



Department of Precision and Microsystems Engineering

Novel design of robust and lightweight lattice materials

Hrishikesh Gopakumar Menon

Report no : 2024.088
Coach : Dr. Can Ayas
Professor : Dr. Can Ayas
Specialisation : Computational Design and Mechanics
Type of report : MSc. Thesis
Date : 30th September 2024

Novel design of robust and lightweight lattice materials

by

Hrishikesh Gopakumar Menon

to obtain the degree of Master of Science

at Delft University of Technology,

to be defended publicly on September 30, 2024 at 9:00 AM.

Student number: 5747783

Thesis committee:	Dr. Can Ayas,	Delft University of Technology
	Dr. Alejandro Aragón,	Delft University of Technology
	Dr. Trayana Tankova,	Delft University of Technology

An electronic version of this thesis is available at <http://repository.tudelft.nl/>.

Preface

As my tenure at TU Delft draws to a close, I look back at these two years with a mix of deep gratitude and mild disbelief. Not only did I learn to cope with rigorous standards of the curriculum, but also to (mostly) keep myself together in the process. I owe this feat to the amazing people around me who have constantly supported me throughout this journey. This work is not just a reflection of my efforts but a testament of their love and belief.

First and foremost, I dedicate this work to my guru- Amma. Any amount of gratitude would fall short for your unflinching love and compassion.

I would like to thank my thesis supervisor, Dr. Can Ayas for all the guidance and support throughout the past year. Your insights and constant encouragement has been vital for the progress and quality of my work. I have thoroughly enjoyed our discussions and working with you has been simply delightful. Further, I extend my appreciation to Dr. Anton Akhmerov, whose feedback on quantum descriptions of Kagome lattices has been valuable.

I am immensely grateful to my parents who have been my pillars of strength throughout. Your endless love, guidance, and sacrifices have shaped the person I am today. Without your support, I am fairly certain that none of this would have been possible. I hope you are proud. Devika, I cannot find words to express my gratitude for your unwavering support and for believing in me throughout this journey. You shared my highest moments with me, and you were there to lift me up when I needed it most, and for that, I am deeply grateful. I am also thankful to Nidhin (a.k.a ikkakka), for being more than an elder brother to me. Your advice and company has played a crucial role in what I am and where I stand now.

My heartfelt gratitude to all my friends here and those back in India for all your love and camaraderie. Your belief in me, whether through late-night discussions, shared laughter, or simply being there when I needed it most, has meant more than words can express.

Finally, I would like to use this opportunity to share a profound phrase that has helped me through the tough times, and more importantly, kept me grounded during the highs- "This too, shall pass".

*Hrishikesh Gopakumar Menon
Delft, September 2024*

Abstract

Lattice materials have been studied extensively for their advantageous mechanical properties like high stiffness-to-weight and strength-to-weight ratios. These properties make them suitable for a multitude of applications like load-bearing structures, energy absorption and impact attenuation. Amongst several planar microarchitectures, the Kagome topology is found to be optimal for effective mechanical properties like macroscopic elastic modulus. However, it has been shown that lattice defects such as nodal misalignments are detrimental to the macroscopic stiffness of the Kagome lattice. From a realistic standpoint, any manufactured lattice is expected to inevitably have these defects, which naturally makes the favorable stiffness properties of the Kagome inaccessible.

This work takes a step towards designing planar lattices with defect insensitive macroscopic stiffness. A novel design strategy is proposed for generating stiff, lightweight and robust lattice materials. The Kagome lattice is chosen as base architecture for the developed designs due to its excellent stiffness-to-weight property and extreme sensitivity towards defects. The generated designs involve appending the Kagome bulk with two unique and carefully designed microarchitectures. The first is a lattice developed using combinatorial design strategies, which demonstrates properties like perturbation-dependent switching between mechanism-states and load-bearing states. The second is a polarised lattice that enables localisation of mechanisms at specific sites of the lattice. This arrangement forms a "composite" lattice which when appropriately designed demonstrates robustness against manufacturing defects.

Development of such an architecture is carried out through an iterative design and analysis process which is based on reformulated matrix methods. A mass-spring model is used in contrast to regular pin-jointed models and a dynamical matrix method is developed as an alternative to traditional matrix analysis. Suitable designs formed out of this iterative process are verified for their stiffness properties using Finite Element models. Robustness against nodal defects is observed in well-designed lattice models. Satisfactory performance of such designs indicates the efficacy of the adopted design strategy which could potentially be applied to any lattice microarchitecture other than Kagome for robustness.

Contents

Preface	I
Abstract	II
Nomenclature	IX
1 Introduction	1
1.1 Lattice materials	1
1.2 Static and kinematic determinacy	2
1.2.1 Mechanisms	3
1.2.2 Stretching-dominated vs. Bending-dominated behaviour	4
1.3 Relevant literature and research gap	5
1.4 Research objective	6
1.5 Thesis outline	7
2 Design methodology	8
2.1 Adopted design protocol	8
2.1.1 Combinatorial designs	8
2.1.2 Topological polarisation	11
2.2 Intended solution strategy	14
2.3 Reformulation of matrix methods	15
2.3.1 Dynamical lattice model	15
2.3.2 Automated matrix evaluation algorithms	17
2.4 Benchmark tests	17
2.4.1 Global modes	18
2.4.2 Localised modes	20
2.5 Information from Eigenvalues	21
2.5.1 Implication of eigenvalues for welded-jointed models	23
2.6 Numerical identification of mechanism types	23
2.6.1 Infinite Lattices	24
2.6.2 Finite lattices	26
2.7 Limitations of the dynamical matrix method	27
2.8 Concluding remarks	28
3 Development of novel designs	29
3.1 Developed designs	29
3.1.1 Rationale behind the design process	31
3.2 Matrix analysis	32
3.3 Concluding remarks	36
4 Numerical verification of designs	37
4.1 Numerical model setup	37
4.2 Macroscopic stiffness calculations	38
4.3 Concluding remarks	44
5 Conclusions	45
References	48
A Algorithms	50
A.1 Repeating members	50
A.2 Repeating nodes	52

A.3	Finite lattices	53
B	Mechanisms	54
C	CL designs	56
C.1	Polarising the Kagome	56
C.2	CL truncation for matrix analysis	58
C.3	Relative density expressions	59

List of Figures

1.1	Schematic representation of 3D lattices with their unit cells (reproduced from [2]).	1
1.2	Unconstrained node p and assembly of the the equilibrium expressions in \mathbf{A} matrix.	2
1.3	a. Triangular lattice $Z = 6$; b. Hexagonal lattice $Z = 3$	4
1.4	Stiffness decay in Kagome lattices: a. Pristine Kagome; b. Example of Kagome with nodal misalignments due to manufacturing errors (indicated by red circles); c. Representative trend of the decay in Kagome macroscopic stiffness due to nodal misalignments observed under a global uniaxial compression test.	6
2.1	Textured surfaces through combinatorial designs (Reproduced from [29]): a. Unit cell with the two collapse mechanisms indicated by '+' and '-'; b. Representation of the combinatorial strategy using cubes with cavities (black) denoting inward movement, and protrusions (white) denoting outward movement; c. Two collapse modes along each orthogonal direction in space; d. Pre-defined texture of a 'smiley face' obtained when the lattice is compressed. Inset shows the undeformed lattice.	9
2.2	Combinatorial design strategy (Reproduced from [30], [31]) a. Supertriangle with edge bonds (grey), internal bonds (black), corner nodes (black), "majority edge nodes" (blue) and a "minority edge node" (pink); b. Collapse mechanisms of the supertriangle; c. Combinatorial rules: Interaction between two supertriangles is governed by the nature of the common node (majority or minority) shared between them; d. Compatible superhexagon (left) with an inner-loop count of 8, and frustrated superhexagon (right) with an inner-loop count of 9 (purple cross indicates a possible site of frustration); e. Demonstration of the global collapse mechanisms of superhexagons with different inner-loop lengths. Inner-loop member count is indicated by the adjacent numeric; f. Evolution of a fully compatible structure to a structure with a topological defect through supertriangle rotations. Supertriangles being rotated are indicated in yellow.	10
2.3	Phonon spectrum of Kagome: a. Real space and reciprocal space of the Kagome with corresponding base vectors. The reciprocal space is the dotted hexagon mapped using base vectors a^1 and a^2 , and the inner hexagon indicates the BZ. The shaded triangle indicates the irreducible BZ; b. Phonon spectrum of the untwisted and twisted Kagome. Dashed lines represent the untwisted kagome and solid lines represent the twisted kagome. Inset- BZ with the three symmetry directions (Reproduced from [34]).	12
2.4	Accumulation of collapse modes and states of self-stress on domain walls (indicated by dashed lines) through polarisation. Arrows indicate the collapse mode and thickened bonds indicate states of self-stress (Reproduced from [33]).	13
2.5	Intended design strategy.	14
2.6	Lattice structures for benchmark tests: a. Kagome with concentric Triangles, otherwise termed as KT (Reproduced from [20]); b. Triangular; c. Demi-regular (Reproduced from [38]); d. Hexagonal-Cupola; e. Kagome; f. Set of finite lattices constructed using a combinatorial strategy. Inner loops are indicated by black lines and numeric insets indicate the inner-loop count (Reproduced from [30]).	18
2.7	Lattice structures with domain walls. Domain walls are indicated by black dashed lines. Polarisation in the lattice is indicated by red arrows: a. Structure 1 with two domain walls. Domain wall on the left harbours states of self-stresses and domain walls on the right harbours collapse mechanisms, as is also indicated by the polarisation vectors; b. Structure 2, again with 2 domain walls. The left wall harbours collapse mechanisms here; c. Structure 3, is an extension of structure 1 with two more domain walls.	20
2.8	Mechanisms of a compatible network: a. Compatible network; b. Non strain-producing infinitesimal mechanism that becomes strain-producing in the finite regime. The original lattice is shown in grey which is overlapped by the lattice mechanism in red.	22

2.9	Collapse mechanism and state of self-stress of the lattice shown in Figure 2.7b: a. Collapse mechanism corresponding to λ_3 of \mathbf{D} . The original lattice is shown in grey which is overlapped by the lattice mechanism in red. Notice the accumulation of the mode at the corresponding domain wall; b. State of self-stress corresponding to λ_3 of \mathbf{D}^h . Absolute values of stresses are irrelevant (entries in an eigenvector). Again, notice the accumulation of the self-stresses around the corresponding domain wall.	23
2.10	Kagome unit cell.	24
2.11	Strain-producing mechanisms observed in two polarised lattices. The original lattice is shown in grey which is overlapped by the lattice mechanism in red. Notice the accumulation of mechanisms at the respective domain walls.	25
2.12	FE results indicating the axial strains observed in members of two pin-jointed polarised lattices. Notice higher strains near the domain wall with states of self-stress and lower strains at the other domain wall.	25
2.13	Compatible MT lattice. O stands for an <i>open mode</i> and C stands for an <i>closed mode</i> (see Figure 2.2b). The black arrows indicate applied loads: a. Lattice architecture, designed such that all inner loops are even in number, thereby making the structure compatible; b. Collapse mechanism predicted by matrix analysis. The original lattice is shown in grey which is overlapped by the lattice mechanism in red; c. Loading scenario A where the loads warrant a collapse mechanism. No internal frustration in the lattice; d. Loading scenario B where the loads can be supported by the lattice and therefore indicates a <i>fitted load</i> case.	26
2.14	FE results indicating the axial strains observed in members of two pin-jointed compatible MT lattices: a. Scenario A: where the applied loads are in accordance with the global collapse mechanism of the lattice; b. Scenario B: where the applied loads do not support the presence of the collapse mechanism.	27
3.1	Lattice design according to the developed rationale. Domain walls are indicated by dashed lines. Black dashed lines indicate domain walls expected to harbour collapse mechanisms, and red ones indicate those for the state of self-stresses. Green arrows indicate the direction of polarisation.: a. Process flow of the iterative design procedure based on analytical predictions; b. Composite Lattice-1 (CL1), with 2 domain walls on each end; c. Composite Lattice-2 (CL2), with 5 domain walls on each end; d. Composite Lattice-2 (CL3), again with 5 domain walls but with larger distances between a few domain walls.	30
3.2	Truncated version of CL designs for computationally feasible matrix analysis: a. CL1; b. CL2; c. CL3.	32
3.3	Strain-producing mechanism of the outer layer of pristine (without defects) CL1 design corresponding to an eigenvalue of λ_8	33
3.4	Set of strain-producing mechanisms of the outer layers of pristine (without defects) CL2 design corresponding to eigenvalues: a. λ_8 ; b. λ_9 ; c. λ_{10} ; d. λ_{11}	34
3.5	Set of strain-producing mechanisms of the outer layers of pristine (without defects) CL3 design corresponding to eigenvalues: a. λ_7 ; b. λ_8 ; c. λ_9 ; d. λ_{10}	35
4.1	Decay in Macroscopic Young's modulus (E). K-Hex stands for Kagome-Hexagonal and K-Tri for Kagome-Triangular: a. Strain-controlled test; b. Stress-controlled test. ϵ_m indicates the maximum strain endured by the lattice.	39
4.2	Strain energy measures for all designed lattices in their pristine and imperfect models. K-Hex stands for Kagome-Hexagonal and K-Tri for Kagome-Triangular: a. Distribution of strain energy (in percentage) amongst the outer layer and Kagome core; b. Strain energy density in the outer layers and Kagome cores for each lattice model.	40
4.3	a. Specific stiffness of all pristine lattice models; b. Absolute stiffness of selective lattices (pristine and imperfect models).	41

4.4	Presence of cell wall buckling in pristine lattice models: a. Decay in stiffness of models analysed through a geometrically linear framework. Only the pristine model is analysed through a linear setting, the imperfect model is studied through the same nonlinear framework; b. Distribution in strain energy at three different strain levels during the process. Only pristine models are studied here, under the established nonlinear setting. Stage 1 is at low macroscopic strains, stage two is a few increments before buckling ensues and stage 3 is the maximum strain level.	42
4.5	Decay in macroscopic Young's modulus for lattices with different amounts of nodal defects: a. CL2; b. Kagome.	43
A.1	Representation of both <i>criteria-for-design</i> and <i>criteria-for-analysis</i> on Kagome unit cells: a. Kagome unit cell with boundary crossing members suitable for an infinite-model; b. Kagome unit cell with periodic nodes suitable for an infinite-model, with set of periodic nodes highlighted by the same colour; c. Process flow starts from the selection of appropriate unit cell with boundary crossing members that satisfy <i>criteria-for-design</i> to fulfilment of <i>criteria-for-analysis</i> which ultimately results in a proper implementation of periodicity in the matrices.	51
B.1	Visual comparison of the non strain-producing mechanism obtained for the lattice shown in Figure 2.7a. Notice the accumulation of mechanisms near the domain wall (region indicated by the dashed box). Mechanism obtained using: a. Traditional matrix method; b. Dynamical matrix method.	55
C.1	Convention and associated parameters (x_1, x_2, x_3) for distorting the Kagome to obtain a polarised Kagome. g_i represents nodes of the same triangle but indicated at different sites to aid visualisation of the movement of each of those nodes independently.	56
C.2	Polarised Kagome: a. Distortion of a single triangle to a polarised one. The original Kagome configuration is illustrated in grey, and the distorted Kagome in black; b. Tessellating the obtained triangle to fill the space. Since asymmetry is not allowed, a single triangle (in black) is enough to generate the whole lattice. Blue dots indicate 3 nodes of the same triangle marked by g'_1, g'_2 and g'_3 . Green arrow indicates the direction of polarisation.	57
C.3	Incremental truncation of the Kagome core of CL2 model: a. Case 1; b. Case 2; c. Case 3.	58
C.4	Schematic of the supertriangle which is the unit cell of the MT lattice.	59
C.5	Unit cell for the polarised Kagome lattice. Distortion of the Kagome is carried out such that the unit cell obtained is a regular hexagon.	59

List of Tables

2.1	Verification of the performance of the dynamical matrix method in comparison to the symbolic matrix method - infinite lattices. Calculated metrics are for local computer with AMD 6000 series CPU.	19
2.2	Verification of the performance of the dynamical matrix method in comparison to the symbolic matrix method - finite lattices. Calculated metrics are for local computer with AMD 6000 series CPU.	19
2.3	Verification of the performance of the dynamical matrix method in comparison to the symbolic matrix method - lattices with domain-walls. Calculated metrics are for local computer with AMD 6000 series CPU. In the case of structure 2, nullspace computation from the symbolic matrix fails due to lack of memory and computation resources.	20
B.1	Visual comparison of non strain-producing mechanisms of infinite lattices obtained using the traditional matrix method (using symbolic matrices) against the dynamical matrix method. Original unit cells are shown in grey, with mechanisms overlaid.	54
B.2	Visual comparison of mechanisms of network lattices obtained using the traditional matrix method (using symbolic matrices) against the dynamical matrix method.	55

Nomenclature

Abbreviations

Abbreviation	Definition
CL	Composite Lattice
MT	Meta-Triangular
FE	Finite Element

Symbols

Symbol	Description
b	Number of lattice members
j	Number of lattice joints (also referred to as nodes)
A	Equilibrium matrix
B	Compatibility matrix
f	Nodal force vector
t	Member tension vector
d	Nodal displacements
e	Member strain
s	Number of states of self-stress
m	Number of mechanisms
Z	Nodal connectivity number
a_i	Real space base vectors
a^i	Reciprocal space base vectors
n	Winding number
P_T	Polarisation vector
D	Dynamical matrix
M	Mass matrix
U	Strain energy
u	Strain energy density
E	Macroscopic Young's Modulus
t	Cell wall thickness (in-plane)
h	Edge length of a supertriangle unit cell
$\bar{\rho}$	Relative density
λ	Eigenvalues
ε	Macroscopic strain
σ	Macroscopic stress

Introduction

1.1. Lattice materials

Lattice materials are a class of engineered materials composed of periodic arrangements of interconnected struts or members, forming a highly ordered, lightweight structure. Periodicity in lattices is represented by a unit cell which when repeated in plane (or space) generates the whole lattice. Figure 1.1 represents two examples of 3D lattices with their unit cells. Generally, the global length scale of a lattice is much larger than the characteristic length scale of its unit cell, making it an alternative "material" of its own virtue. Owing to this difference in length scales, the lattice material can be treated like a continuum with macroscopic properties like elastic modulus [1]. If this difference in length scales does not exist, the lattice is not a material, but a structure.

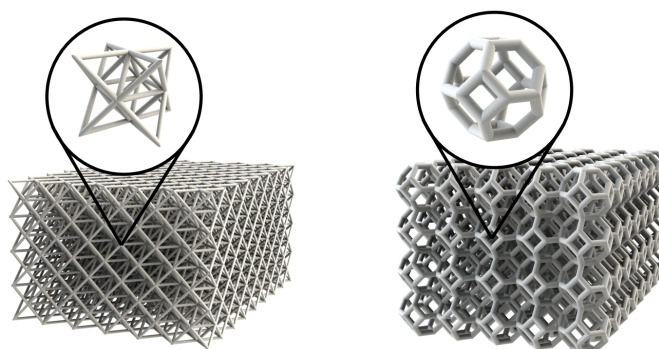
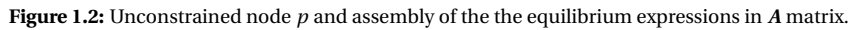


Figure 1.1: Schematic representation of 3D lattices with their unit cells (reproduced from [2]).

The unit cell design or the internal arrangement of members is also termed the microarchitecture of the lattice. Macroscopic properties of the lattice depend on 3 factors: the base material of the struts, the microarchitecture and the relative density ($\bar{\rho}$) [3]. Relative density quantifies the volume fraction of members relative to the volume of the lattice (discussed in more detail in section 1.2). Due to the carefully designed microarchitecture, lattice materials exhibit unique mechanical properties like high stiffness-to-weight and strength-to-weight ratios [4][5], making them useful for applications where weight savings are critical. This has led to their use in aerospace, automotive and biomedical industries where both structural performance and material efficiency are important [6].

In most real-world applications, lattice materials are manufactured with elastic joints which transfer forces and moments between members. These models are referred to as "welded-jointed" lattices. Information regarding the behaviour of these welded-jointed models can be extracted from a "pin-jointed" model, where the joints are friction-less pins that transfer only forces and not moments. However, extending the observations of pin-jointed models to welded-jointed models is not trivial. Pellegrino and Calladine [7] introduce a linear algebra-based analytical method that can be used for examining the properties of pin-jointed lattices.

1.2. Static and kinematic determinacy

$$At = f \tag{1.1}$$
$$\begin{aligned}(x_p - x_w)t_r + (x_p - x_q)t_s &= f_p^{(x)} \\ (y_p - y_w)t_r + (y_p - y_q)t_s &= f_p^{(y)}\end{aligned}\tag{1.2}$$

$$\mathbf{B}d = e \tag{1.3}$$

A lattice is statically determinate if equilibrium expression (Equation 1.1) has a unique solution (of member tensions) for every case of nodal force. Similarly, a lattice is kinematically determinate if the compatibility expression (Equation 1.3) has a unique solution (of nodal displacements) for every case of member strains. This information can be obtained from the four fundamental vector subspaces of either of the two matrices.

They are row space, column space, nullspace and left nullspace. Consider the equilibrium matrix \mathbf{A} . The column space represents the range of nodal forces \mathbf{f} that can be supported by the geometry without exciting nodal movements. For convenience, they are termed as *fitted loads*. The left nullspace represents the range of loads \mathbf{f} that cannot be supported by the assembly. In other words, these loads excite a particular set of internal nodal movements that do not warrant any member tensions. Such a motion is called an inextensional mechanism of the lattice. The size of the left nullspace (m) can be accessed via the rank-nullity theorem. If r_A denotes the rank of \mathbf{A} , then $m = nj - k - r_A$ independent inextensional mechanisms exist in the lattice. The row space denotes the set of member tensions that are in equilibrium with fitted loads. Lastly, the nullspace denotes member tensions that are in equilibrium with zero-loads, also termed as the states of self-stress. Again, from rank-nullity theorem, the set of independent states of self-stress $s = b - r_A$.

The presence of states of self-stress indicates that the lattice is statically indeterminate. The number of unknowns in this case is more than the number of equilibrium equations making the solution of member tensions non-unique. Similarly, if nodal positions cannot be uniquely determined by the member lengths, the lattice is kinematically indeterminate and harbours inextensional mechanisms. If the lattice is both statically and kinematically determinate, it is termed to be *just-rigid* or *isostatic*. The Maxwell-Calladine¹ theorem [7] comes to aid in determining if the lattice is *isostatic*. It is as follows,

$$b - nj + k = s - m \quad (1.4)$$

For finite lattices, the *necessary* condition for isostaticity is that it satisfies Equation 1.4. However, it also requires a suitable arrangement of members and proper nodal connectivity to ensure isostaticity. Therefore, the *sufficient* condition for isostaticity is to have $s = m = 0$. For infinite lattices, Equation 1.4 reduces to $b - nj = s - m$ as foundational constraints cannot exist. While the necessary condition for isostaticity remains the same, the sufficiency condition is different. Guest & Hutchinson [9] prove that an n -dimensional infinite lattice is statically determinate *iff* it has $3(n - 1)$ states of self-stress, and kinematically determinate *iff* it has n mechanisms. In 2D, this translates to the fact that the lattice supports three possible external loads (σ_{xx} , σ_{yy} , σ_{xy}) or any combination of them at infinity without giving rise to any nodal forces; and has two inextensional mechanisms corresponding to rigid body modes along the two independent directions. This means that the equilibrium matrix should be rank deficient by 3 while the compatibility matrix should be rank deficient by 2. Since this is not possible, it is concluded that infinite lattices cannot be isostatic.

1.2.1. Mechanisms

Along with detecting mechanisms, it is also important to understand their nature. Lattice mechanisms can be put into two categories: finite and infinitesimal. A finite mechanism is one that allows the nodes to be displaced by finite amounts without causing strains in the associated members. However, an infinitesimal mechanism causes a change in the member lengths upon nodal displacements. These changes can be of second order or higher in terms of displacements. Consequently, an infinitesimal mechanism tightens up upon excitation. It is important to note that the described matrix method cannot distinguish between finite and infinitesimal mechanisms since the equations are linearised in the original configuration without the capacity to track the ensuing changes in geometry. That is, the matrix method is only capable of detecting first-order changes in member lengths and not higher order. To identify the mechanism type, one can model the nonlinear kinematic behaviour of the mechanism through a general motion function and monitor the mechanism to check if it causes any change in member lengths upon finite nodal movements [10].

The mechanisms can also be categorised in yet another manner: strain-producing and non strain-producing. A strain-producing mechanism is one that is excited when the lattice is subjected to a macroscopic load, that is, exciting such a mechanism causes a macroscopic strain in the lattice. On the other hand, a non strain-producing mechanism is one that is not excited under a macroscopic load. Conversely, the infinitesimal version of a non strain-producing mechanism does not cause any macroscopic strain in the lattice. It should be noted that any finite mechanism of a lattice is, in essence, strain-producing. However, its infinitesimal version can be non-strain producing. Guest & Hutchinson [9] introduce an augmented matrix method to categorise the appearing mechanisms of an infinite lattice into strain-producing or non strain-producing categories.

¹This is a modification by Pelegrino & Calladine to the original Maxwell expression $b - nj + k = 0$.

1.2.2. Stretching-dominated vs. Bending-dominated behaviour

For pin-jointed models of both infinite and finite lattices, if $b > nj$ (or $nj - k$ for finite cases), the states of self-stress increase, indicating an increasing redundancy of members in the lattice. This is directly related to the lattice stiffness. Deshpande *et al.* [8] show that for an infinite planar lattice, a nodal connectivity (Z) of 4 is the necessary condition for rigidity, while $Z = 6$ ensures sufficiency. However, these limits render highly redundant structures like the fully-triangulated lattice featuring multiple states of self-stress and no mechanisms. On the other hand, hexagonal lattices with $Z = 3$ are not rigid and feature strain-producing mechanisms. Schematic representations of both triangular and hexagonal lattice architectures is shown in Figure 1.3. Therefore, for isostaticity in an infinite lattice, it is instructive to have a Z number between 3 and 6.

In most applications, lattice materials are manufactured with elastic-joints that transfer moments. Such a model is called the welded-jointed model. Although all the observations made for pin-jointed models can be translated to welded-jointed models, there are a few subtleties here. If the pin-jointed equivalent has strain-producing mechanisms, the response of the welded-jointed equivalent to a macroscopic load is predominantly via the bending of members. Consequently, its macroscopic stiffness is largely derived from the bending stiffness of members and nodes. Welded-jointed lattices exhibiting this manner of response are categorised under *bending-dominated* structures. In general, lattices with a lower Z number exhibit this characteristic. One example is the hexagonal lattice ($Z = 3$). On the other hand, if the pin-jointed equivalent does not have any strain-producing mechanisms, the welded-jointed response will be largely via member stretching. In this case, the macroscopic stiffness primarily comes from the axial stretching of members. These welded-jointed lattices are categorised under *stretching-dominated* structures. Lattice with a higher Z numbers display this characteristic. An example of this is the fully-triangulated lattice ($Z = 6$).

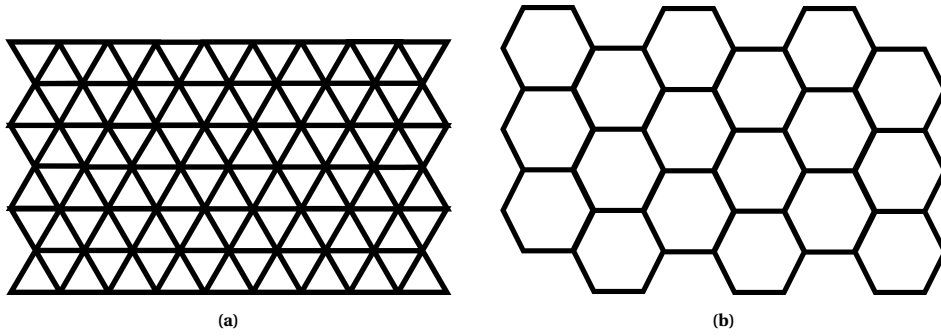


Figure 1.3: a. Triangular lattice $Z = 6$; b. Hexagonal lattice $Z = 3$.

The aspect of rigidity is not only interconnected with the Z number but also with the relative density of the lattice. Relative density ($\bar{\rho}$) is defined as the ratio of the density of the lattice material to the density of its constituent material. In other words, it denotes the volume fraction of the material occupied. For a planar lattice, a straightforward estimation of this quantity can be done by dividing the in-plane cumulative area of the members to the total area of the unit cell. For rectangular members, relative density ($\bar{\rho}$) is expressed as follows,

$$\bar{\rho} = \frac{1}{A_c} \sum_{i=1}^n l_i w_i \quad (1.5)$$

Here, l represents the length of the strut, w stands for the strut width, n for number of members, and A_c denotes the unit cell area. Relative density is closely related to macroscopic elastic moduli. It is shown that if the macroscopic elastic modulus scales with $\bar{\rho}$, the lattice is stretching-dominated and bending-dominated if it scales with $\bar{\rho}^3$ (2D) and $\bar{\rho}^2$ (3D) [5].

With the background on lattice determinacy properties in place, a literature survey is presented next that builds towards the research gap. The thesis objective and outline is presented thereafter.

1.3. Relevant literature and research gap

For a high stiffness characteristic, higher Z numbers are suitable. However, as the Z number increases, the lattice becomes increasingly heavier. Naturally, a need for discovering stiff lattices with lower Z numbers becomes apparent, since lattice materials are chosen for their high specific stiffness, and not absolute stiffness. The Kagome proves to be an ideal candidate in this regard. With $Z = 4$, its stiffness does not come from redundancy in members, but from the fact that it harbours 3 states of self-stress that provide it the ability to withstand any in-plane loading scenario. Hyun & Torquato arrive at the same conclusion in their search for optimal lattices satisfying the Hashin-Shtrikman (HS) upper bounds for bulk and shear moduli [4]. HS bounds define the limiting characteristics for several mechanical and electrical properties of dual-phase composites [11]. The ensuing optimal designs from this study are triangular and Kagome architectures. However, the triangular lattice is twice as heavy as the Kagome for the same material and dimensions.

In light of this, welded-jointed models of the Kagome architecture have been subject to numerous assessments for its properties like elastic modulus [3], [5], Poisson's ratio [3], fracture toughness [12] and damage tolerance [13]. In addition, the pin-jointed equivalents have also been studied for their static and kinematic properties and actuation performance [9], [14], [15]. The pin-jointed version of infinite Kagome is shown to harbour a non strain-producing mechanism. Megen [10] geometrically modelled the motion of this mechanism and analysed the elastic properties of Kagome under a finite amount of excitation of the mechanism. It was found that as the mechanism ensues, the macroscopic stiffness (measured via the macroscopic Young's modulus) of the Kagome lattice decays exponentially. In other words, the mechanism turns into a strain-producing one and thereby changes the response of its welded-jointed equivalent from stretching-dominated to a bending-dominated one. From the matrix method perspective, as soon as the Kagome nodes are displaced from their original symmetry lines, the structure loses a state of self-stress and therefore its welded-jointed equivalent becomes susceptible to bending deformations under an in-plane loading scenario.

However, a more fundamental problem exists here. The presence of a non strain-producing collapse mechanism indicates that under a minute nodal perturbation of a single lattice joint, its kinematic property changes and a strain-producing mechanism is born. This raises a critical concern over the accessibility of favourable stiffness properties of manufactured Kagome for real-world applications. As of today, no manufacturing process guarantees a 100% accuracy in design. Consider the example of laser powder bed fusion, which is one of the most common techniques used for manufacturing metal lattice materials. While this technique makes it possible to construct highly intricate and precise micro-architectures [16], issues with process robustness and repeatability exist. Residual-stresses due to rapid expansion-contraction cycles cause imperfections like nodal misalignments and cell wall rupture in the manufactured lattices. Therefore, manufactured lattices are expected to inevitably have geometrical defects. This necessitates an investigation into the effect of imperfections on the mechanical properties of lattices like Kagome and other configurations intended for practical applications.

Romijn & Fleck [17] report the effect of randomised nodal misalignment on macroscopic elastic modulus and fracture toughness in welded-jointed planar lattices like the Kagome, triangular and square lattices. They observe that the macroscopic properties of Kagome and square lattices are highly imperfection sensitive with the triangular lattice being least sensitive. In other words, nodal defects cause a considerable decay in the macroscopic stiffness of periodic lattices with a nodal connectivity of $Z = 4$. Figure 1.4 represents nodal misalignments in Kagome and the ensuing decay in stiffness. Symons & Fleck [18] observe similar results for Kagome and also investigate the effect of defects in the welded-jointed hexagonal lattice. They observe a drastic drop in its bulk modulus only but not in the shear modulus. This is however an expected outcome as the pristine hexagonal lattice is stretching dominated under hydrostatic loading and bending dominated under deviatoric loading. Tankasala *et al.* [19] perform a similar study as in [17], but investigate the effect of imperfections on ultimate tensile strength and macroscopic ductility of these lattices. This is done by modelling the lattice response considering geometry-induced stiffening at large strains. They observe that with an increasing percentage of defects, there is a similar decay in macroscopic ductility and ultimate tensile strength as that of the macroscopic Young's modulus of the elastic-brittle Kagome (work by [17]).

Gencoglu *et al.* [15] investigated the effect of imperfections like fractured members, non-uniform member thickness and member waviness on the actuation performance and Young's modulus of welded-jointed models of novel lattices designs introduced by Nelissen *et al.* [20]. These designs show similar characteristics to that of

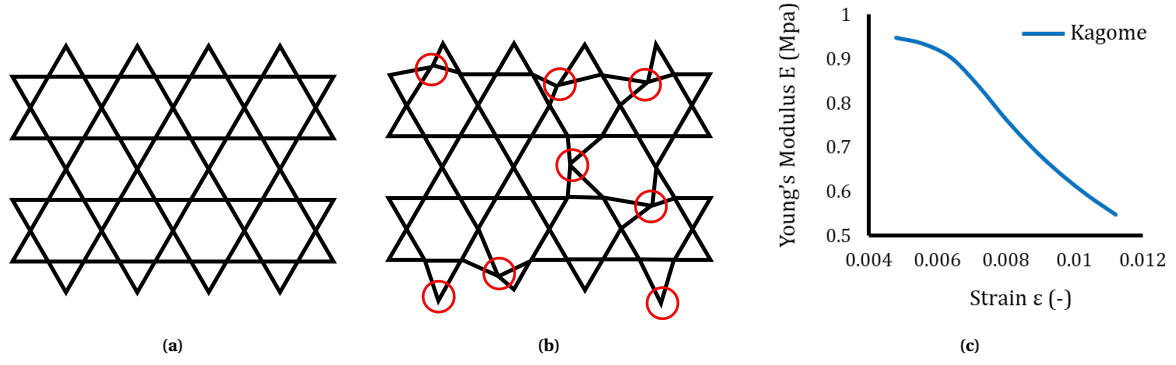


Figure 1.4: Stiffness decay in Kagome lattices: **a.** Pristine Kagome; **b.** Example of Kagome with nodal misalignments due to manufacturing errors (indicated by red circles); **c.** Representative trend of the decay in Kagome macroscopic stiffness due to nodal misalignments observed under a global uniaxial compression test.

the Kagome. It was observed that fractured members cause a greater knock-down in the macroscopic stiffness of most investigated lattices compared to nodal misalignments. However, from a practical stand-point more severe defects like fractured members are detectable during post-processing stages after manufacturing and hence can be addressed before its application.

Furthermore, imperfection sensitivity of properties like stiffness, yielding, buckling and collapse behaviour of planar welded-jointed hexagonal lattices (regular and voronoi tessellations) have also been thoroughly explored [21],[22],[23],[24]. The key finding again being the reduction in stiffness due to defects like nodal misalignments and fractured walls. Similar work has been carried out for investigating the imperfection sensitivity of 3D lattices using numerical and experimental methods [25],[26],[27],[28]. An underlying observation in these studies concerns the relation between Z number and defect sensitivity, where lattices with higher Z numbers are more impervious to defects. Notably, the response of lattices with $Z \geq 12$, in the presence of defects, is almost indistinguishable from that of a homogeneous material.

Although the imperfection sensitivity of planar and spatial lattices has been extensively studied, little to no work has been carried out to remedy this issue. In the face of the defect sensitivity of lattices, the prospect of achieving robustness in stiffness without increasing the weight of the structure becomes critical for obtaining robust and lightweight lattice materials. Therefore, addressing the imperfection sensitivity of lattices is of key importance. With this in mind, the exact research problem addressed as part of this thesis is presented next.

1.4. Research objective

This work is aimed at addressing the issue of decay in the stiffness of planar lattices under the influence of manufacturing defects. The direction pursued is a geometry-based modification of lattices such that imperfections have minimal effect on the stiffness properties. Therefore, the objective here is to accept the presence of manufacturing defects and construct (or equivalently, propose a developmental protocol for) a lattice material capable of retaining its macroscopic stiffness. The Kagome lattice is chosen as the base architecture due to its excellent stiffness properties and extreme vulnerability towards defects. Defects like nodal misalignments are considered since they have a detrimental effect on the Kagome stiffness and are subtle enough to not be identified by most post-processing techniques. It is important that the developed lattice conserves the core properties of Kagome in order to retain the benefits of its structural optimality.

To this end, a novel design approach is adopted. The Kagome is combined with novel and carefully designed lattices exhibiting unconventional properties like localisation of mechanisms and states of self-stress and load-dependent switching between mechanism states and load-bearing states. This lattice design derives inspiration from domains outside traditional mechanics like solid-state physics and quantum mechanics. Importantly, the modifications made are themselves impervious to defects. The design and analysis of these structures are based on a new reformulated matrix method introduced here. This method proves to be computationally more efficient than the traditional matrix method and provides an easier alternative to the augmented matrix method ([9]) for finding strain-producing mechanisms. The observations from matrix analysis is also verified numerically via finite element analysis which also provides new insights.

1.5. Thesis outline

This thesis is structured in the following manner.

- Chapter 2 presents the strategy used to address the research objective along with a discussion of the pertinent literature. A novel solution strategy is established that derives inspiration from domains outside traditional mechanics. This is followed by the development of the computational tools required to generate and analyse the design-solutions. A computationally inexpensive dynamical method is presented which is used for studying lattice determinacy. Benchmark tests are conducted to validate the accuracy of this method and compare its feasibility against traditional matrix methods. Numerical (FEM) protocols used for characterising certain lattice properties are also outlined. This forms the complete set of tools used for analysis in this work.
- Chapter 3 presents the solution protocol, a set of novel designs developed, the underlying motivation and an initial assessment of the lattice properties through matrix methods.
- Chapter 4 presents the observations of the numerical tests conducted pertaining to the research objective and follows it up with necessary discussions.
- Chapter 5 draws out the essence of this work and closes the thesis with key conclusions and recommendations for future work.

2

Design methodology

This chapter provides a detailed overview of the strategy used to address the research objective and key literature relevant to this. Section 2.1 presents a comprehensive coverage of the fundamental principles that form the design approach. This is followed by a brief discussion of the intended solution strategy and how the introduced concepts inspire the solution. Section 2.3 presents a reformulated matrix method which is required to implement the solution. Next, algorithms devised for automating matrix analysis are presented. Benchmark tests are also carried out to verify the accuracy of the new matrix method and the devised algorithms. The chapter culminates with a discussion of the developed numerical protocol used to verify the nature of mechanisms predicted by matrix analysis.

2.1. Adopted design protocol

The developed strategy for design rests on two pillars. The first one, combinatorial designs, is inspired by the geometry of atomic arrangement in stable crystalline lattices. The second one, topological polarisation, is a concept derived from phenomena observed in solid-state devices like topological insulators. Details regarding the background and nuances of both these domains are omitted as it falls outside the purview of this thesis. Rather, the most important points are covered and connections are made between these domains and lattice determinacy concepts (presented in the previous chapter). This includes detailed interpretation and discussions regarding the manner in which the solution strategy is born out of these domains.

2.1.1. Combinatorial designs

A combinatorial design process for lattice structures is essentially a strategy of arranging unit cells in a pre-defined fashion to induce a global or local structural property. Here, the unit cell, itself having a set of mechanical properties, is tessellated in-plane (or space) without being restricted to conventional rules of orientation or connectivity. For this thesis, the mechanical property in consideration is collapse mechanisms. Through a combinatorial process, one could design a collection of these unit cells exhibiting unique global finite mechanisms. In other words, under the application of an external load, the collection of unit cells can cohesively adapt into a global shape.

Coulais *et al.* [29] illustrate this concept using a 3D lattice, with each unit cell having two distinct collapse modes. They propose a combinatorial strategy for tessellating this unit cell so as to generate global mechanisms that result in unique surface topologies - referred to as "textured surfaces". Figure 2.1a shows the designed unit cell with its collapse mechanisms. There are two distinct modes along each axis as shown in Figure 2.1c. Since this is an elastic body, the collapse mode manifests through member bending. Designing the lattice following a local stacking rule ensures that the unit cells change shape cooperatively and guarantees that the deformed cells fit perfectly with each other as in a jigsaw puzzle. An example of one such rule is shown in Figure 2.1b. Under a compressive load, a harmonious cell collapse results in the predicted textured surface as shown in Figure 2.1d. An arrangement that renders such a response is termed as a *compatible*. However, if the arrangement violates local combinatorics, it renders a load-bearing response and the lattice is termed as *frustrated*.

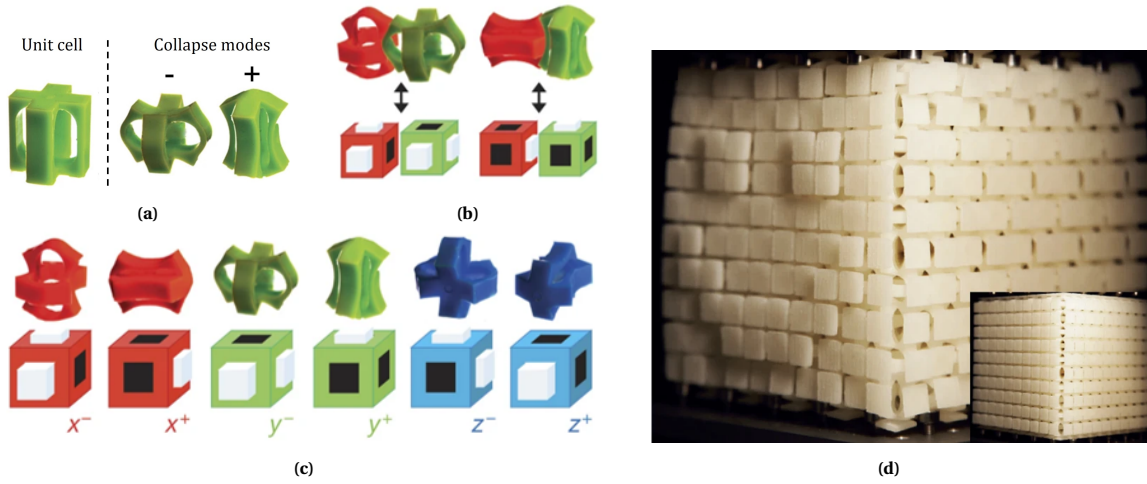


Figure 2.1: Textured surfaces through combinatorial designs (Reproduced from [29]): **a.** Unit cell with the two collapse mechanisms indicated by '+' and '-'; **b.** Representation of the combinatorial strategy using cubes with cavities (black) denoting inward movement, and protrusions (white) denoting outward movement; **c.** Two collapse modes along each orthogonal direction in space; **d.** Pre-defined texture of a 'smiley face' obtained when the lattice is compressed. Inset shows the undeformed lattice.

Meeussen *et al.* [30] propose a planar lattice formed by tessellating a suitable unit cell following a combinatorial strategy. A triangular unit cell with 3 extra nodes situated at the mid-points of each member is used here. Figure 2.2a and Figure 2.2b shows the unit cell and the ensuing two distinct collapse mechanisms. For convenience, the unit cell is termed as a *supertriangle* since there exist two *inner-triangles* (shaded in grey in Figure 2.2a) in the unit cell. The mechanism with inner-triangles rotating outwards produces an *open* mode, while the other produces a *close* mode. The arrows in Figure 2.2b indicate the movement of the internal nodes, blue indicating inward movement while red indicating outward. An immediate application of the Maxwell-Calladine theorem (Equation 1.4) on this unit cell gives $b - nj = -2$. This indicates the presence of two mechanisms more than the number of states of self-stress, which is in accordance with the collapse modes found in [30].

The combinatorial rules for stacking the supertriangles together are highlighted in Figure 2.2c. There are four possibilities for stacking two supertriangles together in a compatible fashion. For a larger compatible structure, geometry dictates that the stacking should be such that any given closed-loop of inner-triangle members has an *even* number of members. Even if any one of the loops has *odd* number of members, the structure loses its global collapse mechanism and becomes frustrated. An example of this is illustrated in Figure 2.2d. Here, the left structure is a compatible *superhexagon* formed by arranging 6 supertriangles together such that the inner-loop count is even (here 8). The superhexagon on the right is frustrated with an inner-loop count of 9 and does not harbour a collapse mechanism. This is achieved by the rotation of just one of the supertriangles in the structure. Several compatible superhexagons can be designed with different inner-loop counts. An example of the ensuing collapse mechanisms of such superhexagons is illustrated in Figure 2.2e.

It is now evident that a simple rotation of one supertriangle can transform a compatible lattice into a frustrated one [31]. For larger compatible lattices, one rotation of the supertriangle changes the parity of the loops and locally generates two adjacent odd loops, as shown in Figure 2.2f. The odd loops are highlighted in red. This is called a local/structural defect. Furthermore, by a sequence of supertriangle rotations, one of the odd loops can be "moved" to the edge and made even. This leaves only one odd loop inside the lattice bulk and is termed as a topological defect. While a local defect can be instantly removed with a small number of supertriangle rotations, a topological defect requires an extensive and precise sequence of supertriangle rotations. Therefore, an on-the-fly switching between frustrated and compatible lattices becomes challenging due to the requirement of rotating supertriangles in the bulk.

The aforementioned were some of the examples of designing lattices that exhibit unique mechanical properties using combinatorial strategies. However, there are some critical observations that need to be discussed.

The presence of a finite mechanism in a pin-jointed compatible lattice is not only the result of its geometry, but

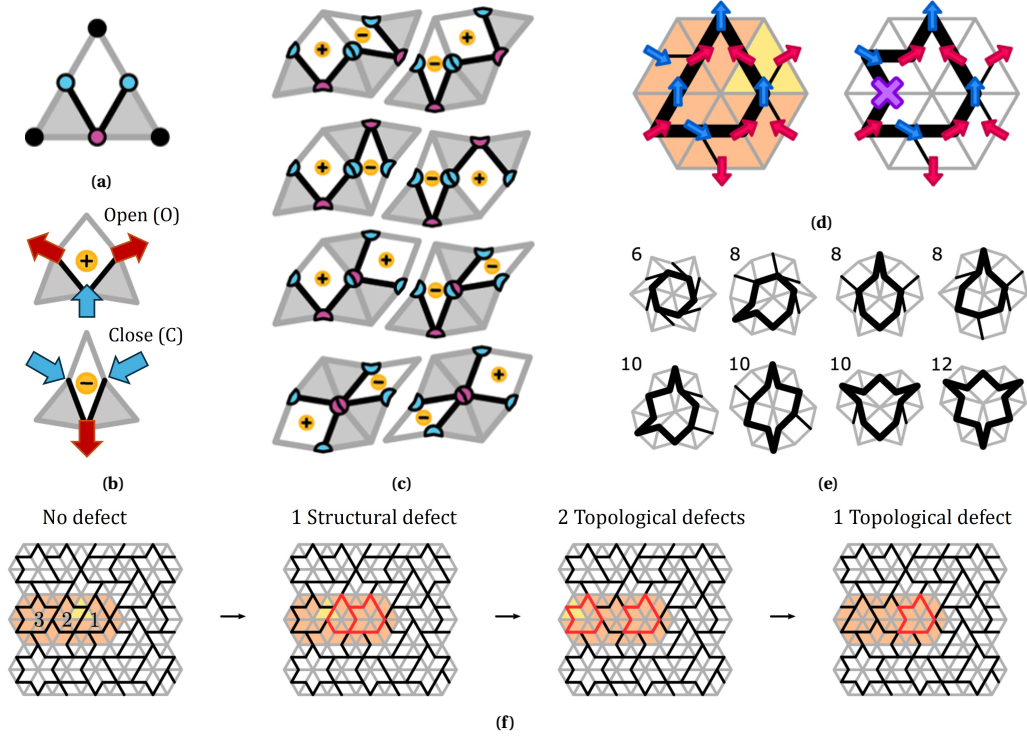


Figure 2.2: Combinatorial design strategy (Reproduced from [30], [31]) **a.** Supertriangle with edge bonds (grey), internal bonds (black), corner nodes (black), "majority edge nodes" (blue) and a "minority edge node" (pink); **b.** Collapse mechanisms of the supertriangle; **c.** Combinatorial rules: Interaction between two supertriangles is governed by the nature of the common node (majority or minority) shared between them; **d.** Compatible superhexagon (left) with an inner-loop count of 8, and frustrated superhexagon (right) with an inner-loop count of 9 (purple cross indicates a possible site of frustration); **e.** Demonstration of the global collapse mechanisms of superhexagons with different inner-loop lengths. Inner-loop member count is indicated by the adjacent numeric; **f.** Evolution of a fully compatible structure to a structure with a topological defect through supertriangle rotations. Supertriangles being rotated are indicated in yellow.

also of the load case [30]. While loads at certain locations give rise to global finite mechanisms, loads applied elsewhere, either directly become a supported load or warrant an infinitesimal mechanism mode. That is, the load-bearing property of the frustrated lattice can be realised in a compatible lattice as well. Again, it is useful to recall that, if the pin-jointed equivalent has finite mechanisms (which is true in the case of compatible lattices), its welded jointed equivalent will respond in a bending-dominated manner.

A crucial benefit to these architectures is the fact that a pin-jointed compatible structure exhibits a collapse mechanism for a long range of physically allowable nodal displacements. Since compatibility predominantly depends on the satisfaction of combinatorial rules, a manufacturing defect such as nodal misalignment will not affect the presence of the collapse mechanism. Although the extent of "finite-ness" of nodal movements could be restricted, the mechanism remains intact. It should be noted that severe defects like fractured members can potentially change the mechanism landscape altogether, but still do not eliminate the global mechanism. Similarly, the presence of defects will not affect the load-bearing response. An external load that renders the original lattice frustrated will cause the same response even under manufacturing defects. This is because frustration only requires to manifest in one loop for it to reflect in the lattice response. That is, defects in a location will not affect the global frustration of the lattice.

Although lattices formed out of this strategy turn out to be aperiodic in nature, they offer a way of designing a lattice with high nodal connectivity which also exhibits collapse mechanisms. For the welded-jointed equivalent, this means that the bending-dominated response of a compatible lattice could potentially demonstrate a relatively stiffer behaviour compared to regular lattice models that exhibit bending-dominated behaviour ($Z \leq 4$), due to the higher nodal connectivity. While combinatorial design strategies present a unique method of generating lattices with high nodal connectivity that also harbour mechanisms, topological mechanics offers an interesting prospect, that is, of localising these mechanisms at pre-defined regions in the lattice bulk. The following section discusses how.

2.1.2. Topological polarisation

The Maxwell-Calladine expression predominantly aids in counting the number of mechanisms and states of self-stress, and relating it to a number of members and joints present in the lattice. For infinite lattices, the obtained mechanisms and states of self-stress reflect throughout the bulk. It is however found that a topological modification to certain lattice structures successfully renders a localisation of collapse mechanisms and states of self-stress at isolated regions in the infinite lattice bulk. This is inspired from the behaviour of topological insulators that exhibit a surface conducting property while being insulating in the bulk [32]. This section discusses this aspect of localisation of modes in detail and makes a connection to the research objective of this thesis.

It was shown by Kane & Lubensky [33] that states of self-stress and mechanisms can have a topological origin in a lattice structure. By means of minor topological manipulation to the unit cell, a *polarisation* is generated in the lattice that allows localisation of mechanisms. In a loose sense, polarisation denotes the flow of net degrees of freedom from throughout the lattice to a particular region and is denoted by a spatial (or planar) vector. It can be visualised as being similar to an electrical polarisation that results in a separation of charges. Through such a manipulation of the structural geometry, mechanisms can be accumulated at certain regions without disrupting the Z number. This is particularly useful in applications where the mechanical properties need to be tuned without disrupting thermal/electrical or other properties.

Polarisation is best understood via the phonon spectra of lattice structures. The phonon spectra is an illustration of all the possible vibration modes of the lattice. In crystal systems, the electronic arrangement creates a potential energy landscape. This governs the allowable momentum states (corresponding to energy states) that the electrons can be in for that system. The relationship between the vibration modes and the energy of electrons in a crystal is described by the electronic band structure, represented by the phonon spectrum. This spectrum is devised from the reciprocal space (also called the k -space or momentum-space) and maps the vibration modes to the wavevectors along various symmetry directions of the Brillouin zone (BZ). Each point in the BZ is represented by a unique wavevector and each wavevector describes a momentum state of the system. Note that each of these momentum states represents a particular energy state allowed in that periodic potential. Following is an example for a better understanding of the phonon spectra.

Kagome phonon spectrum

Figure 2.3a illustrates the real space and reciprocal space of the Kagome lattice with their corresponding base vectors. The reciprocal space is purely a mathematical construct (like a complex plane). Derivation of the reciprocal lattice base vectors is as follows. Consider a Kagome lattice with a real space unit cell as shown in Figure 2.3a (left). Assume the characteristic length of this unit cell is l , which gives the real-space vectors,

$$\mathbf{a}_1 = l\hat{\mathbf{i}} \quad \text{and} \quad \mathbf{a}_2 = \frac{l}{2}\hat{\mathbf{i}} + \frac{l\sqrt{3}}{2}\hat{\mathbf{j}} \quad (2.1)$$

The reciprocal lattice vectors, \mathbf{a}^1 and \mathbf{a}^2 , corresponding to \mathbf{a}_1 and \mathbf{a}_2 are derived as follows,

$$\mathbf{a}^1 = 2\pi \frac{\mathbf{a}_2 \times \hat{\mathbf{k}}}{\mathbf{a}_1 \cdot (\mathbf{a}_2 \times \hat{\mathbf{k}})} \quad \text{and} \quad \mathbf{a}^2 = 2\pi \frac{\hat{\mathbf{k}} \times \mathbf{a}_1}{\mathbf{a}_1 \cdot (\mathbf{a}_2 \times \hat{\mathbf{k}})} \quad (2.2)$$

which gives,

$$\mathbf{a}^1 = \frac{2\pi}{l}\hat{\mathbf{i}} - \frac{2\pi}{l\sqrt{3}}\hat{\mathbf{j}} \quad \text{and} \quad \mathbf{a}^2 = \frac{4\pi}{l\sqrt{3}}\hat{\mathbf{j}} \quad (2.3)$$

A quick sanity check of the calculations can be done by ensuring that $\mathbf{a}_m \cdot \mathbf{a}^n = 2\pi\delta_{mn}$ where m and $n = \{1, 2\}$ and δ_{mn} is the Kronecker delta function. The reciprocal vectors \mathbf{a}^1 and \mathbf{a}^2 form the reciprocal space (see Figure 2.3a (right)).

The phonon spectrum of the Kagome is as shown in Figure 2.3b. The inset here indicates the BZ of Kagome. Each point in this inset corresponds to a wavevector which in turn corresponds to a vibration mode of the lattice with a certain energy mark. The BZ represents a reduced form of the reciprocal lattice, akin to a unit cell of a lattice in real space. The BZ can further be reduced owing to symmetry and this results in the irreducible Brillouin Zone (BZ). The reduction is done based on three symmetry directions- $\Gamma - M$, $M - K$, $K - \Gamma$. These directions can be traced back to the real-space of the Kagome easily.

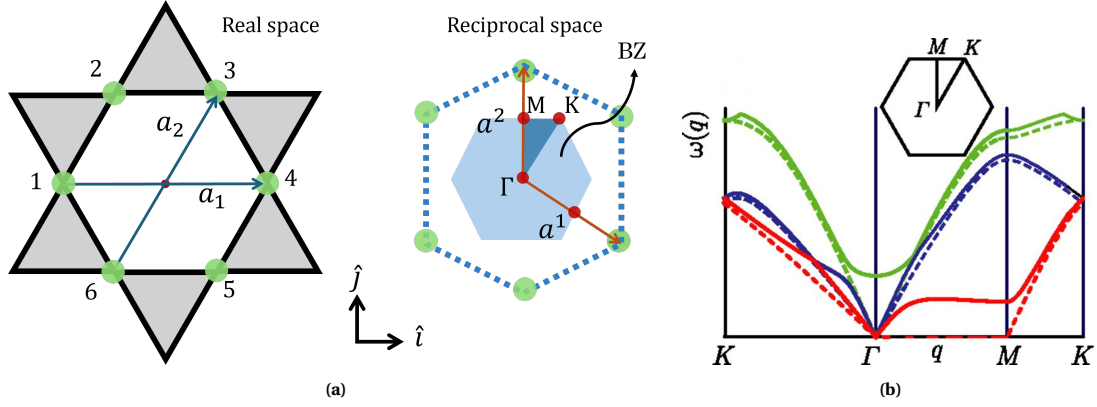


Figure 2.3: Phonon spectrum of Kagome: **a.** Real space and reciprocal space of the Kagome with corresponding base vectors. The reciprocal space is the dotted hexagon mapped using base vectors a^1 and a^2 , and the inner hexagon indicates the BZ. The shaded triangle indicates the irreducible BZ; **b.** Phonon spectrum of the untwisted and twisted Kagome. Dashed lines represent the untwisted kagome and solid lines represent the twisted kagome. Inset- BZ with the three symmetry directions (Reproduced from [34]).

For the Kagome, at each wavevector, there are 6 possible vibration modes each with an increasing energy requirement. The lowest three are shown in Figure 2.3b represented by each of the coloured lines. Beware, that each line does not indicate a mode in itself, but each point that constitutes the line is a mode on its own. It can be observed that there are zero-energy modes along the $\Gamma - M$ symmetry line (dashed red line). This symmetry line runs along each of the reciprocal space vector directions and hence corresponds to the direction a_1 and a_2 in the real space. The presence of zero energy modes along the $\Gamma - M$ lines indicates the presence of non-strain producing mechanisms along a_1 and a_2 in the real space. This zero-energy vibration can be visualised as triangle rotations about a pivot node. This is precisely the attribute of Kagome, since triangle rotations along that direction is the manner in which its non-strain producing mechanism manifests in the lattice. A non-strain producing mechanism essentially is one where no energy is required for movement of internal nodes in the lattice bulk, since it does not warrant any macroscopic strains. Naively put, it means that in an infinite pin-jointed lattice, one could perturb nodes without using any energy.

Now, as soon as the Kagome mechanism ensues, the phonon spectrum changes and is as shown in Figure 2.3b. It can be seen here that the previous zero-energy mechanism is lost and is shifted to higher energy (solid red line). This is reminiscent of the fact that the Kagome mechanism turns into a strain producing one after finite nodal movements, meaning that it requires a finite amount of energy to mobilise the mechanism since it causes macroscopic strains. Since the phonon spectra exhibit all possible vibration modes, from zero-energy ones to the highest-energy ones, it is analogous to the augmented matrix method mentioned in Section 1.2. This analogy is discussed more in detail in Section 2.5.

It should be noted that the phonon spectra are built on the original configuration of Kagome and no information about the mechanism evolution is encoded in it. Therefore, like matrix methods, it only predicts the presence of a mechanism but cannot identify whether it is infinitesimal or finite.

Polarisation

Consider the phonon spectrum of the twisted Kagome again Figure 2.3b. Once the zero-energy mode is lifted to higher-energies, it generates a *gap* in the spectrum (indicated by the lift in the red line). The modes at wavevector $q = 0$, indicate the low-energy rigid-body modes which are the two in-plane translations. This gap in the spectrum can only be closed by drastic geometric changes in the lattice. Minor nodal displacements do not close this gap. Therefore this is a "topologically protected" state [35],[36]. That is, the mechanical properties of the lattice are protected by the topology, in that, only drastic changes away from this topology alters its properties.

Kane & Lubensky [33] identify that collapse mechanisms and states of self-stresses can have a topological origin, apart from nodal connectivity mismatch. A topological origin refers to the advent of modes solely due to a pre-defined distortion of the Kagome unit cell. For convenience, assume that regular nodal connectivity is maintained throughout the lattice. A counting scheme can be devised for topological modes that reveal the

presence of collapse mechanisms and states of self-stress. Details of this derivation are however not relevant from the purview of this thesis. Interested readers are invited to refer to [33] and the associated supplementary information.

The *winding number* (n) sits at the heart of this scheme. It is an integer quantisation of the amount and type of topological modes present in the lattice. The winding number is computed based on the unit cell geometry. A positive winding number indicates the presence of collapse mechanisms and a negative winding number indicates the presence of states of self-stress. These modes localise at regions which are termed as *domain walls*. A domain wall is the imaginary boundary separating two lattices with different topological behaviour. The absolute boundaries at the ends of a finite lattice are also domain walls. The localisation of these modes on domain walls is dictated by the polarisation vector P_T . It is as follows,

$$\mathbf{P}_T = \sum_i n_i \mathbf{a}_i \quad (2.4)$$

where \mathbf{a}_i indicates the real space base vectors and n_i are the corresponding winding numbers. A positive winding number indicates that the domain wall pointed to by the corresponding base vector harbours a collapse mechanism. Similarly, a negative winding number indicates that the domain wall pointed to by the corresponding base vector harbours a state of self-stress. If the directions of base vectors are inverted, the corresponding winding numbers also switch signs.

Upon a suitable distortion of the Kagome unit cell, its phonon spectra become gapped which can then be associated with a winding number. If these distortions follow a specific rule-set ([33], [35], [34]), it changes the lattice property altogether. Collapse mechanisms which used to be present throughout the bulk, accumulate at domain walls in the lattice. If nodal connectivity is not disrupted in the Kagome, $b - nj = 0$ (from Equation 1.4). In such cases, the topological modes appear in pairs and for every collapse mechanism, there is a state of self-stress. Two such domain walls are shown in Figure 2.4 separating lattices with different topological behaviour. The left and right end patches are simply the regular twisted Kagome, with no polarisation indicated by $\mathbf{P}_T = 0$ (meaning that modes are diffused throughout the bulk). The central section is a lattice formed out of a particularly distorted Kagome, which has a polarisation in a specific direction, again indicated by its \mathbf{P}_T . Notice the accumulation of mechanisms at the domain wall which lies in the direction of polarisation, and self-stresses at the domain wall which lies against the direction of polarisation.

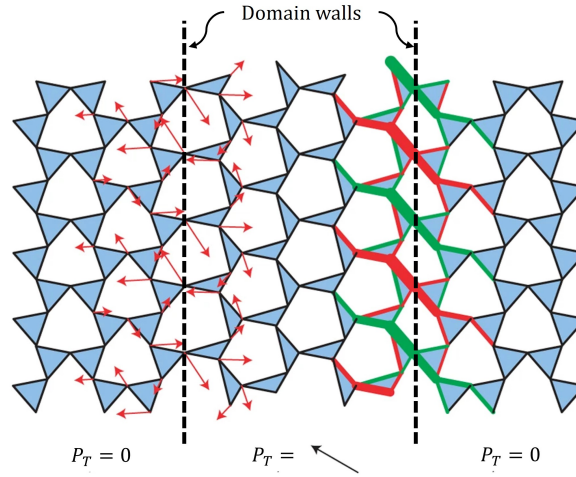


Figure 2.4: Accumulation of collapse modes and states of self-stress on domain walls (indicated by dashed lines) through polarisation. Arrows indicate the collapse mode and thickened bonds indicate states of self-stress (Reproduced from [33]).

Therefore, polarisation helps to control the presence and location of mechanisms and states of self-stress in the lattice. It should be noted that no information about the mechanism can be gathered solely from polarisation. One should consult the phonon spectrum also to identify whether the collapse mechanisms found are strain-producing or non strain-producing. Importantly, this study also reveals that strain-producing mechanisms

belonging to any un-polarised lattice model also can be associated with individual energy requirements. However, unlike the case of the Kagome lattice where its phonon spectrum aids in determining the energy levels, in the case of large and more complicated unit cells, associating the strain-producing mechanisms to their energies is non-trivial.

There are two distinct advantages to topological polarisation. First, it is indistinguishable from the bulk in terms of nodal connectivity which allows freedom to tune the mechanical response locally without altering other physical features like thermal/electrical conductivity. Second, for a gapped spectrum, the winding number is a topological invariant. That is, smooth local perturbations that do not drastically change the topology do not affect the winding number and the polarisation remains intact. In other words, polarisation remains intact under manufacturing defects. Conversely, even the slightest distortion of the Kagome will generate a gap in the phonon spectrum and is enough to induce topological behaviour.

With details of both combinatorial designs strategies and topological polarisation in mind, the envisioned design strategy is discussed next.

2.2. Intended solution strategy

The objective of this work is to develop a design to make the elastic response of Kagome lattice impervious to manufacturing defects. The strategy here focuses on designing appropriate exterior sections to a Kagome core that delivers a blend of robustness and high stiffness to the whole lattice.

It is well established that the presence of strain-producing mechanisms in a pin-jointed lattice model indicates a bending-dominated elastic behaviour of its welded-jointed equivalent. Recall that, compatible lattices carefully formed out of combinatorial designs harbour mechanisms while having a high nodal connectivity. Furthermore, topological mechanics have shown that the nature of these mechanisms can be associated with their energy requirements. In other words, the topology of the lattice dictates the amount of energy associated with each mechanism excitement (if their presence is guaranteed). This exact feature is utilised to address the aforementioned research problem.

The idea here is to design a lattice model combining both combinatorial designs and topological polarisation to embed different "energy-rated" strain-producing mechanisms at selective regions. The intended manner of design is to append the Kagome core with these newly designed architectures. A schematic of this strategy is shown in Figure 2.5. Such a design aids in mitigating the effect of external loads as the work done on the lattice can be neutralised by mobilising the strain-producing mechanisms in the external layers (in its pin-jointed model), keeping the rest of the lattice intact. For a welded-jointed model, this means that the loads will be mitigated by bending-dominated deformations. However, the advent of deformations will be governed by the "energy" associated with that strain-producing mechanism. Designing a Kagome lattice combined with these regions, and tuning the design appropriately could aid in addressing the issue of stiffness decay in Kagome. Rationale behind this strategy and the significance of such a design is elaborated in detail in Chapter 3.

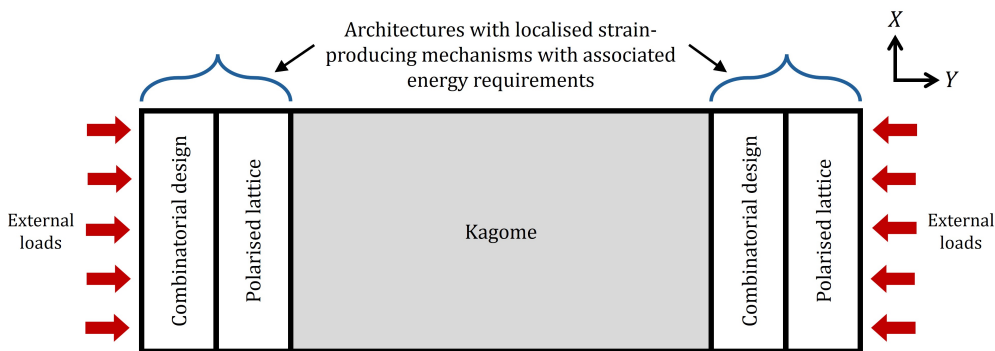


Figure 2.5: Intended design strategy.

Polarisation is utilised to localise the ensuing deformations to selective regions. Further, given that the welded-jointed models of compatible lattices formed out of combinatorial designs show a bending-dominated

elastic response, it is natural to wonder why such a design is used and not conventional lattices that show bending-dominated behaviour. This is due to two reasons. Primarily, most of the conventional lattices whose welded-jointed equivalents demonstrate a bending-dominated response are severely sensitive to manufacturing defects like nodal misalignments, as discussed in Section 1.3. Secondly, due to their low nodal connectivity, the macroscopic stiffness of these models is low. In contrast to this, combinatorial designs are not sensitive to nodal misalignments and feature a higher nodal connectivity causing it to be stiffer in nature. Due to these reasons, they are selected for the design.

However, to pursue this idea, appropriate analytical tools must be developed. The existing matrix methods ([7], [14]) do not aid in identifying energy-levels of an obtained strain-producing mechanism. It should also be noted that augmenting the matrix for discovering strain-producing mechanisms could get extremely cumbersome for lattices with aperiodic internal geometries. Furthermore, the existing method of using symbolic matrices for assessing lattice determinacy is computationally intractable. Due to these reasons, the existing matrix method needs to be reformulated to incorporate the intended solution strategy. Details of this novel procedure are elaborated below.

2.3. Reformulation of matrix methods

Nullspaces of the equilibrium matrix and compatibility matrix provide key information about the determinacy of the lattice structures. A symbolic representation of this matrix is imperative for the complete extraction of nullspaces. However, as the architecture becomes complicated in terms of the internal angles between the members and member lengths itself, evaluation of nullspaces becomes substantially expensive even for small matrices. The simplest solution would be to compute all parameters- member lengths, nodal positions and angles in numeric data-types, resulting in numeric matrices which makes the nullspace computation inexpensive. However in these cases, finite precision greatly affects the nullspace. An easy remedy would be to construct the matrices in a symbolic manner and only convert them to double-precision numbers when evaluating the nullspace. Although this works a majority of the time, loss of information here also affects the nullspaces and leads to discrepancies in some cases. This is because Singular Value Decomposition (SVD) solvers are extremely sensitive to data precision and hence they produce different nullspaces when working with symbolic and numeric representations of the same matrices.

Therefore, a computationally feasible method is required to extract the nullspaces. This is done by using an alternate representation of the equilibrium and compatibility matrices. As mentioned in Section 2.1.2, the phonon spectrum of a lattice model helps in identifying and distinguishing strain-producing mechanisms from non strain-producing mechanisms. Further, it is well established that phonon spectra are generated using dynamical models. Therefore, a dynamical model is developed to describe the kinematic properties of pin-jointed lattices. Since a band-gap analysis is not the focus of this study, the dynamical lattice models are restricted to real-space representations.

2.3.1. Dynamical lattice model

Consider a pin-jointed lattice as a mass-spring system by assuming point masses at the nodes and elastic springs as members. Friction is neglected and the connection between masses and springs is assumed to be conservative in nature. Under the assumption that the original lattice configuration corresponds to a stable dynamic state, the mechanism modes can be modelled as vibrations around that stable equilibrium.

The following is a simple derivation of the dynamical matrix. For a simple 2D mass-spring system with a single mass (m) connected to ground via a spring (with coefficient k), the dynamics dictate,

$$\begin{aligned} \text{Potential energy } (V) &= \frac{1}{2} k(x^2 + y^2) \\ \text{Kinetic energy } (T) &= \frac{1}{2} m(\dot{x}^2 + \dot{y}^2) \end{aligned} \tag{2.5}$$

where x and y denote the orthogonal components of mass displacement, and \dot{x} and \dot{y} denote corresponding velocity components. A straightforward application of Lagrangian principles gives the equations of motions,

$$\begin{bmatrix} m & 0 \\ 0 & m \end{bmatrix} \begin{bmatrix} \ddot{x} \\ \ddot{y} \end{bmatrix} + \begin{bmatrix} k & 0 \\ 0 & k \end{bmatrix} \begin{bmatrix} x \\ y \end{bmatrix} = \begin{bmatrix} 0 \\ 0 \end{bmatrix} \tag{2.6}$$

where \ddot{x} and \ddot{y} denote the acceleration components.

Similar to the traditional matrix methods, the dynamical model for an infinite lattice is also defined for its unit cell. For a finite lattice, it is defined as the whole lattice. Consider the unit cell of an infinite n dimensional lattice model with j nodes. Both the mass and stiffness matrix become of size $nj \times nj$. For an arbitrary arrangement of masses and springs, both matrices would be dense. This information of the lattice geometry and connectivity is encoded in both the equilibrium (\mathbf{A}) and compatibility (\mathbf{B}) matrices (refer to Section 1.2 for details).

Now consider such an arbitrary lattice configuration. The potential energy is a function of the spring elongations (\mathbf{e}) which is itself a function of the nodal displacements (\mathbf{d}). It is expressed as,

$$V = \frac{1}{2} \mathbf{e}^T \mathbf{K} \mathbf{e} \quad (2.7)$$

where \mathbf{K} is essentially a diagonal matrix with all entries K_{bb} as the spring constants corresponding to spring b . Using Equation 1.3, Equation 2.7 can be expanded as,

$$\begin{aligned} V &= \frac{1}{2} \mathbf{d}^T \mathbf{B}^T \mathbf{K} \mathbf{B} \mathbf{d} \\ &= \frac{1}{2} \mathbf{d}^T \mathbf{D} \mathbf{d} \end{aligned} \quad (2.8)$$

where $\mathbf{D} = \mathbf{B}^T \mathbf{K} \mathbf{B}$ is the *Dynamical matrix*. Similarly, the kinetic energy can be expressed as,

$$T = \frac{1}{2} \dot{\mathbf{d}}^T \mathbf{M} \dot{\mathbf{d}} \quad (2.9)$$

where \mathbf{M} is a diagonal matrix with entries M_{jj} as the mass values of nodes j .

Here, both \mathbf{K} and \mathbf{M} are considered to be identity matrices, indicating a unit mass for all nodes and a unit spring constant for all springs. The equations of motion are then obtained through a Lagrangian formulation which is as follows,

$$\frac{d}{dt} \frac{\partial T}{\partial \dot{\mathbf{d}}} - \frac{\partial T}{\partial \mathbf{d}} + \frac{\partial V}{\partial \mathbf{d}} = 0 \quad (2.10)$$

$$\implies \mathbf{M} \ddot{\mathbf{d}} + \mathbf{D} \mathbf{d} = \mathbf{0} \quad (2.11)$$

The free motion solution of this system takes the form $\mathbf{d} = \mathbf{q} e^{\lambda t}$. Here, \mathbf{q} defines the shape of motion and $e^{\lambda t}$ is the time-dependent component with λ being a complex number. Therefore, Equation 2.11 takes the form,

$$\lambda^2 \mathbf{M} \mathbf{q} + \mathbf{D} \mathbf{q} = \mathbf{0} \implies (\lambda^2 \mathbf{M} + \mathbf{D}) \mathbf{q} = \mathbf{0} \quad (2.12)$$

The system is considered to be stable in its original configuration. That is, the manufactured state of the lattice is a stable equilibrium of its mass-spring equivalent. Linearised vibration modes around this equilibrium state indicate the mechanisms present in the lattice. For a stable system, \mathbf{M} and \mathbf{D} are positive definite and hence λ^2 should be real and negative. As a result, λ can be denoted as $i\omega$ with ω being a real number. Therefore Equation 2.12 becomes,

$$(\mathbf{D} - \omega^2 \mathbf{M}) \mathbf{q} = \mathbf{0} \implies (\mathbf{D} - \omega^2 \mathbf{I}) \mathbf{q} = \mathbf{0} \quad (2.13)$$

Disregarding the trivial solution $\mathbf{q} = \mathbf{0}$, Equation 2.13 represents an eigenvalue problem. The eigenvalues indicate the frequencies of vibration around the stable equilibrium state and the corresponding eigenmodes denote the shape of vibration.

A simple reformulation of Equation 2.13 gives a similar alternate to find states of self-stress. Pre-multiplication of this expression with \mathbf{B} results in

$$\mathbf{B} \mathbf{D} \mathbf{q} = \omega^2 \mathbf{B} \mathbf{q} \quad (2.14)$$

Considering time independence of states of self-stress, \mathbf{q} can be replaced with \mathbf{d} . Therefore, Equation 2.14 can be reformulated as,

$$\mathbf{B} \mathbf{B}^T (\mathbf{B} \mathbf{d}) = \omega^2 \mathbf{B} \mathbf{d} \implies \mathbf{B} \mathbf{B}^T \mathbf{e} = \omega^2 \mathbf{e} \quad (2.15)$$

Assuming a linear elastic material relation between spring strains (\mathbf{e}) and tensions (\mathbf{t}), Equation 2.15 can be expressed as,

$$\mathbf{B}\mathbf{B}^T \mathbf{t} = \omega^2 \mathbf{t} \implies (\mathbf{D}^h - \omega^2 \mathbf{I}) \mathbf{t} = \mathbf{0} \quad (2.16)$$

where $\mathbf{D}^h = \mathbf{B}\mathbf{B}^T$.

In summary, numeric eigenvalues of $\mathbf{D} = \mathbf{B}^T \mathbf{B}$ and their corresponding eigenvectors indicate the lattice mechanisms. Similarly, eigenvalues and eigenvectors of $\mathbf{D}^h = \mathbf{B}\mathbf{B}^T$ reveal the states of self-stress.

The primary advantage of this method is that instead of precision-sensitive SVD, an eigensolver could be used. Nullspace of a matrix is nothing but the set of eigenvectors corresponding to zero-eigenvalues. Even so, an eigenvalue estimation of a symbolic large matrix is still computationally extremely expensive. Again, converting the matrix to a finite precision data-type solves the issue but results in a loss of information and therefore inaccuracy in eigenvectors and sometimes even missing eigenvectors. This is because minor discrepancies due to numeric representation directly affects the member lengths and nodal positions in the equilibrium and compatibility matrices and hence the eigenvectors get affected. However, in a dynamical representation of these matrices (\mathbf{D} and \mathbf{D}^h), these discrepancies only affect the scaling of the energy marks, ensuring that the stable equilibrium remains intact. The only difference that the data-type conversion makes is that the potential energy landscape becomes minutely different in the vicinity of the stability point and hence affects the potential energy associated with the linearised modes of vibration around that point. Hence, all vibration modes are extracted albeit with some at almost-zero eigenvalues which is accepted as an artifact of data-type conversion. This makes the computation significantly inexpensive. A nonzero eigenvalue however indicates a high energy mechanism in itself and is not an artifact of data-type conversion. It should be noted that in this case, instead of absolute 0, zero eigenvalues are obtained upto computer precision which is $\approx 10^{-16}$ for double data-types.

2.3.2. Automated matrix evaluation algorithms

For infinite lattices with small unit cells, it is possible to derive the compatibility and equilibrium matrices manually. However, as the structure gets more complicated and larger, including finite lattices, an automated methodology is required. Here, a workflow is developed capable of constructing the compatibility and equilibrium matrices for any given lattice microarchitecture. The lattice microarchitecture information is extracted from an *input file*. Here, the input files are generated from their geometric representations within Abaqus 2023 [37] which outputs complete information regarding nodal connectivity, node positions and corresponding member lengths.

Simple algorithms are developed to generate the required matrices. The advantage of these algorithms is their capability to analyse large lattice models, be it complex unit cell microarchitectures of infinite lattices or large aperiodic finite lattices. Different sets of algorithms are developed for infinite and finite lattices. The primary challenge in infinite lattices is to properly model periodicity of the unit cell. Appropriate unit cell design is critical for periodicity to be maintained and for the correct usage of algorithms. For finite lattices, the process is relatively straightforward since the aspect of periodicity does not exist. The only challenge here is to incorporate proper boundary conditions (if existing). Information regarding boundary conditions is also extracted from the input file generated.

Details of all the algorithms (including the pseudo-codes) and the process of designing appropriate unit cells is elaborated in Appendix A.

2.4. Benchmark tests

The developed algorithms and the dynamical matrix method are tested against benchmark lattice models available in the literature. First, regular lattices from [20] and [38] are tested using both the traditional nullspace method and the novel method. Then more complicated lattices from [31] and [33] are also tested. Both collapse mechanisms as well as states of self-stress are extracted.

For convenience, collapse mechanisms are categorised into two. Global collapse mechanisms are those that manifest throughout the bulk of the lattice. All mechanisms predicted by the unit cell of an infinite lattice is by default a global mechanisms. However, in some cases with large irregular unit cells, mechanisms could

exist in selective regions within it. A prime example of this is the presence of domain walls where mechanisms reside. One could design a large unit cell with a few domain walls. These mechanisms are categorised as *localised*. In this section, both global and localised mechanisms are replicated through the dynamical method in benchmark lattice models. The computational efficacy is brought to light here. DelftBlue [39] computing facilities are used wherever necessary.

2.4.1. Global modes

Existing lattice structures with global collapse mechanisms are analysed using the traditional matrix method and the novel dynamical matrix method. The obtained results from the dynamical matrix method are compared to the ones obtained from traditional matrix methods to check the accuracy of the proposed method and the developed algorithms. For robustness in testing, the chosen set of lattices includes both infinite and finite ones. Figure 2.6[a-e] shows five periodic lattices retrieved from [20] and [38], and their corresponding unit cells. The analysis and verification are done based on the count of states of self-stresses and mechanisms, and the computation time (wall-clock time) required for estimation of the nullspaces through both the traditional symbolic matrices (\mathbf{A}, \mathbf{B}) and through dynamical matrices (\mathbf{D}, \mathbf{D}^h). For some selective cases, mechanisms obtained through both methods are illustrated in Appendix B. Algorithms 1 and 3 are used for analysis here. Computation time is measured only for the calculation of the nullspaces and not for the whole algorithm. The results are compiled in Table 2.1 and Table 2.2.

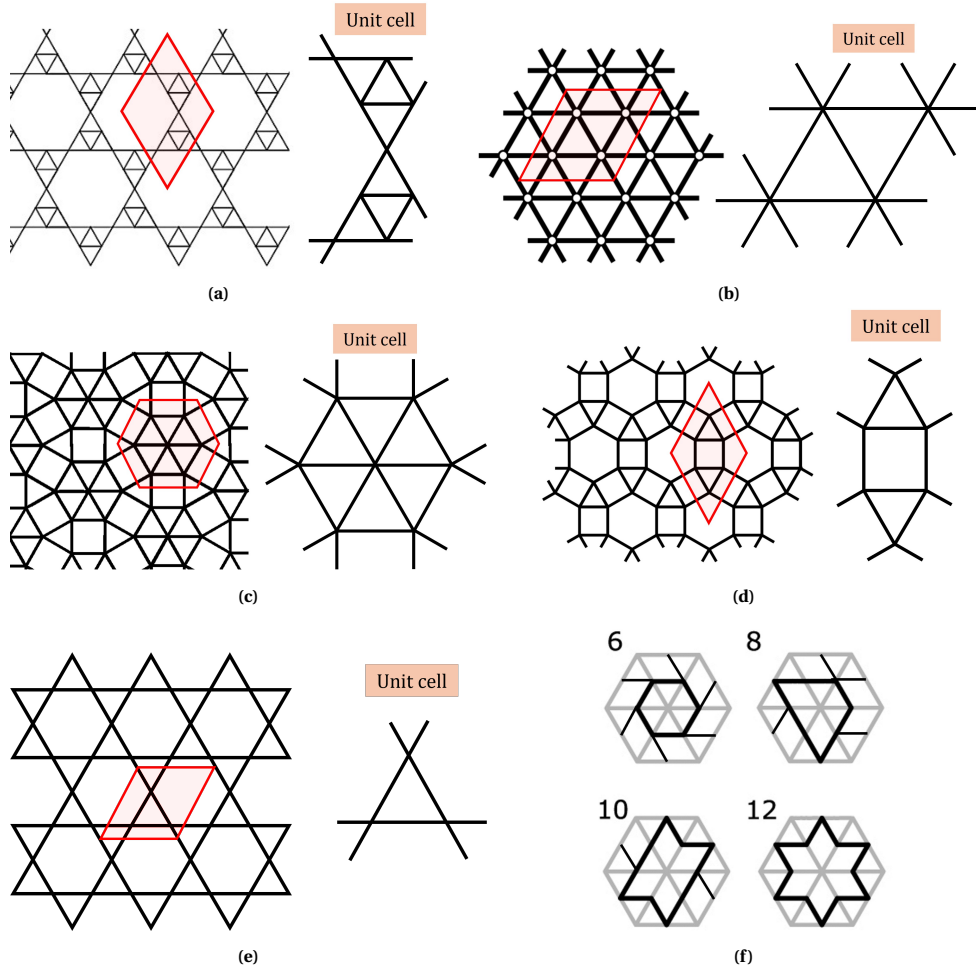


Figure 2.6: Lattice structures for benchmark tests: **a.** Kagome with concentric Triangles, otherwise termed as KT (Reproduced from [20]); **b.** Triangular; **c.** Demi-regular (Reproduced from [38]); **d.** Hexagonal-Cupola; **e.** Kagome; **f.** Set of finite lattices constructed using a combinatorial strategy. Inner loops are indicated by black lines and numeric insets indicate the inner-loop count (Reproduced from [30]).

Lattice	nj and b	Symbolic matrix		Dynamical matrix	
		s and m	Computation time (s)	s and m	Computation time (s)
Kagome	$nj = 6 ; b = 6$	$s = 3 ; m = 3$	0.0039	$s = 3 ; m = 3$	3.23×10^{-4}
KT	$nj = 18 ; b = 18$	$s = 3 ; m = 3$	0.0201	$s = 3 ; m = 3$	3.95×10^{-4}
Triangular	$nj = 8 ; b = 12$	$s = 6 ; m = 2$	0.0074	$s = 6 ; m = 2$	3.51×10^{-4}
Demi regular	$nj = 14 ; b = 18$	$s = 7 ; m = 3$	0.0199	$s = 7 ; m = 3$	3.727×10^{-4}
Hex-Cupola	$nj = 12 ; b = 12$	$s = 3 ; m = 3$	0.0116	$s = 3 ; m = 3$	3.78×10^{-4}

Table 2.1: Verification of the performance of the dynamical matrix method in comparison to the symbolic matrix method - infinite lattices. Calculated metrics are for local computer with AMD 6000 series CPU.

For the set of finite lattices shown in Figure 2.6f, irrespective of the combinatorial arrangement, the joints and member counts are the same with $nj = 38$ and $b = 36$. Meeussen *et al.* [30] prove that each of these superhexagons only has 2 states of self-stress ($s = 2$). Therefore, the matrix analysis (through both symbolic and dynamical methods) should yield $m = 4$, in order to satisfy the Maxwell-Calladine condition (Equation 1.4).

Inner-loop count	Symbolic matrix		Dynamical matrix	
	s and m	Computation time (s)	s and m	Computation time (s)
6	$s = 2 ; m = 4$	0.0926	$s = 2 ; m = 4$	0.0018
8	$s = 2 ; m = 4$	0.0933	$s = 2 ; m = 4$	0.0021
10	$s = 2 ; m = 4$	0.09405	$s = 2 ; m = 4$	0.0019
12	$s = 2 ; m = 4$	0.1107	$s = 2 ; m = 4$	0.0023

Table 2.2: Verification of the performance of the dynamical matrix method in comparison to the symbolic matrix method - finite lattices. Calculated metrics are for local computer with AMD 6000 series CPU.

As observed, for both infinite and finite lattices, both methods provide the same results and all of them satisfy the Maxwell-Calladine condition (Equation 1.4). In conjunction with the mechanisms shown in Appendix B, these results are sufficient proof to validate the authenticity of the dynamical method and the designed algorithms 1 and 3. Furthermore, although the absolute computation time is minimal for both cases, the difference in time between both methods is significant. This is primarily because the dynamical matrix method allows the freedom to operate with numeric type matrices instead of symbolic ones, which considerably reduces the computation effort. This highlights the efficiency of the new method. Therefore, it can be concluded that the proposed method and algorithms are accurate and are fit for use.

To appreciate the complete power of this algorithm, one needs to evaluate more complicated lattices. If the members and angles of the lattices are not of the same dimensions, its representation in the matrix becomes increasingly complicated and the nullspace evaluation becomes a cumbersome endeavour. All the lattices analysed previously have the same member lengths and angles. The only exceptions here are the 90° angles in hexagonal cupola and the demi-regular architectures. These nevertheless result in a 0 or 1 for some entries of the equilibrium/compatibility matrices due to the trigonometric operations (\sin / \cos) during the matrix formation and therefore do not cause any complexity in the nullspace estimation. In these cases, the symbolic representation of matrices \mathbf{A} and \mathbf{B} suffices for the SVD solvers to extract the nullspaces. In order to observe the effect of increasing computation complexity due to geometry, lattice structures with domain walls are analysed. Domain walls guarantee a change in topology in the lattice and therefore these structures offer a sufficient test of this phenomenon.

2.4.2. Localised modes

Localised modes are observed in specifically designed lattice structures as indicated in [33]. Three structures with domain walls (see Figure 2.7) are tested for their determinacy properties and the computation time required for nullspace estimation is also measured. All three structures are made by tessellating a distorted Kagome. Details of this geometrical distortion are elaborated in Appendix C. Again, these calculations have been done using both traditional matrices (\mathbf{A}, \mathbf{B}) in their symbolic forms and dynamical matrices (\mathbf{D}, \mathbf{D}^h). The results are presented in Table 2.3. It should be observed that each structure fundamentally differs from the rest. For structures 1 and 3, the change in topology on either sides of the domain walls is not as severe as in structure 2. Additionally, each of these structures are unit cells in itself of a larger infinite lattice. The unit cells here are modelled with boundary nodes that are responsible for periodicity. The coloured dots indicated on either sides of the structures indicate the repeating direction. Each green dot is periodic with its partner green dot lying on the same vertical axes. The same goes for purple dots with the periodic nodes on corresponding horizontal axes. Algorithm 2 is used for analysis. Again, an illustration of the ensuing mechanisms found from both the symbolic and dynamical methods is shown in Appendix B.

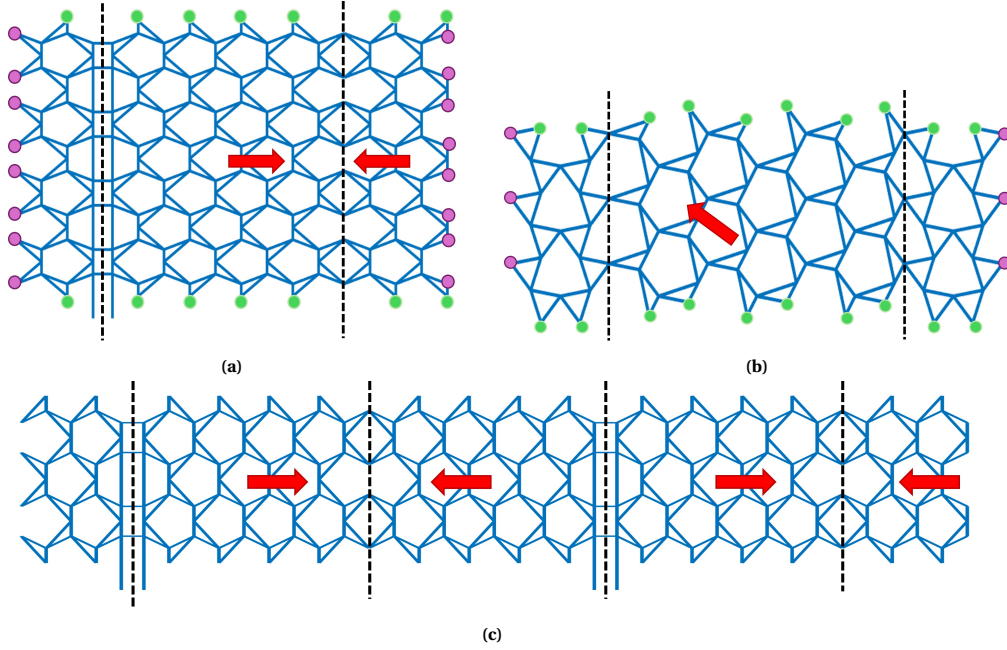


Figure 2.7: Lattice structures with domain walls. Domain walls are indicated by black dashed lines. Polarisation in the lattice is indicated by red arrows: **a.** Structure 1 with two domain walls. Domain wall on the left harbours states of self-stresses and domain walls on the right harbours collapse mechanisms, as is also indicated by the polarisation vectors; **b.** Structure 2, again with 2 domain walls. The left wall harbours collapse mechanisms here; **c.** Structure 3, is an extension of structure 1 with two more domain walls.

Structure #	Symbolic matrix		Dynamical matrix	
	s and m	Computation time (s)	s and m	Computation time (s)
1	$s = 3 ; m = 3$	1.165×10^3	$s = 3 ; m = 3$	0.0114
2	–	–	$s = 2 ; m = 2$	0.1228
3	$s = 7 ; m = 7$	235.5185	$s = 7 ; m = 7$	0.0380

Table 2.3: Verification of the performance of the dynamical matrix method in comparison to the symbolic matrix method - lattices with domain-walls. Calculated metrics are for local computer with AMD 6000 series CPU. In the case of structure 2, nullspace computation from the symbolic matrix fails due to lack of memory and computation resources.

Primarily, the algorithm for evaluating lattice determinacy properties for infinite lattices with boundary nodes

is verified. Second, the efficacy of the dynamical method is evident since it takes significantly fewer resources to compute the same nullspace calculated using the symbolic matrices. It is interesting to note that for structure 2 shown in Figure 2.7b, MATLAB does not compute the nullspace from the symbolic matrix due to lack of memory and computation resources. Since structure 2 is directly inspired from [33], the results obtained from the dynamical matrix method are verified against the reported material. This highlights the advantage of using the dynamical matrix method.

2.5. Information from Eigenvalues

An important feature of the dynamical method of investigation is that strain-producing mechanisms can be identified using the original compatibility matrix itself, and an augmented matrix method ([9]) is not required. Although implementation of an augmented matrix is relatively straightforward, it can become increasingly cumbersome if the unit cell of a lattice is complicated with a large number of entities. The manner in which this method investigates strain-producing mechanisms is by consulting the eigenvalues. Non-zero eigenvalues indicate strain-producing mechanisms. This can be reasoned as follows.

Recall that, the lattice is no more represented by members and nodes, but by springs and masses free to oscillate about its stable equilibrium. Each mode of oscillation can be associated with eigenvalues that indicate mechanisms with their respective linearised potential energies. This can be better understood by observing the modal stiffness corresponding to each of these modes. Note that the algorithms presented here use normalised eigenvectors such that their norm is unity. Therefore the modal mass ($\mathbf{q}_r^T \mathbf{M} \mathbf{q}_r$) corresponding to all obtained modes is unity (since \mathbf{M} is also an identity matrix). In such a scenario, the eigenvalue corresponding to a particular mode equals the modal stiffness ($\mathbf{q}_r^T \mathbf{D} \mathbf{q}_r$). The relation between modal stiffness, modal mass and eigenvalues are as follows,

$$\frac{\mathbf{q}_r^T \mathbf{D} \mathbf{q}_r}{\mathbf{q}_r^T \mathbf{M} \mathbf{q}_r} = \lambda_r \quad (2.17)$$

Therefore, high eigenvalues directly indicate a high modal stiffness. This naturally means that exciting the set of mechanisms residing at higher eigenvalues causes finite spring elongations. Similarly, mechanisms at low frequencies do not cause as high spring elongations. If the eigenvalues are almost zero, spring elongations are also zero. From the pin-jointed model perspective, mechanisms that do not cause spring elongations are synonymous with non strain-producing mechanisms, and the ones that cause spring elongations are strain-producing mechanisms (cause member tensions if mobilised). Since the eigenvalues are directly linked to the linearised potential energies of the respective modes around the stable equilibrium point, a mechanism mode with a high eigenvalue is loosely termed a "high-energy" mode, and the one with a lower eigenvalue a "low-energy" mode. In essence, eigenvalues of the dynamical matrices help in segregating strain-producing mechanisms from the non strain-producing mechanisms. It should be noted that eigenvalues of both \mathbf{D} and \mathbf{D}^h matrices are always exactly the same.

Not only does this method provide a safe estimation of nullspaces, but also is a tool for categorising strain-producing and non strain-producing mechanisms. Due to these advantages, all matrix analysis henceforth in this thesis are carried out through the dynamical matrix method.

Four cases are used to highlight the significance of eigenvalues. First, the Kagome lattice is investigated. The pristine Kagome has three mechanisms, two of which are rigid body modes along orthogonal directions and the last is a mechanism involving rotating triangles [14], [40]. This mechanism, in the linear regime, is non strain-producing. However, as soon as the mechanism evolves and nodes move by finite amounts, it becomes a strain-producing mechanism [10]. Therefore, if the Kagome, in its mobilised state, is subjected to matrix analysis, only two mechanisms corresponding to rigid body modes can be found. However, if an augmented matrix is used ([9]), the third mechanism which is strain-producing, is also found. The dynamical matrix method provides an alternative to this. The first four eigenvalues corresponding to the pristine Kagome is,

$$\lambda_1 \approx 10^{-15}, \quad \lambda_2 \approx 10^{-15}, \quad \lambda_3 \approx 10^{-15}, \quad \text{and} \quad \lambda_4 \approx 10^1 \quad (2.18)$$

This indicates that there are 3 non strain-producing mechanisms and the fourth one is a strain-producing mechanism. The corresponding eigenvectors indicate the mechanisms. Now, when the Kagome mechanism is activated, the obtained eigenvalues are,

$$\lambda_1 \approx 10^{-15}, \quad \lambda_2 \approx 10^{-15}, \quad \lambda_3 \approx 10^1, \quad \text{and} \quad \lambda_4 \approx 10^1$$

As observed, the third eigenvalue which corresponds to the mechanism has increased to a nonzero eigenvalue indicating that it is a strain-producing mechanism. The other three eigenvalues remain unchanged. Therefore, without using an augmented matrix, one could directly predict the nature of the mechanism through the eigenvalues in the dynamical matrix. This feature is revealed completely when a lattice with simultaneously existing non strain-producing and strain-producing collapse mechanisms is analysed.

Consider the Hexagonal cupola, as shown in Figure 2.6d. A simple matrix analysis using symbolic matrices yields 3 nullspace vectors of the compatibility matrix. This includes two translation modes and a mechanism mode. However, when the analysis is carried out via an augmented matrix method, 2 more mechanisms appear, apart from the already existing 3 [40]. These two mechanisms are strain-producing mechanisms which are qualitatively different from the non strain-producing mechanism found through the non-augmented matrix. Therefore, after augmenting the compatibility matrix, both strain-producing and non strain-producing mechanisms are found.

The same procedure when carried out using the dynamical matrix, gives 3 eigenvalues of the order of 10^{-16} , indicating non strain-producing mechanisms representing 2 translation modes and 1 mechanism mode. The higher eigenvalues obtained are as mentioned in Equation 2.19. The matrices here are 12×12 and hence 12 eigenvalues are obtained.

$$\lambda_p = 4; \quad \lambda_q = 12; \quad \lambda_{12} = 16 \quad \text{where } p \in \{4, 5\} \quad \text{and} \quad q \in \{6, 7, 8, 9, 10, 11\} \quad (2.19)$$

These eigenvalues correspond to degenerate modes where any linear combination of the eigenvectors is also a valid solution. For example, the 4th and 5th modes share the same eigenvalue. Individually, they do not correspond to any of the strain-producing mechanisms found in symbolic matrices, however, a linear combination of them yields one of the mechanisms. Similarly, an appropriate linear combination of the other higher modes (from 6th to 11th), yields the other strain-producing mechanism. This is also an example of the fact that the dynamical matrix method is capable of discovering strain-producing mechanisms without the need for augmented matrices.

This advantage becomes particularly useful when modelling large unit cells of infinite lattices. For example consider a compatible network as shown in Figure 2.8a, which is periodic only along the horizontal direction but not along the vertical direction. Matrix analysis of this lattice shows 3 eigenvalues of the order of 10^{-16} and higher energy modes of the order of 10^{-1} . The 3 non strain-producing mechanisms found correspond to two translations and a collapse mechanism which is shown in Figure 2.8b. It is expected that this collapse mechanism becomes strain-producing under finite nodal movements (which is in fact the case for all non strain-producing mechanisms). To test this fact, the same network is modelled with an initial configuration that resembles its mechanism. Nodes are moved by a distance which is $\frac{1}{50}^{th}$ the member lengths. Matrix analysis of this configuration (still being periodic), reveals 2 eigenvalues of the order of 10^{-15} , and the third eigenvalue, which still represents the mechanism, is now of the order of 10^{-1} . This particular practice also brings out the convenience in the analysis offered by the dynamical matrix method.

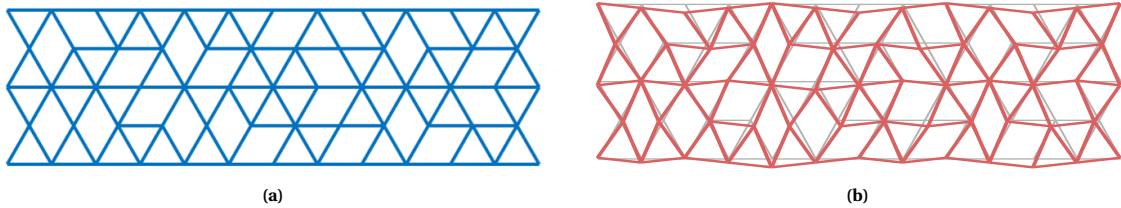


Figure 2.8: Mechanisms of a compatible network: **a.** Compatible network; **b.** Non strain-producing infinitesimal mechanism that becomes strain-producing in the finite regime. The original lattice is shown in grey which is overlapped by the lattice mechanism in red.

Next, consider the lattice shown in Figure 2.7b. This is a doubly periodic unit cell of an infinite lattice. When analysed through a dynamical matrix method, the first four eigenvalues of \mathbf{D} are,

$$\lambda_1 \approx 10^{-15}, \quad \lambda_2 \approx 10^{-15}, \quad \lambda_3 \approx 10^{-3}, \quad \text{and} \quad \lambda_4 \approx 10^{-3}$$

The third eigenvalue indicates the presence of a strain-producing mechanism. When the eigenvectors are investigated, one can observe the accumulation of the mechanism around the respective domain wall. Similarly,

if eigenvectors of \mathbf{D}^h are investigated, an accumulation of states of self-stress around the other domain wall can be observed. Figure 2.9 shows the mechanism corresponding to λ_3 of \mathbf{D} and the state of self-stress corresponding to λ_3 of \mathbf{D}^h . Proof that the mentioned mechanism here is a strain-producing one is discussed in the Section 2.6.

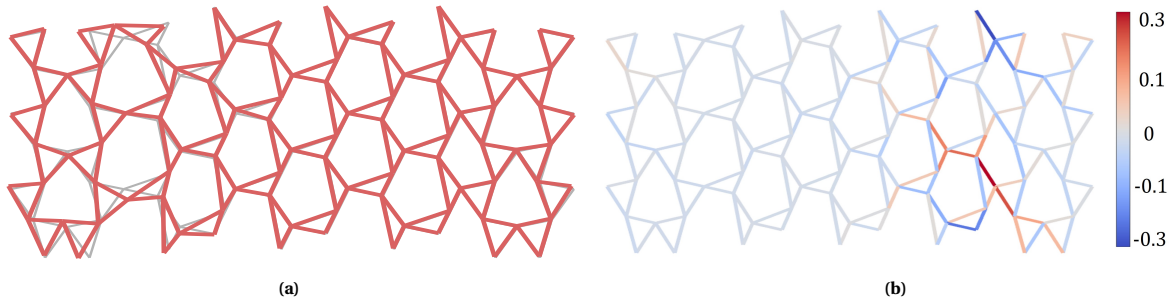


Figure 2.9: Collapse mechanism and state of self-stress of the lattice shown in Figure 2.7b: **a.** Collapse mechanism corresponding to λ_3 of \mathbf{D} . The original lattice is shown in grey which is overlapped by the lattice mechanism in red. Notice the accumulation of the mode at the corresponding domain wall; **b.** State of self-stress corresponding to λ_3 of \mathbf{D}^h . Absolute values of stresses are irrelevant (entries in an eigenvector). Again, notice the accumulation of the self-stresses around the corresponding domain wall.

2.5.1. Implication of eigenvalues for welded-jointed models

Eigenvalues obtained for strain-producing mechanisms of the pin-jointed models provide key information about the lattice behaviour of its welded-jointed equivalents. As mentioned above, high eigenvalues indicate high member tensions corresponding to the mechanism. In other words, movement of nodes corresponding to that mechanism causes high member tensions in the lattice. Conversely, only an external load capable of generating those tensions in the members would warrant excitement of that mechanism. For the welded-jointed model, this indicates that mechanisms with high eigenvalues manifest as bending-deformations only after a suitable load-level.

Although no parallel can be drawn between the exact load-level and eigenvalue of a mechanism, a spectrum of eigenvalues (and corresponding eigenvectors) indicate the compliant and stiff regions of the lattice. Consider the example of polarised lattices harbouring mechanisms with a spectrum of eigenvalues on multiple domain walls. The location of a mechanism with a low eigenvalue represents a compliant characteristic region of its welded-jointed equivalent. Similarly, location of a higher eigenvalue mechanism represents a stiffer region. For a pin-jointed lattice with a range of nonzero eigenvalues, under an increasing external load, deformations in the welded-jointed equivalent primarily ensue at locations corresponding to the mechanism with lowest eigenvalues. It is perfectly possible that the same region of a lattice harbours multiple eigenvalue mechanisms, in which case, deformations ensue corresponding to the lowest one. Furthermore, it should be noted that the geometry of mechanism of a pin-jointed model cannot be related to the manner of deformations of its welded-jointed equivalent, since this depends on the load-case as well.

So far, it has been demonstrated that the dynamical matrix methods help in identifying and categorising strain-producing mechanisms from non strain-producing mechanisms. Moreover, eigenvalues aid in correlating the obtained mechanisms with associated linearized potential energies. However, matrix methods cannot distinguish between finite and infinitesimal mechanisms. In rare cases, if an accurate motion function can be generated for an evolving mechanism of a lattice, information regarding whether it is finite or infinitesimal can be extracted. Since, this is not possible for all cases, an alternate method is required to collect information about the nature of mechanisms. Numerical models prove to be useful in this regard. The following section revolves around understanding the nature of these mechanisms from a numerical perspective.

2.6. Numerical identification of mechanism types

Although mechanisms are identified through the dynamical method, it is important to note that these are linearised around the assumed stable configuration. Therefore, this method also cannot detect if the mechanisms are finite or infinitesimal. To distinguish between finite and infinitesimal mechanisms, Finite Element (FE) analysis is used. The numerical protocol used here relies on strain energy estimates and pin-jointed

models are analysed. The pin-jointed model is modified to a "pin-jointed elastic" model where the members are elastic, but connected to each other via pin-joints. Therefore only displacement degrees of freedom are passed at the joints and moments are not. The modification of the pin-jointed model to pin-jointed elastic is done so that the strain energy can be monitored during excitation of the mechanism. Moreover, periodicity is a requirement when modelling an infinite lattice and is ensured by prescribing appropriate relations between the degrees of freedom of periodic nodes.

For a lattice with a finite mechanism, mobilising the mechanism in its pin-jointed equivalent should not cause any strains in the members. Consequently, the strain energy computed for this lattice should be extremely low. However, if the lattice harbours an infinitesimal mechanism, its pin-jointed equivalent exhibits a higher strain energy due to strained members. This difference is more prominent in pin-jointed models than the welded-jointed models, as in the latter, the finite mechanism also exhibits a finite strain energy due to the torsional rigidity of nodes which also leads to bending of the members. For strain-producing mechanisms, a macroscopic load on the lattice triggers the mechanism. The amount of strains observed in the members contributing to the mechanism dictates whether it is a finite mechanism or an infinitesimal mechanism.

The purpose of this section is two fold. First, to highlight the developed numerical protocols used for identifying the mechanism features. Second, since characteristics of the mechanism in Kagome are well established in the literature, to explore features of mechanisms observed in lattices built with combinatorial strategies (Section 2.1.1) and those with domain walls (Section 2.1.2). For convenience, lattices made with combinatorial strategies are hereafter called *Meta-Triangular* (MT) lattices, due to the supertriangle unit cell which in essence is a modified triangular lattice unit cell. In addition, lattices with domain walls are called *polarised* lattices.

The numerical protocols developed here are for both finite and infinite lattices. MT lattices are used as the finite lattice models for this study, and polarised lattices as the infinite ones. For infinite lattice, periodicity is critical and hence is ensured by prescribing *paired* natural boundary conditions at the respective nodes. For example, consider the Kagome lattice and a chosen unit cell shown in Figure 2.10 with a unit cell length H along X axis. This unit cell is chosen to represent periodicity in two orthogonal directions X and Y (points on the respective axes are denoted by x and y). Periodicity demands that nodes at $x = -a$ have a suitable motion corresponding to their pairs at $x = a$. Similar for nodes at $y = -b$ and $y = b$. This is dependent on the loads (a macroscopic stress/strain field) applied to the lattice. Consider a uniaxial compressive scenario: $\sigma_{xx} \neq 0$ with $\sigma_{yy} = 0, \sigma_{xy} = 0$. For every node i and its counterpart i' ,

$$u_1^{(i)}|_{x=-a} = -u_1^{(i')}|_{x=a} \quad u_2^{(i)}|_{x=-a} = u_2^{(i')}|_{x=a} \quad \phi^{(i)}|_{x=-a} = \phi^{(i')}|_{x=a} \quad (2.20)$$

$$u_1^{(i)}|_{y=-b} = u_1^{(i')}|_{y=b} \quad u_2^{(i)}|_{y=-b} = -u_2^{(i')}|_{y=b} \quad \phi^{(i)}|_{y=-b} = \phi^{(i')}|_{y=b} \quad (2.21)$$

$$|u_1^{(i)}|_{x=-a}| = \frac{1}{2}\epsilon_{xx}H \quad (2.22)$$

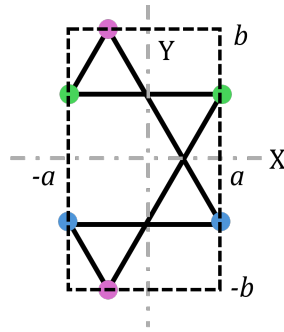


Figure 2.10: Kagome unit cell.

2.6.1. Infinite Lattices

The lattices shown in Figure 2.11 are the representative unit volumes of an infinite lattice. Matrix methods show the presence of the domain walls harbouring mechanisms and states of self-stress. However, their nature is unknown. This is identified through FE analyses where the unit cell, modelled as a pin-jointed structure, is

subjected to a macroscopic compressive uniaxial load. If the mechanism is excited, it is a strain-producing mechanism. Furthermore, if finite nodal movements are allowed without excessive strains in the members, it is a finite mechanism. If the strains considerably increase with initial nodal movements, the mechanism is infinitesimal. It should be noted that the lattice modelled in Figure 2.11a is a smaller version of the lattice illustrated in Figure 2.7a. This modification does not change the behaviour of the lattice since the domain walls are maintained at the same distance and periodicity is intact.

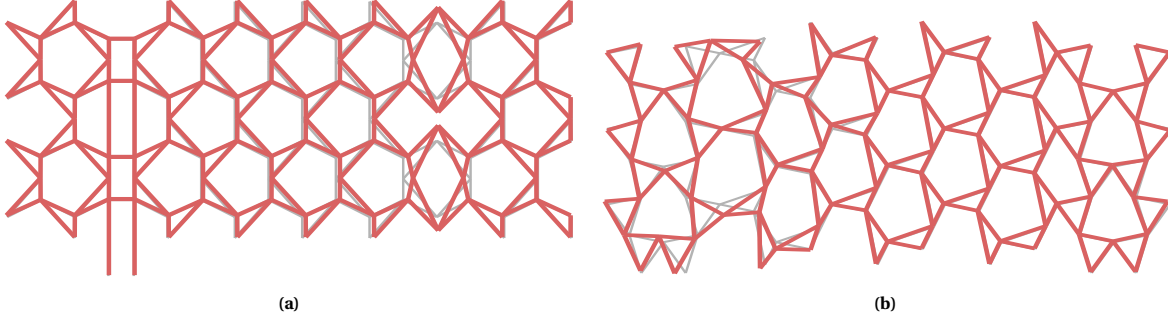


Figure 2.11: Strain-producing mechanisms observed in two polarised lattices. The original lattice is shown in grey which is overlapped by the lattice mechanism in red. Notice the accumulation of mechanisms at the respective domain walls.

Figure 2.11a shows one of the strain-producing collapse mechanisms observed from matrix analysis. This observed mode is the eighth eigenvalue and is of the order of 10^{-1} , while the non strain-producing modes reside at orders of 10^{-15} . Next, consider the lattice shown in Figure 2.7b. Figure 2.11b shows a strain-producing mechanism of this particular lattice, as observed from matrix analysis. The strain-producing mechanism observed here has an eigenvalue of the order of 10^{-3} , with the non strain-producing mechanisms for this lattice at 10^{-15} .

FE results provide greater insight into the nature of these mechanisms. The generated FE models are periodic in nature to model an infinite lattice. Uniaxial compressive loads are applied along the X axes (horizontal direction) via displacement boundary conditions. Figure 2.12 represents the results of the FE analysis. It can be noted that, in both cases of Figure 2.12, the mechanism present at the domain wall is excited and hence is a strain-producing one. Maximum nodal displacements (at the domain walls) in both cases is observed to be $\frac{1}{5}^{th}$ that of member lengths. Furthermore, members strains at the domain walls are not observed to dramatically increase as the external loads are increased. It can also be observed that the mechanism predicted through matrix methods (see Figure 2.11) is in accordance with the results from FE analysis. Therefore it can be concluded that, although strains at the domain walls are not negligible, both mechanisms still are finite. This is due to the fact that in periodic lattices with strain-producing finite mechanisms, the strains tend to be finite and never negligible.

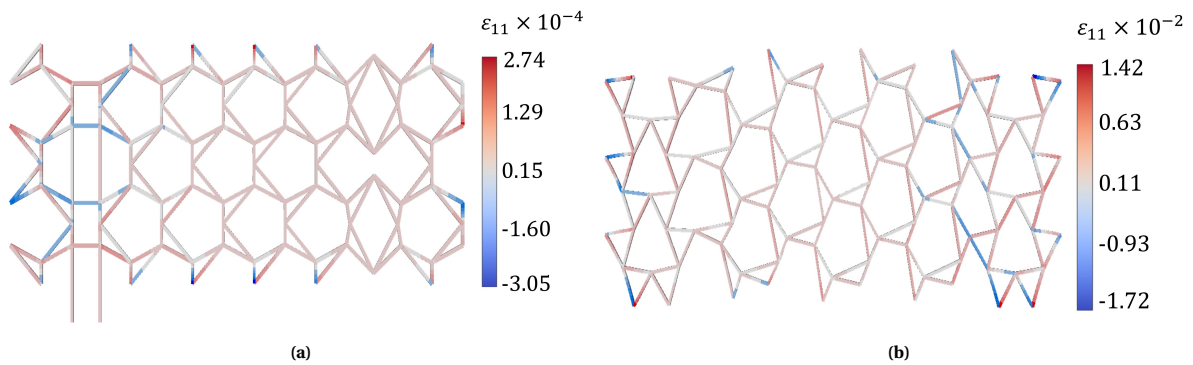


Figure 2.12: FE results indicating the axial strains observed in members of two pin-jointed polarised lattices. Notice higher strains near the domain wall with states of self-stress and lower strains at the other domain wall.

This highlights the utility of supplementing matrix analysis with FE calculations, as it provides a complete

picture of the lattice properties.

2.6.2. Finite lattices

Figure 2.13a shows a finite MT lattice generated by a combinatorial design process. The unit cell of this lattice is the same as in [30], which is a supertriangle. As can be observed, all inner loops of the lattice are even-numbered and hence it is a compatible structure. However, its response is dependent on the loads applied as well. Information regarding the application of loads can be gathered from two sources: matrix analysis and combinatorial rules. Through matrix analysis, one could observe the ensuing collapse mechanisms and decide the placement of loads such that it excites the mechanism. The second solution starts with assigning loads to external nodes in a completely random fashion and observing the combinatorics to see if all supertriangles in the network can harmoniously harbour either of its two collapse modes or give rise to a conflict. If there is a conflict, the lattice exhibits a load-bearing behaviour and is referred to as "frustrated" (see Section 2.1.1).

The collapse mechanism observed through matrix analysis is shown in Figure 2.13b. Figure 2.13c shows a loading scenario where the loads cannot be supported by the lattice architecture and hence warrants a global collapse mechanism. The presence of the collapse mechanism is conditional to compatibility being satisfied everywhere in the lattice. In this case, individual modes of each unit cell harmoniously exist with all its neighbours simultaneously. Compatibility satisfaction of a network of such supertriangles is governed by the rules highlighted in Figure 2.2c. Therefore, for a given load, the lattice response can be predicted by simply following the combinatorics. In the case where there is a conflict arising in any one of the internal supertriangles with respect to its collapse mode, compatibility is lost and the structure becomes frustrated. That is, disruption in the combinatorics leads to a load-bearing response instead of a mechanism-response. Such a situation is highlighted in Figure 2.13d where, upon application of loads, a conflict arises in one of the unit cells (indicated by the question mark) since it cannot satisfy compatibility conditions with all its neighbours simultaneously.

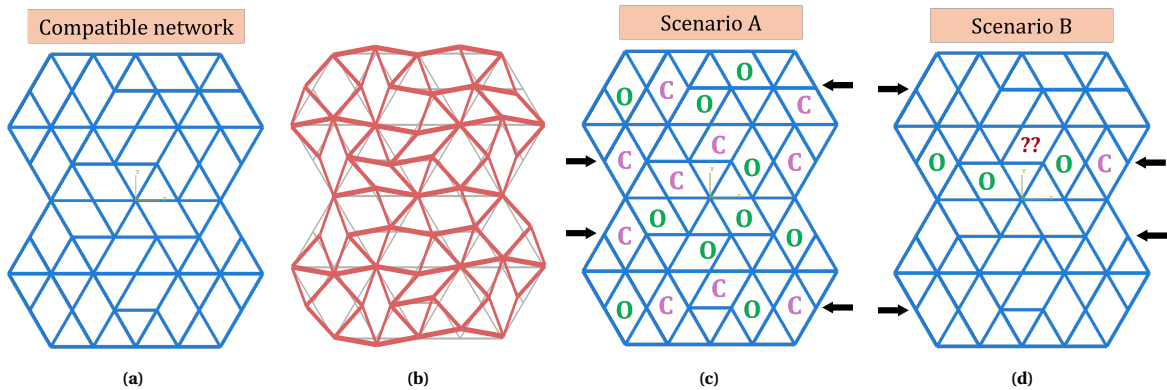


Figure 2.13: Compatible MT lattice. ○ stands for an *open mode* and ● stands for an *closed mode* (see Figure 2.2b). The black arrows indicate applied loads: **a.** Lattice architecture, designed such that all inner loops are even in number, thereby making the structure compatible; **b.** Collapse mechanism predicted by matrix analysis. The original lattice is shown in grey which is overlapped by the lattice mechanism in red; **c.** Loading scenario A where the loads warrant a collapse mechanism. No internal frustration in the lattice; **d.** Loading scenario B where the loads can be supported by the lattice and therefore indicates a *fitted load* case.

An FE model is developed to test this behaviour. Pin-jointed model of this lattice is generated and subjected to both loading scenarios individually. Loads are applied via displacement boundary conditions. Figure 2.14 represents the strain response of each scenario. For scenario A, maximum internal nodal movements are observed to be $\frac{1}{5}^{th}$ that of member lengths and for scenario B, it is $\frac{1}{100}^{th}$. This already hints at the fact that scenario A harbours a finite mechanism while scenario B shows a load-bearing scenario. As predicted, the first case warrants a collapse mechanism response, indicated by minimal strains. The second one results in a load-bearing response, indicated by the high strains in the members. Strain energy measures also provide the same results. The strain energy for scenario A is $\approx 10^{-17}$ while for scenario B it is of the order of $\approx 10^4$. A high strain energy indicates a load-bearing state and the low strain energy indicates a mechanism. This validates the analytical methods presented above and more importantly, shows the finite nature of the mechanism present in scenario A which cannot be predicted otherwise using matrix methods.

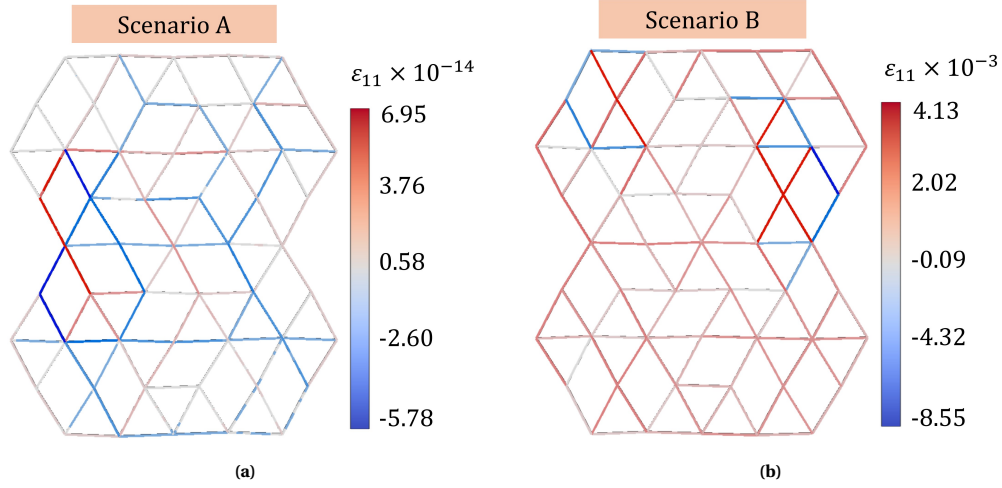


Figure 2.14: FE results indicating the axial strains observed in members of two pin-jointed compatible MT lattices: **a.** Scenario A: where the applied loads are in accordance with the global collapse mechanism of the lattice; **b.** Scenario B: where the applied loads do not support the presence of the collapse mechanism.

In summary, this section highlights the utility of using appropriate numerical models to understand the mechanism features. More importantly, this points to the fact that both- domain wall mechanisms of polarised lattices and global mechanisms of MT lattices can be finite in nature. Further, it verifies the claim from dynamical matrix analysis that the domain wall mechanisms are strain-producing in nature, which is key to the design-solution proposed as part of this thesis.

As evidenced in the current and previous sections, the advantages of the dynamical matrix method makes it a beneficial tool for matrix analysis. Nevertheless, there are a few limitations that need to be kept in mind while using this technique. A brief discussion on these limitations is presented next.

2.7. Limitations of the dynamical matrix method

One of the main advantages of the dynamical matrix is that it allows the usage of numeric data-types which reduces computational expense. However, the usage of double precision data-types causes the eigenvectors to be "diffused". That is, eigenvectors have finite values distributed across all its entries which for symbolic cases would be sharp entries along with absolute zeros. Due to this "diffusion" of eigenvectors, calculation of mechanisms and states of self-stresses show finite nodal movements and member tensions for certain regions which otherwise would have been zero if estimated using the symbolic matrices. Therefore, it can be misleading to use this technique while studying effects like mechanism propagation between domain walls.

Estimation of the eigenvalues of any matrix is only limited by its number columns. Therefore, for large lattices, thousands of eigenvalues could be extracted corresponding to both non strain-producing and strain-producing mechanisms. However, the actual number of each of these mechanisms is generally a small number as found through the traditional matrix methods. When the results of the dynamical method are carefully observed, it is understood that the many of the eigenvectors with finite eigenvalues correspond to completely distorted unit cells. In the case of Kagome, these distortions (corresponding to λ_5 and λ_6 of Equation 2.18) result in scalene and asymmetrical triangles. Distorted unit cell modes cannot be classified under strain-producing mechanisms as it is physically impossible to generate those distortions through macroscopic loads. Therefore it becomes important to make a distinction between these modes.

In some cases the distinction can be made fairly easily. Consider the hexagonal cupola for example. Due to the possibility of visual comparison with results from traditional matrix methods, the correct strain-producing mechanisms can be identified. The eigenvalues corresponding to the strain-producing mechanisms happen to appear right after the eigenvalues of non-strain producing mechanisms. All higher eigenvalues correspond to distorted unit cells. This is in fact a common trend where the eigenvalues corresponding to distortion modes are higher compared to those of the strain-producing modes, and do not appear in a mixed manner. However, a distinction cannot always be made as to which eigenvalues correspond to the last of the strain-producing

mechanisms. Therefore, although the dynamical matrix method allows for discovery of strain-producing mechanisms, it cannot provide a direct means to distinguish between this set, and eigenmodes that correspond to distortions of the unit cell. To circumvent this issue, the mechanism modes are studied closely to assess change in member lengths. For mechanism modes that cause distortion in unit cells, the change in member lengths is observed to be clearly higher than the other modes. Although rudimentary, this check is used in all analyses further for distinguishing mechanism modes and modes that cause lattice distortions.

2.8. Concluding remarks

A dynamical lattice model is introduced that drastically reduces the computational expense involved in calculating the nullspaces of large matrices. It also provides an alternative strategy for discovering strain-producing mechanisms without the use of augmented matrices (as proposed by [9]). Further explanation is provided regarding the implications of the eigenvalues of strain-producing mechanisms in a pin-jointed lattice for its welded-jointed counterpart. Accuracy of the dynamical matrix method is verified by testing it against the traditional matrix method on lattice structures whose determinacy properties are already established. Algorithms are developed for automating matrix analysis of infinite and finite lattices, which makes the matrix analysis convenient for large lattice models. FE models are established that identify the mechanism types for polarised and MT lattices. It is demonstrated that domain walls of polarised lattices can harbour finite strain-producing mechanisms and compatible MT lattices also have finite mechanisms. In summary, all computational tools required to investigate lattice structures for their determinacy properties are developed. These tools are used extensively in designing a lattice structure suitable for retaining the Kagome stiffness with inevitable manufacturing defects.

3

Development of novel designs

This chapter discusses the design solutions in accordance with the objective of this thesis. The traditional matrix method is a useful tool for assessing the mechanical properties of a lattice. However, with the development of a dynamical matrix model, a completely new perspective on the kinematics of lattice materials is obtained. Through eigenvalues of the dynamical matrix, one could discover strain-producing mechanisms and associate them with different levels of perturbation (loads/strains) that trigger them. Eigenvalues of the dynamical matrix form the basis of the design process here. Details of the development of designs are elaborated in this chapter. The resultant structural properties predicted via these eigenvalues are then supported by detailed FE calculations, presented in Chapter 4.

3.1. Developed designs

The solution proposed here relies on using the dynamical matrix method to design lattice structures with regions manifesting strain-producing mechanisms with specific eigenvalues. Recall the design strategy proposed in Section 2.2, where a Kagome bulk is combined with designs formed out of combinatorial processes and polarised lattices. The presence of such regions aids in concentrating the effect of external loads through mechanism excitement (deformations in a welded-jointed model). Eigenvalues and the observed mechanisms are key factors that help in deciding if the design is favourable or not.

An iterative process is adopted for the development of suitable designs. The rationale behind the development of designs and details of the iterative process are elaborated in the following section. The dynamical matrix method forms the basis of the iterations carried out here. Details of the initial unsuitable designs are omitted from this report for brevity since the iterative process is fairly straightforward. A process-flow of the iterative procedure is illustrated in Figure 3.1a. The resultant set of designs is shown in Figure 3.1 [b-d]. The MT lattice regions are developed in a straightforward manner following combinatorial rules of the supertriangle. The polarised region uses topologically polarised Kagome as the unit cell. Details of the geometrical transformation of the regular Kagome to the polarised Kagome are outlined in Appendix C.

It is important to note the manner in which the designs are set-up. A large Kagome bulk is considered. The overall dimensions of the lattice are kept constant and exterior regions of the Kagome are replaced with the designed structures. The smallest designed layer accounts for approximately 8% of the overall lattice length (in Y direction), and the largest accounts for 20%. The Kagome core is attached to polarised Kagome regions, and the lattice exteriors are designed to have compatible MT lattice regions. By design, these lattices are periodic only in the X direction. For convenience, they are named Composite Lattices 1, 2 and 3 (CL1, CL2 and CL3).

The implication of the outer layer architecture of each of these designs is detailed here. Since the Kagome core is appended by two similar layers at both its ends, only one of them is referred to here for ease of discussion. For the CL1 structure, the added layers have two domain walls separated by a small distance. One harbours collapse mechanisms and the other has a state of self-stress. CL2 has a larger outer layer compared to CL1 and houses 5 domain walls. Three of these are for collapse mechanisms and two for states of self-stress. The outer layer of the CL3 structure is the largest of the three. In CL3, while the number and nature of the domain walls are the same as in CL2, the eigenvalues corresponding to the collapse mechanisms and states of self-stress

are expected to be lower compared to CL1 and CL2 as the distance between domain walls is higher. This is because the larger distance between domain walls facilitates the presence of a low-energy mechanism, while smaller distances warrant higher-energy mechanisms.

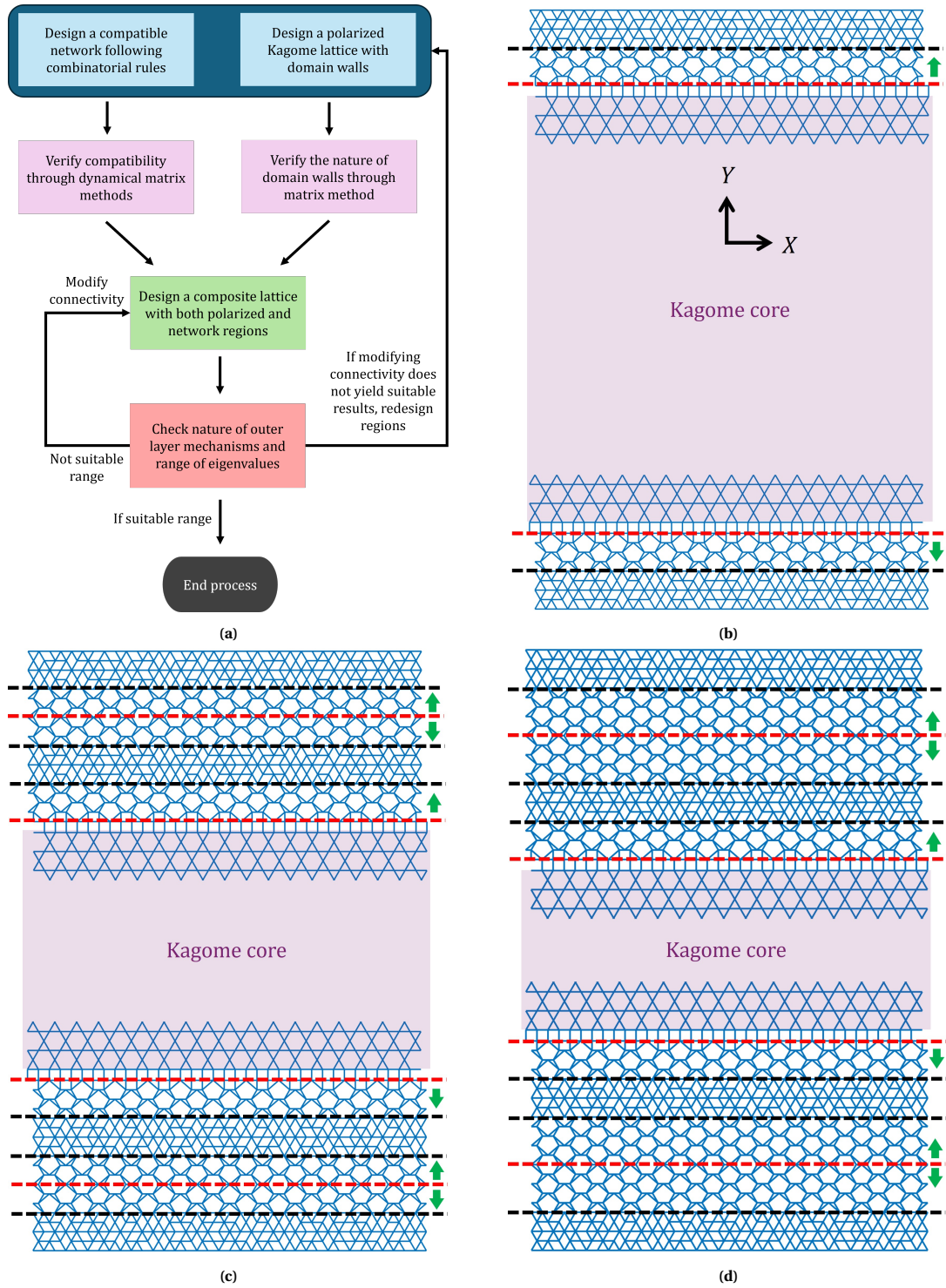


Figure 3.1: Lattice design according to the developed rationale. Domain walls are indicated by dashed lines. Black dashed lines indicate domain walls expected to harbour collapse mechanisms, and red ones indicate those for the state of self-stresses. Green arrows indicate the direction of polarisation.: **a.** Process flow of the iterative design procedure based on analytical predictions; **b.** Composite Lattice-1 (CL1), with 2 domain walls on each end; **c.** Composite Lattice-2 (CL2), with 5 domain walls on each end; **d.** Composite Lattice-2 (CL3), again with 5 domain walls but with larger distances between a few domain walls.

3.1.1. Rationale behind the design process

The idea central to the designs developed is that the external layers should harbour mechanisms with a suitable range of eigenvalues. This idea forms the rationale behind the developed designs and is explained in this section. Here, it is useful to recall the discussions presented in Section 2.2 and Section 2.5.1. It is established that strain-producing mechanisms can be associated with their energy requirements and that this information is extracted through the dynamical representation of the lattice models. Furthermore, the presence of strain-producing mechanisms in the pin-jointed models indicates that under an external load, the welded-jointed equivalent deforms in a bending-dominated manner. It should be noted that the geometry of the mechanism of a pin-jointed lattice, cannot always predict the manner of deformation of its welded-jointed equivalent. Deformation of the welded-jointed model also depends on the load case.

Consider the CL designs presented in the previous section. When a welded-jointed model of a pristine (no defects) CL design is subjected to external loads, deformations ensue in the external layers (since the external layers are guaranteed to have strain-producing mechanisms). Each of the strain-producing mechanisms can be associated with their eigenvalues. It should be noted that just by virtue of the addition of such external layers to Kagome, its macroscopic stiffness already becomes lower relative to the macroscopic stiffness of a fully Kagome lattice of the same dimensions. This is because, a fully-Kagome lattice deforms in a stretching-dominated manner, but the presence of such external layers causes bending-dominated deformations. While being a disadvantage for macroscopic stiffness, it is the presence of these external layers that aid in robustness against defects. This phenomenon is explained now.

Consider a welded-jointed CL design with nodal defects (imperfect CL design), subjected to an external load along Y direction (see Figure 3.1b for axis direction). Under an external load, deformations ensue throughout the lattice, and not just in the external layers, since the Kagome core also harbours strain-producing mechanisms. Again, each of the strain-producing mechanisms can be associated with their eigenvalues. Recall that, low eigenvalues indicate compliance of the welded-jointed models, and high eigenvalues indicate stiffer responses (see Section 2.5.1). For simplicity, consider 3 distinct cases of eigenvalue balance as follows,

- Case 1: Eigenvalue of external layer mechanisms are higher than Kagome strain-producing mechanisms. In such cases, deformations in the welded-jointed equivalent will be localised to the Kagome cores, causing a knock-down in macroscopic stiffness.
- Case 2: Eigenvalue of external layer mechanisms are significantly lower than Kagome strain-producing mechanisms. In this case, the macroscopic stiffness of the lattice will be considerably low due to the overly compliant external layer.
- Case 3: Eigenvalue of the external layer mechanisms are minutely lower than Kagome strain-producing mechanisms. In this case, deformations will be largely localised to the external layers, without comprising greatly on the macroscopic stiffness of the lattice. This is because, neither the external layers are overly compliant, nor are deformations localised to the imperfect Kagome core. In other words, this case falls in between a spectrum where case 1 and 2 are the extremes.

Therefore, case 3 is the ideal scenario and the designs should be made to achieve this balance between the eigenvalues of the external layer mechanisms and Kagome mechanisms. If such a balance is maintained between the eigenvalues of Kagome mechanisms and external layer mechanisms, robustness could be achieved without greatly sacrificing the macroscopic stiffness.

A crucial aspect of this whole idea is the defect sensitivity of external layers. If the amount of nodal defects disrupts the eigenvalue balance between the external layer and Kagome core mechanisms, either robustness or macroscopic stiffness could be lost. Therefore, designs with defect-insensitive characteristics are required as external layers. To this end, both MT and polarised lattices prove to be ideal candidates. Robustness in these lattices is owing to the impervious nature of MT lattice combinatorics and topological polarisation to nodal defects (see Section 2.1).

Topological polarisation facilitates the localisation of mechanisms at domain walls. Unless designed with weak polarisation, these domain walls generally harbour mechanisms with considerably low eigenvalues. Consequently, in a setting where the Kagome bulk is combined with a polarised lattice, external loads would cause bending deformations at the domain walls. Although such an arrangement localises the deformations

without causing any propagation towards Kagome bulk, the macroscopic response will be overly compliant due to the low eigenvalues of domain wall mechanisms. This is similar to case 2 mentioned above.

On the other hand, consider a Kagome bulk combined with MT lattices. A stand-alone periodic compatible MT lattice has a non strain-producing mechanism (see Section 2.5). However, when connected to Kagome, the MT lattice loses its non strain-producing mechanism altogether, as the connectivity cannot support the simultaneous existence of the MT lattice mechanism and the Kagome mechanism. In such a situation, the MT lattice will only harbour high-energy strain-producing mechanisms, indicative of the example mentioned in case 1 above. However, the property of harbouring strain-producing mechanisms despite high nodal connectivity makes the MT lattices favourable for the design solution. They can be re-designed to achieve strain-producing mechanisms with different levels of eigenvalues. Moreover, while itself being bending-dominated, high nodal connectivity ensures a stiffer response compared to conventional bending-dominated lattices like square or hexagonal.

Therefore, the design solution here uses a combination of MT lattices and polarised regions as the external layers for the Kagome bulk. The manner in which they are connected causes a domain wall at the interface between both regions (see Figure 3.1). The compatibility between polarised Kagome mechanisms at the domain wall and mechanism of the MT lattice dictates the eigenvalues of the designed external layers. In this manner, the eigenvalue-balance as in case 3 (mentioned above) is achieved and this process of re-designing for the eigenvalue-balance is the iterative procedure (see Figure 3.1a). Due to the robustness feature of the polarised and MT lattice regions, a well-designed external layer is expected to behave in the same manner even under the influence of defects, with minimal changes in mechanical properties.

3.2. Matrix analysis

In order to understand the distribution of eigenvalues, all three designs are tested via matrix analysis. Moreover, to observe the effect of nodal misalignments, the designs are embedded with defects and again tested through matrix analysis. Periodic lattice models are prepared and analysed via the developed algorithms (Appendix A). From the purview of this thesis, only collapse mechanisms are studied and states of self-stress are not. Smaller models of CL1, CL2, and CL3 (as shown in Figure 3.2) are used for matrix analysis. This is because matrix analysis of the original larger structures produces several zero eigenvalues corresponding to Kagome mechanisms, before highlighting the nonzero eigenvalues corresponding to the strain-producing mechanisms of the outer layers. Since the primary focus here is on the outer layers, it is useful to truncate the Kagome bulk, to make the computation faster and limit excess overload of data. This should be done with special care so as to not tamper with the eigenvalues of the outer layers. Details of this truncation process is presented in Appendix C. First, results for the pristine (no defect) models are presented.

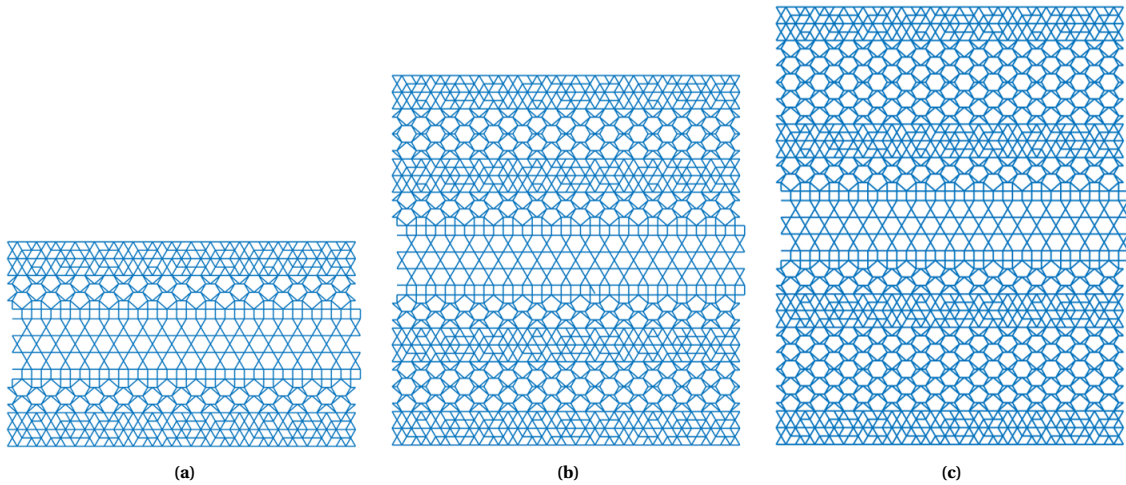


Figure 3.2: Truncated version of CL designs for computationally feasible matrix analysis: **a.** CL1; **b.** CL2; **c.** CL3.

Figure 3.3 shows the eigenvector corresponding to an eigenvalue of $\approx 10^{-4}$ for the CL1 structure. This is the eighth eigenvalue and all previous ones correspond to non strain-producing mechanisms of the Kagome core

and rigid body modes of the whole lattice. That is, λ_8 corresponds to the first strain-producing mechanism of the lattice which is localised to the outer layers. The higher eigenvalue is primarily owing to the connectivity of the MT lattice region and the polarised region, and consequently, its influence on the existence of a simultaneous mechanism at the domain wall. Furthermore, eigenvalues higher than λ_8 correspond to modes representing global shape-changes, including lattice distortions.

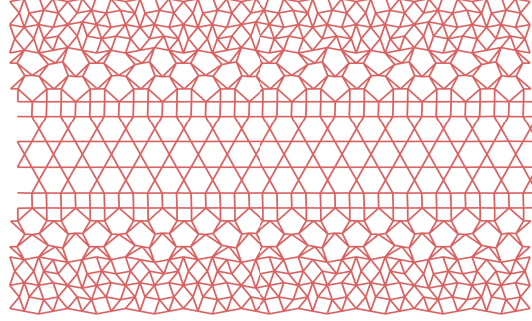


Figure 3.3: Strain-producing mechanism of the outer layer of pristine (without defects) CL1 design corresponding to an eigenvalue of λ_8 .

For CL2, again λ_1 to λ_7 denote non strain-producing mechanisms of the Kagome core and global rigid-body modes. Owing to the presence of additional domain walls and MT lattice regions, there are 4 eigenvalues representing strain-producing mechanisms in the outer layers, and their values are as follows,

$$\lambda_8 \approx 10^{-4}, \quad \lambda_9 \approx 10^{-4}, \quad \lambda_{10} \approx 10^{-3}, \quad \text{and} \quad \lambda_{11} \approx 10^{-3} \quad (3.1)$$

The eigenvectors corresponding to these eigenvalues are as shown in Figure 3.4. Since the distance between the domain walls here is the same as that in CL1, the eigenvalues (λ_8 and λ_9) corresponding to mechanisms in the outermost MT lattice and polarised regions are in the same range as that of CL1. For the other MT lattice and polarised region (the ones closer to Kagome bulk), eigenvalues (λ_{10} and λ_{11}) are relatively higher as the combined collapse mechanisms of the MT lattice and polarised regions at the domain walls are restricted. This is due to its connectivity to polarised regions on both sides.

In the case of CL3, λ_1 to λ_6 denote non strain-producing mechanisms of the Kagome core and rigid-body modes. Since both CL2 and CL3 have the same amount of domain walls, the number of strain-producing mechanisms in the outer layers is the same. Eigenvalues corresponding to those mechanisms are as follows,

$$\lambda_7 \approx 10^{-5}, \quad \lambda_8 \approx 10^{-5}, \quad \lambda_9 \approx 10^{-4}, \quad \text{and} \quad \lambda_{10} \approx 10^{-4} \quad (3.2)$$

The corresponding eigenvectors are illustrated in Figure 3.5. It is important to note the change in eigenvalues from CL1 and CL2 to CL3. As the distance between the domain walls is higher in CL3, the collapse mechanism manifests without being as restricted as in the case of CL1 and CL2. Following the same trend as in CL2, the eigenvalues λ_7 and λ_8 correspond to the outermost MT lattice and polarised regions, and λ_9 and λ_{10} for the other MT lattice and polarised regions.

This assessment of all the 3 designs indicates that under an external load, the mechanisms of the outer layers will be mobilised. It is important to note that a strain-producing mechanism, in essence, represents nodal movements that cause strains in the members. In other words, if the pin-jointed lattice harbours strain-producing mechanisms, its welded-jointed response, under an external load, is through member bending and nodal rotations (in regions where the mechanism is supposed to be). If the strain-producing mechanisms of a region are separated by a large gap in their eigenvalues, the welded-jointed equivalent is expected to deform in a manner predominantly governed by the lower eigenvalue mechanisms. However, if the gap is small enough, multiple mechanism modes influence the deformation behaviour.

As discussed previously, to mitigate the effect of external loads, the eigenvalues of outer layer mechanisms should be slightly lower than the Kagome mechanisms in the face of defects like nodal misalignments. To examine this behaviour, CL1, CL2 and CL3 lattices are modelled in the same manner but with randomly

distributed nodal defects. To ensure robustness in assessment, defects are embedded throughout the lattice and not just in the Kagome core.

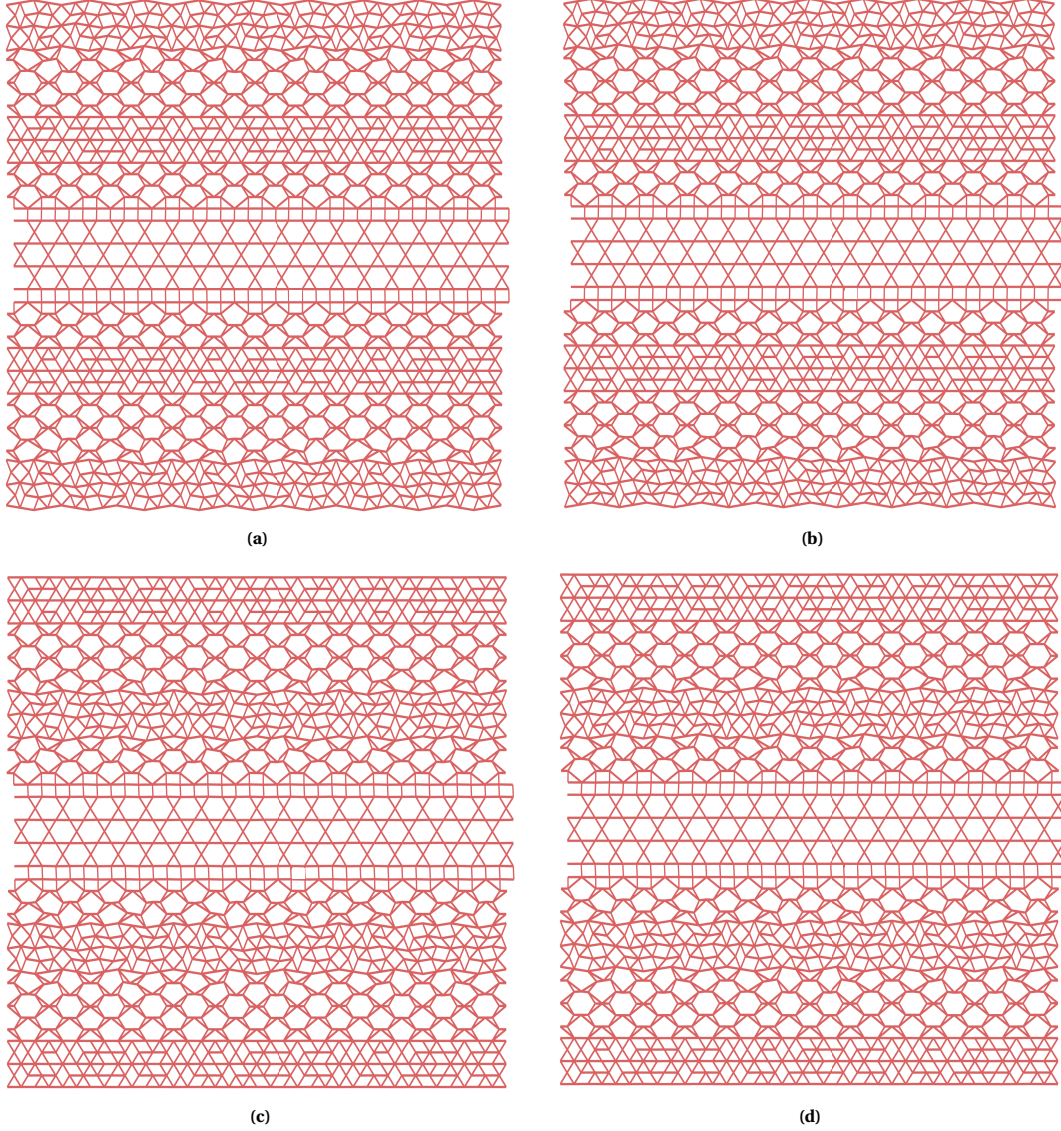


Figure 3.4: Set of strain-producing mechanisms of the outer layers of pristine (without defects) CL2 design corresponding to eigenvalues: **a.** λ_8 ; **b.** λ_9 ; **c.** λ_{10} ; **d.** λ_{11} .

For CL1, as expected, all Kagome non strain-producing mechanisms are lost and the lattice only has two mechanisms of the order of 10^{-16} corresponding to the two rigid body modes. The eigenvector corresponding to $\lambda_8 \approx 10^{-4}$ of the pristine CL1 is retained even after the inclusion of defects with a new eigenvalue of $\lambda_4 \approx 10^{-4}$. There is however a minute change in both these eigenvalues, owing to the loss of polarisation due to defects. All higher eigenvalues start from the range of 10^{-3} and indicate Kagome strain-producing mechanisms and global shape-changing modes. As the eigenvalue corresponding to Kagome mechanisms are established to be of the order of 10^{-3} , it is favourable to have the outer layer mechanisms with slightly lower eigenvalues than 10^{-3} (as is observed here). With further reduction in eigenvalues of the outer layer mechanisms, the outer layer becomes increasingly compliant. This balance of eigenvalue resembles the third case mentioned in Section 3.1.1. Note that the mechanisms of the CL models with defects are not shown since they are exactly similar to the ones shown for CL models without defects (Figure 3.3, Figure 3.4 and Figure 3.5).

The same trend as in CL1 is followed for CL2 and CL3 as well. The first two eigenvalues correspond to rigid-body modes. The next few eigenvalues (λ_5 to λ_8 for CL2 and CL3) correspond to strain-producing mechanisms of

the MT lattice and polarised regions. All higher eigenvalues correspond to strain-producing mechanisms of the Kagome and global shape-changing modes start from the order of 10^{-3} . In the case of the CL2, the eigenvalues are such,

$$\lambda_5 \approx 10^{-3}, \quad \lambda_6 \approx 10^{-3}, \quad \lambda_7 \approx 10^{-3}, \quad \text{and} \quad \lambda_8 \approx 10^{-3} \quad (3.3)$$

Similarly, for CL3, the eigenvalues are as follows,

$$\lambda_5 \approx 10^{-4}, \quad \lambda_6 \approx 10^{-4}, \quad \lambda_7 \approx 10^{-3}, \quad \text{and} \quad \lambda_8 \approx 10^{-3} \quad (3.4)$$

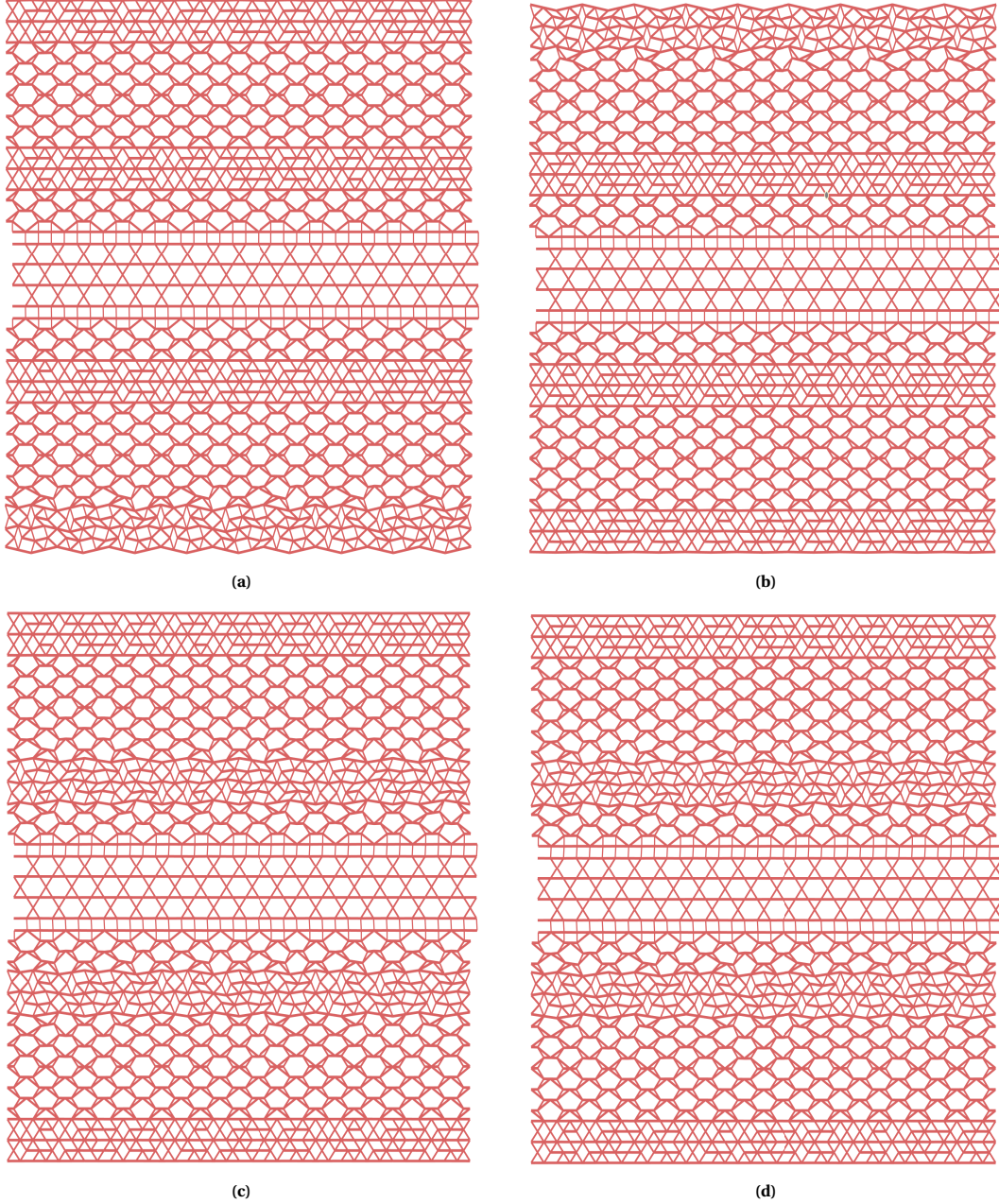


Figure 3.5: Set of strain-producing mechanisms of the outer layers of pristine (without defects) CL3 design corresponding to eigenvalues: **a.** λ_7 ; **b.** λ_8 ; **c.** λ_9 ; **d.** λ_{10} .

It is important to note two points here. First, the eigenvalues corresponding to mechanisms in the polarised and MT lattice regions are lower than the ones corresponding to Kagome. This indicates that the work required

to cause deformations in the outer layers is lower than that required to cause deformations in the Kagome core. Although the difference is not high, comparable eigenvalues like these point to the fact that the energy imparted to the lattice from external sources will be used up partly in the outer layers and partly in the Kagome core. However, matrix methods cannot predict the evolution of mechanisms or the mechanical properties of the welded-jointed equivalents once deformations ensue.

Therefore, it is yet to be determined if this split of energy will hold after the initial stages of deformation in the outer layers. Numerical analysis is required for assessing that behaviour. Numerical results could aid in identifying whether there is any geometry-induced stiffening in the designed outer layers. If this is the case, one could afford to have outer layer mechanisms with even lower eigenvalues to begin with. This feature would increase the robustness of the lattice further.

The second important point to note is that the eigenvalues remain intact (with minimal changes) for the mechanisms of the MT lattice and polarised regions, indicating robustness in those designs. In the polarised region, this is owing to the fact that the winding number is an invariant for a polarised Kagome, and geometrical perturbations at certain sites in the lattice do not drastically affect the overall polarisation (refer to Section 2.1.2). Similarly, for MT lattice regions, nodal perturbations do not affect the combinatorics to a great extent and therefore the compatible nature is retained even under the influence of defects.

Recall that, the presence of strain-producing mechanism only guarantees a bending-dominated deformation, but does not predict the manner in which deformations ensue as that depends on the loading conditions. Moreover, if analysed through a numerical model which accounts for geometric nonlinearities, there can be no parallel drawn between the evolution of mechanisms from matrix analysis (assuming there exists a framework for tracking this) and deformations observed in the numerical model. This is because the equilibrium path followed in the numerical model is highly nonlinear and depends on the effect of changing geometry. Therefore even if we observe a rise in eigenvalues, it cannot be correlated to geometric stiffening directly.

3.3. Concluding remarks

Composite Lattice (CL) designs are proposed where the Kagome bulk is appended with carefully designed MT and polarised lattices at the bulk exteriors. If most of the energy is used up in the CL outer layers, the Kagome core is shielded and hence robustness is maintained in the face of defects. However, if this "absorption" of energy is at the cost of having a compliant lattice, that is a lattice with extremely low eigenvalue mechanisms, the absolute stiffness measured against an external load will be low. On the other hand, if the outer layers harbour high eigenvalue mechanisms (higher than Kagome mechanisms), the energy will be utilised in mobilising the Kagome mechanisms, thereby causing a sharp decay in lattice stiffness. Therefore, the ideal scenario is to have outer layer mechanisms with slightly lower eigenvalues than that of the Kagome core. That way, robustness is maintained without compromising greatly on the macroscopic stiffness. Importantly, the outer layers should be robust against defects themselves. If the eigenvalues change drastically upon the introduction of defects, the energy balance shifts and robustness could be lost. Matrix analysis of CL1, CL2 and CL3 designs shows that the eigenvalue balance is maintained with Kagome mechanisms and that the outer layer mechanisms are robust against defects themselves. To explore the effect of these layers further, a detailed numerical analysis is conducted. This is elaborated in the next chapter.

Numerical verification of designs

The effect of the inclusion of polarised and MT lattice regions on the stiffness of Kagome lattices is illustrated in this chapter. It is instructive to recall the thesis objective here: to generate a Kagome lattice capable of retaining its macroscopic stiffness under manufacturing defects. Although there is a large set of different types of defects that could exist in a lattice [15], the most subtle one is the nodal misalignment. This is so because nodal misalignments are not as easily apparent as other defects but nevertheless affect the Kagome behaviour severely. Therefore, for this thesis, only nodal defects are considered as a cause of imperfections in the lattice. Matrix analysis is the first step in redesigning and analysing the lattice properties. With the help of the dynamical matrix method and eigenvalues, an iterative design process is formulated to predict, in an analytical sense, the mechanical behaviour of lattices (see Chapter 3). All three lattices presented in the previous section have been thoroughly explored via matrix analysis. However, in order to understand their mechanical behaviour completely, FE calculations are necessary. This chapter presents the results of numerical analysis and links it to the observations made from Chapter 3.

4.1. Numerical model setup

Welded-jointed models of all three lattices CL1, CL2 and CL3 are subjected to uniaxial compression tests along Y direction (see Figure 3.1 for axis). These tests are conducted under a strain-controlled and stress-controlled setting. Since the dimensions of all the lattices are kept constant, both tests are carried out within the same range of applied strains and loads. Abaqus 2023 [37] is used to carry out the FE analysis.

The entire lattice has a length of 535 mm along the Y direction. The X directional dimension is not important as it is modelled as a periodic structure in that direction. The characteristic unit cell member length of each of the regions is approximately 2.9 mm. The in-plane thickness for all members throughout the whole model is kept constant at 0.2 mm. This directly influences the relative density of the lattice. Since there are three distinct regions in the model, the relative density changes for each region due to constant member thickness. Derivation of relative density expressions for each of these regions is elaborated in Appendix C. The obtained relative density expressions are,

$$\rho_{MT} = \frac{10t}{\sqrt{3}h}; \quad \rho_{polarised} = \frac{(4\sqrt{7} + 12)t}{3\sqrt{3}h} \quad \text{and} \quad \rho_{kagome} = \frac{2\sqrt{3}t}{h} \quad (4.1)$$

where t represents the member thickness and h represents the outer edge length of a supertriangle of the MT lattice region. For the same member thickness t , $\rho_{MT} \approx 1.67\rho_{kagome}$ and $\rho_{polarised} \approx 1.25\rho_{kagome}$. This points to the fact that if the relative density has to be kept constant throughout the lattice, t_{MT} should be $0.6t_{kagome}$ and $t_{polarised}$ should be $0.8t_{kagome}$. It is shown by Hyun & Torquato [4], that for a particular relative density, the Kagome architecture attains the upper bounds of elastic modulus and hence is the optimal configuration for high specific stiffness lattice materials. Therefore, the polarised and MT lattice layers, if maintained with the same relative density as that of the Kagome, will be considerably more compliant than the Kagome, as it is also established that they harbour strain-producing mechanisms. This situation is analogous to placing a slab of soft elastomer over the Kagome. This results in a lattice model with tremendously low macroscopic Young's

modulus compared to the Kagome. Since this directly goes against the thesis objective, such an approach is avoided and hence, a model with constant member thickness is used.

The cell walls are meshed with B21 Timoshenko beam elements. This element allows for axial, bending and transverse shear deformations. Beam elements are chosen over solid elements to reduce the computational effort. However, one should be careful in choosing the proper beam element depending on the member lengths and thicknesses in the lattice model. For the lattice models designed here, the slenderness ratio (ratio of the cross-sectional dimension to the axial length) is 0.069. This is minutely higher than the limit of the slenderness ratio prescribed for using Euler-Bernoulli beam elements (elements that do not account for shear effects). Due to this reason, Timoshenko elements are used to mesh the cell walls.

A linear-elastic material model is used, with Young's modulus 69 GPa and Poisson's ratio 0.33, representative of aluminium alloys. Further, a geometrically nonlinear framework is adopted for all analyses. This is important as the mechanical properties change with the changing geometry. All tests are carried out here by ramping up the macroscopic strains (and loads). In a pristine Kagome model, if the loads do not exceed the critical limits of buckling, a geometrically linear analysis suffices to extract mechanical properties like Young's modulus. However, the situation is different for a model with nodal defects. Here, as the loads are increased, the lattice undergoes a significant change in shape. To accurately capture the effect of this changing shape on the mechanical properties, geometric nonlinearities have to be considered. In an FE setting, this is implemented by modifying the stiffness matrix. For a geometrically linear case, the stiffness matrix only consists of physical stiffness contributions (effect of material properties like E and ν , and geometrical properties like area moment of inertia I). However, for a geometrically nonlinear case, the stiffness matrix involves stress-induced effects (commonly known as geometric stiffness), along with the physical stiffness matrix. With each increment in the FE analysis, the stresses are updated which updates the geometric stiffness and in turn the overall stiffness matrix. In this manner, the FE model captures the effect of changing geometry.

As mentioned earlier, the model is periodic in the X direction. This is enforced in the FE model by using periodic constraints. For every periodic node on the left (i) and its counterpart on right (i'), the following natural boundary conditions are prescribed,

$$u_x^{(i)} = -u_x^{(i')}; \quad u_y^{(i)} = u_y^{(i')}; \quad \text{and} \quad u_\phi^{(i)} = u_\phi^{(i')}$$

It is important to note that the periodic boundary conditions prescribed here follow the type of mechanical loads.

To examine the stiffness properties of the lattices, a macroscopic Young's modulus measure is used. Depending on the type of test (strain-controlled or stress-controlled), the measurement is appropriately modified. For a stress-controlled test, the stresses are measured by simply dividing the applied loads by the undeformed area of the exterior surface on which the loads are prescribed (also called nominal stress). The change in area in the process of loading is not taken into account as it is minimal. Strains are calculated by dividing the change in total length by the original length. For strain-controlled tests, the reaction forces are divided by the area to obtain the stresses. The rest of the procedure remains the same. This procedure is akin to the kind of measurement a Universal Testing Machine (UTM) would take.

In addition to the macroscopic Young's modulus, strain energy is also examined. This is a useful measure as it can be calculated for any region in the interior of the lattice and provides a qualitative measure of the regions that contribute primarily to the macroscopic stiffness. In addition to this, strain energy density (strain energy normalised with the volume of the region) is also estimated so as to remove the dependency on region-size.

4.2. Macroscopic stiffness calculations

Investigation on the effects of nodal misalignments is carried out by embedding these defects randomly throughout the bulk of the lattice. Two models are generated for each lattice examined here. The first one is a pristine structure with no defects and the second is with nodal defects, otherwise also termed as the imperfect structure. The change in macroscopic Young's modulus (E), is measured by gradually increasing the strains (or loads) and measuring the difference in the obtained macroscopic Young's modulus values of the pristine lattice and the lattice with defects (otherwise termed as imperfect lattice). The difference is calculated as a percentage decay in stiffness with respect to the pristine model stiffness, as expressed in Equation 4.2. The

decay percentage is calculated at every increment of the analysis.

$$\text{Percentage decay} = 100 \times \left(1 - \frac{E_{\text{pristine}} - E_{\text{imperfect}}}{E_{\text{pristine}}} \right) \quad (4.2)$$

Furthermore, since the CL outer layers are designed to be compliant (as they have a fixed strain-producing mechanism even without the influence of defects), it causes a drop in the macroscopic stiffness by default. In other words, the design itself warrants an initial drop in the macroscopic stiffness (irrespective of the presence of defects). To make a comparison of the effect of this "compliant" characteristic of the CL outer layer, two additional lattices are designed. The first one replaces the outer layers of CL2 with a hexagonal lattice (Kagome-Hexagonal), and the second one with a fully-triangular lattice (Kagome-Triangular). The presence of a hexagonal lattice mimics the behaviour of a fully compliant outer layer in a qualitative sense. On the other hand, the presence of a triangular lattice mimics the behaviour of a stiff outer layer (from the dynamical matrix analysis perspective, a lattice with extremely high eigenvalue mechanisms). Details of the numerical results are presented next.

The nodal defects are maintained to be uniform for all the models. That is, the amount and direction of movement of a specific joint is kept the same for all the models. However, as not all sections of all models are the same (for instance, the outer layers of CL2 and the hexagonal layer are geometrically different), there are inevitably small changes in the nature of the introduced nodal misalignments, but not the amount. 224 defects are introduced in these models which account for approximately 3.5% of the total number of nodes. Note that a "node" here refers to a lattice joint and not a FE mesh node.

Figure 4.1 indicates the change in E as the strains (and loads) are increased. As can be noticed, there is a sharp decay in the stiffness of Kagome under the influence of nodal defects. Before the main results are discussed, preliminary checks need to be done. At first sight, it appears as if both the stress-controlled and strain-controlled tests depict different behaviour. However, a close study reveals that it indeed is the same behaviour. For the stress-controlled tests, as each of the lattice models has different stiffness properties, the strain endured by each of them is different (indicated by ϵ_m in Figure 4.1b). For all the structures, the decay in E corresponding to the same level of macroscopic strains is the same, indicating that both tests capture the same behaviour.

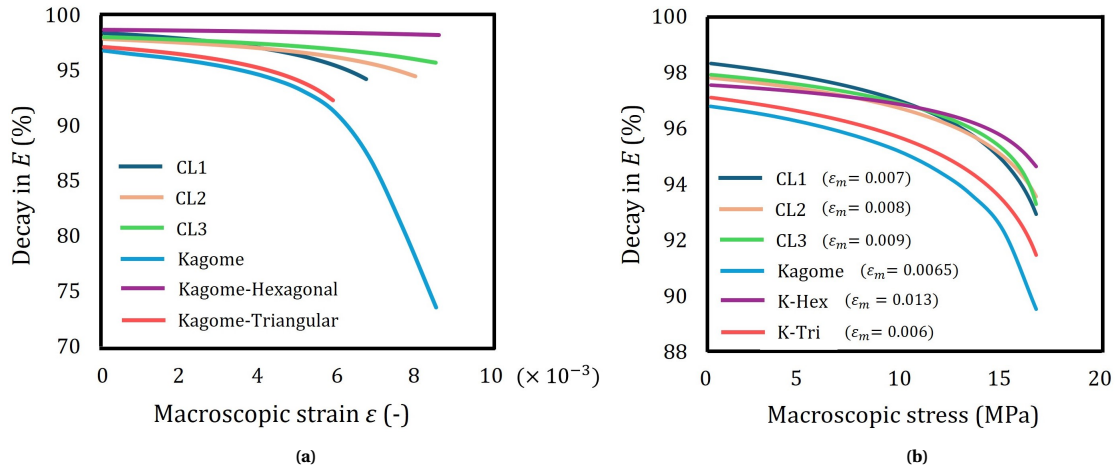


Figure 4.1: Decay in Macroscopic Young's modulus (E). K-Hex stands for Kagome-Hexagonal and K-Tri for Kagome-Triangular: **a.** Strain-controlled test; **b.** Stress-controlled test. ϵ_m indicates the maximum strain endured by the lattice.

As observed, the decay in E for CL1, CL2 and CL3 is significantly lower than Kagome (upto the respective limits of macroscopic strains). Interestingly, this decay is the least in the Kagome-Hexagonal lattice, while the Kagome-Triangular lattice behaves in a similar manner as the Kagome for the most part. The truncation in curves for the CL1, CL2 and Kagome-Triangular will be discussed shortly. These plots indicate the ability of CL outer layers to provide robustness to the lattice stiffness. To discover the reason behind this behaviour, the strain energy (U) of these regions is examined. Figure 4.2a illustrates the computed strain energy distribution

in percentage between the outer layers and Kagome cores of all lattice models, in their pristine and imperfect forms. The percentage is calculated with respect to the total strain energy of the model at the maximum strain level. Furthermore, to conduct a fair comparison, the strain energy associated with a particular region is normalised with its volume. In other words, strain energy density (u) is also consulted. Figure 4.2b shows the corresponding strain energy densities.

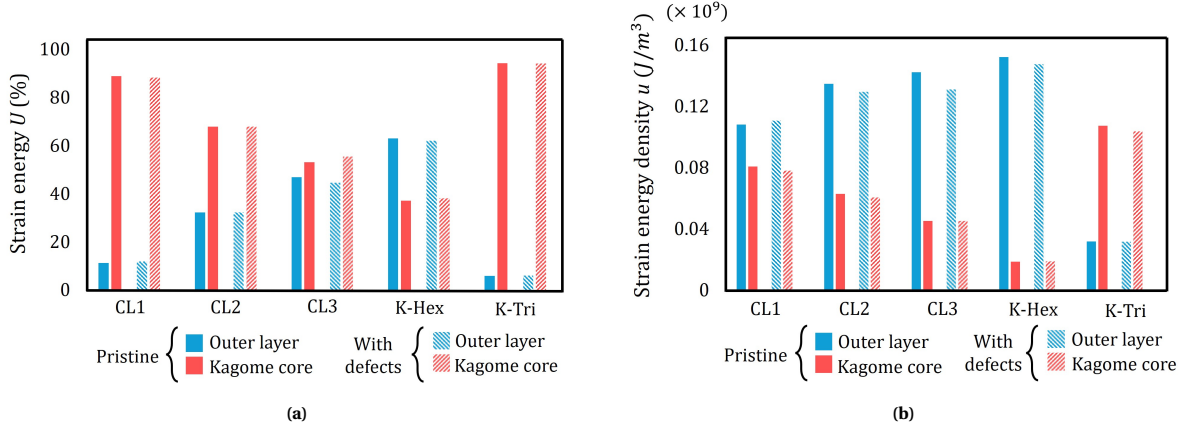


Figure 4.2: Strain energy measures for all designed lattices in their pristine and imperfect models. K-Hex stands for Kagome-Hexagonal and K-Tri for Kagome-Triangular: **a.** Distribution of strain energy (in percentage) amongst the outer layer and Kagome core; **b.** Strain energy density in the outer layers and Kagome cores for each lattice model.

In the case of CL1, CL2 and CL3, it can be observed that, as the outer layer area increases, the distribution in strain energy also shifts (see Figure 4.2a). From 11% in CL1, it has increased to 48% in CL3 at the same macroscopic strains. Here, the increase in strain energy percentages could be reasoned as a direct effect of the increase in the outer layer area in CL3. To this end, the strain energy density provides an accurate measure. In CL1, the strain energy density of the outer layer is approximately 1.3 times that of the Kagome core. However, in CL3, it is approximately 3.5 times that of the Kagome core. This means that the change in architecture between CL1 and CL3 shifts the stiffness contribution largely from Kagome to the outer layers.

The key point to note here is that this trend in strain energy density remains the same even after defects are introduced. As indicated by matrix analysis results (see Chapter 3), all three CL lattices retain the eigenvalues of the outer layer mechanisms even after nodal defects are introduced, meaning that the loads required to trigger them remain approximately the same. Furthermore, these eigenvalues are slightly lower than the eigenvalues of the Kagome strain-producing mechanisms (under the influence of defects). For CL3 and CL2, as multiple such strain-producing mechanisms exist in the outer layers, the stiffness contribution of these layers is high compared to the Kagome cores (indicated by the high strain energy densities). As the CL outer layers are robust against nodal defects, this stiffness contribution is retained even in imperfect lattices. Therefore, multiple low eigenvalues of the robust CL outer layers aid in maintaining the robustness of the whole lattice, up to certain levels of macroscopic strains. Under the influence of defects, the stiffness drop is lowest in CL3 (least outer-layer eigenvalues amongst the designs) and gradually increases till CL1 (highest outer-layer eigenvalues). For CL1, as only 1 mechanism exists, the stiffness contribution of the layer is low.

It should be noted that the calculated strain energy densities here do not necessarily indicate the absolute stiffness of the region, rather it is only a measure of what region of the whole lattice contributes primarily to the stiffness of the lattice. Since the thesis objective is to make the Kagome lattice impervious to these nodal defects, an absolute drop in stiffness at the cost of high robustness is also not desired. Therefore, it is also important to consider the absolute stiffness of the designed lattices. Since all the designed outer layers are of different relative densities, the weight of each lattice model is different. To form a fair comparison, the macroscopic Young's modulus is normalised with the weight. In other words, specific stiffness is calculated. Furthermore, the specific stiffness is then calculated as a percentage of the highest value (that of Kagome lattice) and is presented in Figure 4.3a. Further, this is only calculated for the pristine models as the drop in stiffness due to defects is already evident from Figure 4.1.

From Figure 4.3a, it can be seen that amongst the designed lattices apart from Kagome, the Kagome-Triangular

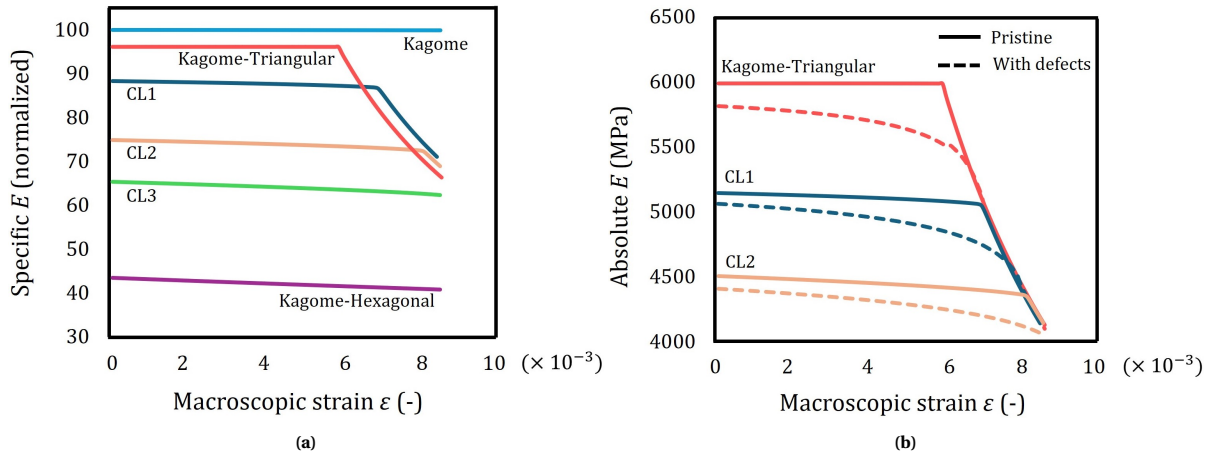


Figure 4.3: **a.** Specific stiffness of all pristine lattice models; **b.** Absolute stiffness of selective lattices (pristine and imperfect models).

has a high specific stiffness. This is expected since the Triangular outer-layer harbours the highest stiffness (similar to Kagome) for a lattice architecture at a given relative density. However, interestingly, the specific stiffness still does not match that of Kagome. This is because the stiffness contribution of the Kagome-Triangular lattice primarily comes from the Kagome core, as evidenced by the strain energy percentages (see Figure 4.2a). Therefore, while the absolute stiffness of the lattice is minimally higher than that of the Kagome, the specific stiffness is lower owing to the considerable increase in weight. Amongst the CL designs, CL1 has the highest specific stiffness. Again, this is because the Kagome core contributes to the most extent to the lattice stiffness (see Figure 4.2a). The drop in stiffness compared to Kagome is however due to the presence of a domain wall harbouring a strain-producing mechanism. For CL2 and CL3, as there are several such domain walls, the absolute stiffness drops further, and by extension, the specific stiffness. For the Kagome-Hexagonal lattice, a majority of the contribution to its macroscopic stiffness comes from the Hexagonal layer, which automatically causes a tremendous drop in the lattice's absolute stiffness. This study reveals that, although the CL designs and Kagome-Hexagonal lattice provide robustness against defects to a good extent, they cause a drop in the absolute stiffness of the lattice.

Apart from this drop in absolute macroscopic Young's modulus, the upper limit to the macroscopic strains endured by CL1, CL2 and Kagome-Triangular lattices is much smaller than the others, as can be seen in Figure 4.1. A close observation of the FE results (stresses and displacements) indicates cell wall buckling in the Kagome core of the pristine models of CL1, CL2 and Kagome-Triangular. Figure 4.3b illustrates the macroscopic Young's modulus of the pristine models against the imperfect models for CL1, CL2 and Kagome-Triangular. It can be seen that the gap between the two lines in each plot increases up to a certain strain level, indicating a decay in stiffness. After a certain point, there is a sharp decline in the stiffness of the pristine models which then causes a sudden change in decay percentage. The decay percentage rises to 100 indicating no drop in stiffness. To verify that this effect is indeed due to buckling, the pristine models of CL1, CL2 and Kagome-Triangular are tested through a geometrically linear analysis. Since a linear analysis does not capture the effect of a changing geometry, it performs the analysis with an increasing load on the original configuration of the lattice and therefore escapes buckling. The results of such an analysis is as shown in Figure 4.4a. Lattice models with defects are analysed through the same geometrically nonlinear framework, while the pristine models are under a linear one.

As can be observed here, the decay percentage drops for these models in a regular manner, pointing to the fact that the anomalous behaviour was indeed the result of buckling in the Kagome core. The trend in the decay of the macroscopic Young's modulus closely resembles what is obtained through a geometrically nonlinear framework. However, there are some subtle differences. Upon close observation, it can be noticed that the decay for all CL models and Kagome-Hexagonal is predicted to be higher when studied under a linear analysis, than when studied under a nonlinear analysis. This is owing to the fact that, even in pristine CL and Kagome-Hexagonal models, there is always a small drop in stiffness due to deformations in the outer layer. This effect is captured in a nonlinear framework but not in a linear framework, which thereby reduces the gap between the pristine model stiffness and the stiffness of the models with defects. Therefore, the decay percentage is smaller

when analysed under a geometrically nonlinear framework.

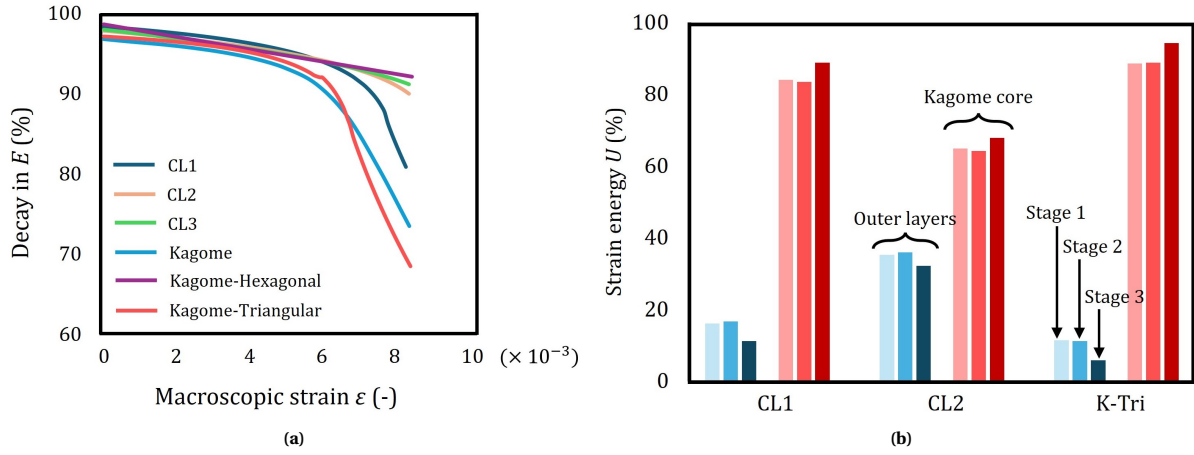


Figure 4.4: Presence of cell wall buckling in pristine lattice models: **a.** Decay in stiffness of models analysed through a geometrically linear framework. Only the pristine model is analysed through a linear setting, the imperfect model is studied through the same nonlinear framework; **b.** Distribution in strain energy at three different strain levels during the process. Only pristine models are studied here, under the established nonlinear setting. Stage 1 is at low macroscopic strains, stage two is a few increments before buckling ensues and stage 3 is the maximum strain level.

The effect of buckling on the macroscopic stiffness of the pristine models can also be understood qualitatively through strain energy estimates. Figure 4.4b represents the strain energy percentage calculated for the outer layers and Kagome cores at three different macroscopic strain levels. The first one is at very low strains, the second at strain levels just below critical limits of buckling and the final one at maximum strains. The critical limit for buckling is not estimated in an analytical manner, but rather by observing FE results (stresses and displacements) at each increments. Figure 4.4b shows that the strain energy percentage is identical for the first and second stages for all models. However after buckling has ensued, the percentage shifts. The buckled Kagome core then contributes, to the stiffness, more than its pristine counterpart, thereby causing a drop in the macroscopic stiffness of the lattice.

The cause for buckling in these models is due to the fact that the load is endured largely by the Kagome core. In the Kagome-Triangular lattice, the loads are endured by the relatively smaller Kagome section (relative with respect to the full Kagome lattice). The situation is similar in CL1 and CL2. Although in CL2, the outer layer endures the effect of external loads to a good extent (see Figure 4.2b), the Kagome core being smaller causes buckling, albeit at higher macroscopic strains compared to CL1. Similarly, for CL3, buckling is expected at even higher strains outside the range investigated here. Naturally, this effect is not seen in the Kagome-Hexagonal lattice as the effect of external loads is endured, for the most part, by the hexagonal layer.

This particular study reveals an important aspect of the designed pristine CL outer layers. The fact that buckling ensues in the Kagome core at certain macroscopic strain levels indicates that the absolute stiffness of the CL outer layers has gone up after deformation in the initial stages. That is, as deformations are triggered at low macroscopic strains, the outer layer region becomes stiffer and moves away from a compliant characteristic to a stiffer characteristic (like a triangular outer layer). This behaviour is most prominent in CL1 and least in CL3, due to the presence of multiple low eigenvalue mechanisms in the outer layer of CL3. Since inclusion of defects does not drastically change the nature of deformations in CL outer layers, the same stiffening behaviour is expected for imperfect CL models as well.

Although the effect of nodal misalignments in Kagome and the designed lattices is established, it is also important to investigate the effect of different levels of defects in the lattices. To this end, two extra models of the Kagome lattice are generated with 2% and 5.4% defects respectively. The same procedure is adopted for the CL2 lattice. The CL1 and CL3 lattices are not modelled as the tendencies observed for CL2 suffices in representing the behaviour of CL1 and CL3 lattices as well. The decay in macroscopic Young's modulus for these lattices is shown in Figure 4.5.

For convenience, the models with 2% defects are categorised under "set 1" and those with 5.4% defects under "set 3", with "set 2" being the original model with 3.5% defects. For the CL2 lattices, the same trend is observed

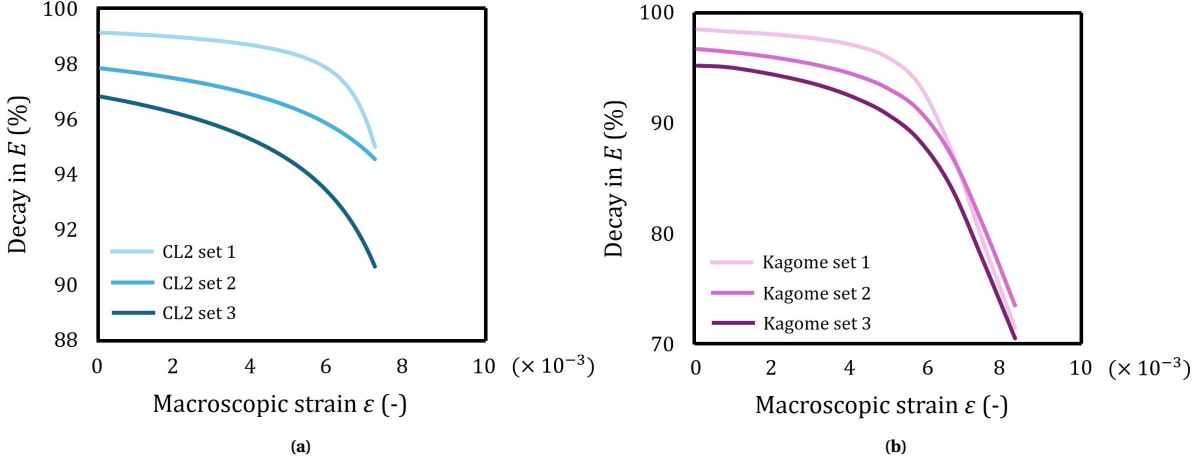


Figure 4.5: Decay in macroscopic Young's modulus for lattices with different amounts of nodal defects: **a.** CL2; **b.** Kagome.

as before, as can be seen in Figure 4.5a. As the strains are increased, the stiffness decays and buckling ensues in the Kagome core. However, the rate at which this decay occurs is different for each case. As the percentage of defects increases from set 1 to set 3, the decay in stiffness accordingly increases. This is however in contrast to what is seen for the Kagome lattices (see Figure 4.5b), as only a minimal difference is observed. For the sake of discussion now, it is assumed that the results shown for Kagome lattices are indeed correct (this assumption will be addressed shortly). With this premise, the increase in decay for CL2, with increasing defects, can only be reasoned by a change in the property of the CL outer layers. To examine this, pin-jointed CL2 models for sets 1 and 3 are assessed through matrix analysis. The same procedure outlined in Chapter 3 is followed.

In the case of the CL2 model of set 1, The eigenvalues corresponding to the outer layer mechanisms and Kagome core mechanisms are as follows,

$$\text{Outer Layer: } \lambda_5 \approx 10^{-4}, \quad \lambda_6 \approx 10^{-4}, \quad \lambda_9 \approx 10^{-3}, \quad \text{and} \quad \lambda_{10} \approx 10^{-3} \quad (4.3)$$

$$\text{Kagome core: } \lambda_7 \approx 10^{-4}, \quad \lambda_8 \approx 10^{-3} \quad (4.4)$$

For the CL2 model of set 3, they are as follows,

$$\text{Outer Layer: } \lambda_8 \approx 10^{-3}, \quad \lambda_9 \approx 10^{-2}, \quad \lambda_{10} \approx 10^{-2}, \quad \text{and} \quad \lambda_{11} \approx 10^{-2} \quad (4.5)$$

$$\text{Kagome core: } \lambda_5 \approx 10^{-3}, \quad \lambda_6 \approx 10^{-3} \quad (4.6)$$

From the distribution of eigenvalues in set 1, it can be seen that the mechanisms of outer layers (and even Kagome) have reduced eigenvalues compared to what was observed in set 2 (Equation 3.3). Multiple lower eigenvalue mechanisms in the outer layer indicate that the external loads primarily affect the outer layer. It is this feature that lends the CL2 lattice of set 1 its robustness for the most part of applied strains (the slope of the curve is not extremely steep). However, as the loads are increased, Kagome core mechanisms are inevitably excited (meaning deformations ensue in the welded-jointed FE models) hence the increase in decay percentage. On the other hand, for set 3, the Kagome core mechanisms have lower eigenvalues compared to the outer layer mechanisms. This indicates that the external loads on the welded-jointed equivalent affects the Kagome core primarily, thereby causing a more severe decay in macroscopic stiffness.

It should be noted that several nodal defects in the polarised regions cause a significant diffusion in the polarisation as it is no more uniformly directed in one direction towards a domain wall. As the number of defects increases, diffusion of polarisation increases and the eigenvalues corresponding to the mechanisms at the domain wall increase, till a point where the domain wall no more harbours mechanisms and therefore stops being a domain-wall altogether. In addition, these nodal defects also affect the combinatorics of the MT lattice region. That is, although nodal defects do not disrupt compatibility, they can affect the eigenvalues associated with the mechanism of the MT lattice region. Severe nodal defects could cause a higher eigenvalue for the strain-producing mechanism of the MT lattice, making its welded-jointed response stiffer in nature.

Now, Figure 4.5b is revisited to address the assumption made earlier. Intuitively, with an increase in defects, one would expect the decay in Kagome stiffness to be pronounced further. However, this is not what is observed

here. This is due to the geometric nonlinear setting in the FE framework. Under any given amount of nodal defects, the Kagome geometry changes upon application of infinitesimal external loads, corresponding to a drop in stiffness. This change in geometry is taken into account by the FE framework. As the geometry changes, nodal defects become 100% in a qualitative sense, since the change in geometry (although minute) is reflected throughout the bulk of the lattice. This phenomenon manifests in all three sets of Kagome considered here and hence the decay in E is approximately similar in all three for higher strain levels. However, the drop in stiffness due to an increase in defects can be seen at infinitesimal strain levels where it falls from 98% in set 1 to 94% in set 3.

4.3. Concluding remarks

The numerical results presented in this chapter are in accordance with the observations made through matrix analysis (presented in Chapter 3). Higher strain energy densities for welded-jointed FE models of CL2 and CL3 are expected from the observed eigenvalues of the pin-jointed CL outer layer mechanisms. Since these were approximately equal (if not smaller) to the eigenvalues of the Kagome mechanisms, work done by the external load manifests in nearly equal percentages in the outer layers and the Kagome. This feature is most apparent for CL3. With outer layer eigenvalues smaller than that of the Kagome core, the strain energy density of the welded-jointed outer layer is approximately 3.5 times that of the Kagome. Robustness against defects is indeed attributed to the presence of outer layer mechanisms with specific eigenvalues, which can be observed in the decay % trends. Characteristics like geometry-induced stiffening of outer layers is also brought to light, along with its effects like Kagome core buckling. The downside to such a design is the overly compliant nature of the outer layer. Although it aids robustness, lower external eigenvalues in the pin-jointed models leads towards more compliant outer layers in the welded-jointed models and hence a low absolute macroscopic stiffness. This feature can be seen in CL3 and more prominently in Kagome-Hexagonal lattice, due to the more compliant response of the hexagonal lattice.

Therefore, this solution demands a suitable trade-off between the robustness against decay in stiffness and the absolute stiffness of the lattice. For structures that exhibit one extreme, the other feature is completely lost.

5

Conclusions

A novel design strategy for reducing the imperfection sensitivity of lattice materials is presented. The Kagome is chosen as the base architecture of the developed designs due to its excellent stiffness properties and extreme vulnerability towards defects. Nodal misalignment is chosen as the primary defect as it is proven to cause a significant knock-down in Kagome macroscopic stiffness and is difficult to detect during regular post-processing techniques. The strategy here focuses on designing appropriate exterior sections to a Kagome core that delivers a blend of robustness and high stiffness to the whole lattice. Satisfactory performance of the developed designs with defect sensitive Kagome at the bulk indicates the efficacy of the proposed design strategy.

The designs are primarily investigated via a reformulated matrix method. This technique removes the lattice from its original space of member lengths and nodal placements and places it in a mass-spring paradigm where the oscillations around a stable equilibrium indicate non strain-producing and strain-producing mechanisms. The benefits of adopting this approach are observed in computational efficiency and ease of implementation where augmenting the matrices is not necessary for identifying strain-producing mechanisms. More importantly, eigenvalues of the dynamical matrix aid in associating the strain-producing mechanisms found with their linearised potential energies. This fact plays a crucial role in the design-development process. The spectrum of potential energies indicates the energy associated with the spring elongations in the pin-jointed model, and thereby represent deformations (in the welded-jointed equivalents) that warrant different levels of strain (tensions) in the members. If eigenvalues corresponding to a strain-producing mechanism are low, the welded-jointed equivalent is compliant and deforms easily. Higher eigenvalues indicate stiffer responses of the welded-jointed model.

The design solution introduced here uses polarised Kagome and compatible MT lattices as thin exterior layers to a regular Kagome bulk. These designs are termed Composite Lattices (CL). The robustness of the CL design comes from the satisfaction of two criteria. First, the exterior layer should harbour strain-producing mechanisms with eigenvalues marginally lower than the strain-producing mechanisms of the Kagome core. Second, the eigenvalues of the exterior layer mechanisms should be impervious to nodal defects. Both conditions are necessary for robustness against defects and for not compromising the absolute macroscopic stiffness of the lattices. Such a design ensures that work done by the external loads is neutralised by deformations localised to the exterior regions. CL designs satisfying both criteria are generated through an iterative design and analysis process which uses dynamical matrix methods. An additional advantage to using the MT lattice design is their tendency to offer stiffer responses compared to conventional lattices that show bending-dominated behaviour. Moreover, the usage of polarisation enables the localisation of deformation to specific regions without having a propagating effect.

Verification of the performance of these designs is carried out via numerical tests on the welded-jointed equivalents. The decay in macroscopic stiffness is investigated through a "Decay %" parameter that measures the drop in macroscopic Young's modulus. Strain energy measurements are also taken to develop a complete picture of the lattice behaviour. The observations made from numerical tests are in agreement with the predictions from matrix analysis. The eigenvalue balance observed from matrix analysis is observed to lend robustness against defects in the CL designs. The sections with lower eigenvalue mechanisms (in the pin-

jointed models) cause deformations easily (in the welded-jointed equivalents) compared to sections with higher eigenvalues. This difference is clearly observed between CL3 and CL1 from a comparison of the strain energy density of the outer layers against the strain energy density of the Kagome core. CL3 design with multiple domain walls harbouring low eigenvalue mechanisms provides the greatest robustness among the designed lattices (excluding the Kagome-Hexagonal) as is indicated by the decay % parameter. Additionally, it is observed that the developed CL outer layers have a property of stiffening after deformation which is clear from the advent of buckling in the Kagome cores. This should be carefully studied as it reduces the applicability of the developed designs to a shorter range of strains.

However, robustness in designs developed through this approach comes at the cost of a drop in absolute macroscopic Young's modulus. The presence of several low eigenvalue mechanisms makes the lattice compliant and hence reduces its stiffness (compared to a fully-Kagome lattice of the same dimensions). Therefore, a trade-off needs to be established between robustness and absolute stiffness of designed lattices. Designs tending towards one extreme inherently lose the other feature, as evidenced by robustness in the Kagome-Hexagonal against the absolute stiffness of the Kagome-Triangular. The proposed method which uses eigenvalues for designing, helps in striking the desired trade-off. The CL1 is an example of a design that is both robust and does not sacrifice on the macroscopic Young's modulus greatly, in addition to having a weight as that of a fully-Kagome lattice of the same dimension. Although not optimal, these designs are indicative of the feasibility of the proposed solution strategy in addressing the problem of stiffness decay in Kagome lattices, without warranting a significant increase in overall lattice weight.

Finally, revisiting the set objective which was to develop robust and lightweight lattice materials, it can be said that a novel design protocol is devised that aids in addressing the issue of robustness while generating stiff and lightweight lattices. Although the issue of imperfection sensitivity can not be removed completely unless a radical change in microarchitecture is introduced, the protocol devised here achieves robustness to a decent extent while also addressing the issue of absolute stiffness. Nevertheless, the designs presented here are far from optimal. There are a few ways in which they can be improved further, resulting in higher robustness without sacrificing the absolute stiffness. They are as listed below:

Recommendations for future work

The following is a set of potential directions that one could adopt for future work. While some are regarding improvements for the proposed designs and the adopted methodology, others are new directions that could be pursued based on this work.

1. The CL designs could be improved through an eigenvalue assessment of the outer layers as the deformations set in. However, since a direct link cannot be made between the mechanism of the pin-jointed model and ensuing deformations in the welded-jointed model, such an improvement is not a straightforward endeavour. For this, accurate numerical models need to be developed to examine the manner in which deformations ensue in a welded-jointed model under a specific loading scenario. Analysing such a model shows the deformed states at various increments which can then be translated into a series of equivalent pin-jointed geometries. Needless to say, the pin-jointed models will only be moderately accurate as it cannot accept bent or buckled members, and therefore is at best, an approximate. Nevertheless, the rise in eigenvalue can be then investigated for the series of pin-jointed geometries.

If the eigenvalue increase in the outer layer mechanisms (as measured from the pin-jointed equivalents of the FE model increments) is more than the Kagome mechanisms, the whole design cycle needs to be restarted with a modified design such that the eigenvalue increase is lesser than that of the Kagome mechanisms. If the eigenvalue increase of the CL outer layers can be contained to be lesser than the eigenvalue increase of the Kagome core mechanisms, robustness can be achieved for larger range of external loads, in accordance with the rationale presented in Section 3.1.1. This could also help in limiting the presence of Kagome core buckling. This whole framework of redesigning the pin-jointed equivalent based on numerical results, although tedious, could gradually lead to a more effective and nuanced design.

2. In addition to maintaining the evolution of eigenvalues corresponding to the CL outer layer mechanisms, a simultaneous objective would be to redesign the polarised and MT lattice regions to increase the absolute stiffness of the lattice. This however should be done carefully without affecting the presence

of mechanisms at domain walls or the associated eigenvalues. Although this measure does not seem to promise a substantial increase in absolute stiffness (as the drop in stiffness is mainly due to domain walls itself), it is nevertheless worthy of investigation.

3. Pursuing the directions mentioned in the previous points through an iterative design process can become extremely cumbersome. To that end, utilising multi-objective optimisation and learning algorithms could prove to be beneficial. A ground structure optimisation technique [41] or novel methods like topology optimisation of modular blocks [42] could be used for this purpose. Data-driven paradigms like the Distance-Minimising technique could be used as a plug-in to the minimisation problem in the optimisation framework. Kirchdoerfer & Ortiz [43] introduce this technique and demonstrate its application for assessing the equilibrium of 3D lattices. This is just one of the many alternate techniques that have been introduced in the past decade. An extensive data-driven study would not only help generate designs with improved performance but also with counter-intuitive functionality. Importantly, implementing a lattice determinacy framework into these techniques would be a challenging yet interesting avenue to explore.
4. Extending the concept of polarised and MT lattices into 3D would most definitely be a rich and interesting aspect to investigate. 3D Kagome models like the KDLG introduced by Symons *et al.* [44] could be used for the core, as the KDLG lattice also demonstrates severe imperfection sensitivity [25]. The KDLG design, with nodal connectivity of 6, is considerably lightweight compared to other designs like the octet lattice with nodal connectivity of 12 [45], which is observed to be insensitive to nodal defects. Therefore, the robustness of the KDLG lattice due to the addition of 3D MT lattice and polarised Kagome could potentially be a lightweight alternative to the octet design and other lattices with $Z \geq 12$. Furthermore, in such an architecture, mechanisms would be spatial and the existence of strain-producing mechanisms could be dependent on directional loading. In addition, mechanism propagation could also be studied.
5. Considering the limitations of the dynamical matrix method (see Section 2.7), it would be beneficial to explore a method that would aid in easy and accurate differentiation of strain-producing mechanism modes and modes that distort the unit cells. Further, implementing a nonlinear kinematic model in the matrix analysis framework could aid in tracking the change in eigenvalues as the mechanisms at the domain wall evolve.
6. In order to study the complete efficacy of the novel CL designs, stiffness decay should be investigated for different lattice microarchitectures as the core. For example, defect sensitive square lattices could be used as the core with appropriately designed MT lattice and polarised regions at its exteriors. Assessment of a variety of such designs could provide more insights into the nuances of the proposed design strategy. Furthermore, the designs should be examined under the influence of other defects as well. These could be defects like fractured cell walls, non-uniform cell wall thickness, and curved/wavy walls [23], [18], [15].

Naturally, pursuing any idea mentioned here should be supplemented with experimental validation. Adopting a direction towards a specific application like impact attenuation or energy absorption could aid in more specific and definitive set of designs, assuming the design strategy presented here suffices for such applications.

Finally, it should be understood that the proposed design strategy is one among the many that could potentially solve the issue of stiffness decay in lattice materials. It would be perfectly valid to develop and adopt a completely different and superior strategy. All the aforementioned points pivot around the current designs. With that, it can be concluded that further steps need to be taken to completely address the problem at hand. It may very well be possible that in the end, no method offers 100% robustness against defects, while simultaneously retaining the macroscopic stiffness of the lattice. Nevertheless, one should leave that speculation for scientific curiosity and pursue the effort till the end.

References

1. Onck, P. R. Cosserat modeling of cellular solids. *Comptes Rendus. Mécanique* **330**, 717–722 (2002).
2. Weeks, J. *Mechanical Response of Lattice Structures under High Strain-Rate and Shock Loading*. Doctoral thesis (California Institute of Technology, 2022).
3. Gibson, L. J. & Ashby, M. F. *Cellular solids: Structure and properties, second edition* 1–510 (Cambridge University Press, 2014).
4. Hyun, S. & Torquato, S. Optimal and manufacturable two-dimensional, Kagomé-like cellular solids. *Journal of Materials Research* **17**, 137–144 (2002).
5. Fleck, N. A., Deshpande, V. S. & Ashby, M. F. Micro-architected materials: past, present and future. *Proceedings of the Royal Society A: Mathematical, Physical and Engineering Sciences* **466**, 2495–2516 (2010).
6. Yin, H. *et al.* Review on lattice structures for energy absorption properties. *Composite Structures* **304**, 116397 (2023).
7. Pellegrino, S. & Calladine, C. R. Matrix analysis of statically and kinematically indeterminate frameworks. *International Journal of Solids and Structures* **22**, 409–428 (1986).
8. Deshpande, V. S., Ashby, M. F. & Fleck, N. A. Foam topology: bending versus stretching dominated architectures. *Acta Materialia* **49**, 1035–1040 (2001).
9. Guest, S. D. & Hutchinson, J. W. On the determinacy of repetitive structures. *Journal of the Mechanics and Physics of Solids* **51**, 383–391 (2003).
10. Van Megen, D. *Predicting the elastic properties of lattice materials, a geometrically nonlinear approach*. Master's thesis (Delft University of Technology, 2022).
11. Hashin, Z. & Shtrikman, S. A variational approach to the theory of the elastic behaviour of multiphase materials. *Journal of the Mechanics and Physics of Solids* **11**, 127–140 (1963).
12. Lipperman, F., Ryykin, M. & Fuchs, M. Fracture toughness of two-dimensional cellular material with periodic microstructure. *International Journal of Fracture* **146**, 279–290 (2007).
13. Fleck, N. A. & Qiu, X. The damage tolerance of elastic–brittle, two-dimensional isotropic lattices. *Journal of the Mechanics and Physics of Solids* **55**, 562–588 (2007).
14. Hutchinson, R. G. & Fleck, N. A. The structural performance of the periodic truss. *Journal of the Mechanics and Physics of Solids* **54**, 756–782 (2006).
15. Gencoglu, C., Tekoglu, C. & Ayas, C. Effect of imperfections on the actuation performance of lattice materials. *International Journal of Solids and Structures* **252**, 111779 (2022).
16. Yan, C., Hao, L., Hussein, A. & Raymont, D. Evaluations of cellular lattice structures manufactured using selective laser melting. *International Journal of Machine Tools and Manufacture* **62**, 32–38 (2012).
17. Romijn, N. E. & Fleck, N. A. The fracture toughness of planar lattices: Imperfection sensitivity. *Journal of the Mechanics and Physics of Solids* **55**, 2538–2564 (2007).
18. Symons, D. D. & Fleck, N. A. The imperfection sensitivity of isotropic two-dimensional elastic lattices. *Journal of Applied Mechanics* **75**, 051011 (2008).
19. Tankasala, H., Deshpande, V. & Fleck, N. Tensile response of elastoplastic lattices at finite strain. *Journal of the Mechanics and Physics of Solids* **109**, 307–330 (2017).
20. Nelissen, W., Ayas, C. & Tekoglu, C. 2D lattice material architectures for actuation. *Journal of the Mechanics and Physics of Solids* **124**, 83–101 (2019).
21. Guo, X. & Gibson, L. J. Behavior of intact and damaged honeycombs: A finite element study. *International Journal of Mechanical Sciences* **41**, 85–105 (1999).

22. Guo, X.-D. E., McMahon, T. A., Keaveny, T. M., Hayes, W. C. & Gibson, L. J. Finite element modeling of damage accumulation in trabecular bone under cyclic loading. *Journal of Biomechanics* **27**, 145–155 (1994).
23. Chen, C., Lu, T. & Fleck, N. Effect of imperfections on the yielding of two-dimensional foams. *Journal of the Mechanics and Physics of Solids* **47**, 2235–2272 (1999).
24. Silva, M. J. & Gibson, L. J. The effects of non-periodic microstructure and defects on the compressive strength of two-dimensional cellular solids. *International Journal of Mechanical Sciences* **39**, 549–563 (1997).
25. Symons, D., Shieh, J. & Fleck, N. Actuation of the kagome double-layer grid. part 2: Effect of imperfections on the measured and predicted actuation stiffness. *Journal of the Mechanics and Physics of Solids* **53**, 1875–1891 (2005).
26. Lu, Z.-X., Liu, Q. & Huang, J.-X. Analysis of defects on the compressive behaviors of open-cell metal foams through models using the FEM. *Materials Science and Engineering: A* **530**, 285–296 (2011).
27. Wallach, J. & Gibson, L. Defect sensitivity of a 3D truss material. *Scripta Materialia* **45**, 639–644 (2001).
28. Gross, A., Pantidis, P., Bertoldi, K. & Gerasimidis, S. Correlation between topology and elastic properties of imperfect truss-lattice materials. *Journal of the Mechanics and Physics of Solids* **124**, 577–598 (2020).
29. Coulais, C., Teomy, E., de Reus, K., Shokef, Y. & van Hecke, M. Combinatorial design of textured mechanical metamaterials. *Nature* **535**, 529–532 (2016).
30. Meeussen, A. S., Oğuz, E. C., Shokef, Y. & van Hecke, M. Topological defects produce exotic mechanics in complex metamaterials. *Nature Physics* **16**, 307–311 (2020).
31. Meeussen, A. S., Oğuz, E. C., Hecke, M. V. & Shokef, Y. Response evolution of mechanical metamaterials under architectural transformations. *New Journal of Physics* **22**, 023030 (2020).
32. Moore, J. E. The birth of topological insulators. *Nature* **464**, 194–198 (2010).
33. Kane, C. L. & Lubensky, T. C. Topological boundary modes in isostatic lattices. *Nature Physics* **10**, 39–45 (2013).
34. Sun, K., Souslov, A., Mao, X. & Lubensky, T. C. Surface phonons, elastic response, and conformal invariance in twisted kagome lattices. *Proceedings of the National Academy of Sciences of the United States of America* **109**, 12369–12374 (2012).
35. Huber, S. D. Topological mechanics. *Nature Physics* **12**, 621–623 (2016).
36. Sun, K., Souslov, A., Mao, X. & Lubensky, T. C. Surface phonons, elastic response, and conformal invariance in twisted kagome lattices. *Proceedings of the National Academy of Sciences* **109**, 12369–12374 (2012).
37. Abaqus. Dassault Systemes. <https://www.3ds.com/products/simulia/abaqus>. 2023.
38. Omid, M. *Material Properties of Planar Lattices*. Doctoral thesis (Aalto University, 2023).
39. DHPC. *DelftBlue Supercomputer (Phase 2)*. <https://www.tudelft.nl/dhpc/system>. 2024.
40. Pronk, T. N., Ayas, C. & Teköglü, C. A quest for 2D lattice materials for actuation. *Journal of the Mechanics and Physics of Solids* **105**, 199–216 (2017).
41. Dorn, W., Gomory, R. & Greenberg, H. Automatic Design of Optimal Structures. *Journal de Mécanique* **3**, 25–52 (1964).
42. Lu, H., Lee, T.-U., Ma, J. & Xie, Y. M. Design optimisation of structures made of a small number of prescribed building blocks. *Engineering Structures* **304**, 117686 (2024).
43. Kirchdoerfer, T. & Ortiz, M. Data-driven computational mechanics. *Computer Methods in Applied Mechanics and Engineering* **304**, 81–101 (2016).
44. Symons, D., Hutchinson, R. & Fleck, N. Actuation of the Kagome Double-Layer Grid. Part 1: Prediction of performance of the perfect structure. *Journal of the Mechanics and Physics of Solids* **53**, 1855–1874 (2005).
45. Deshpande, V., Fleck, N. & Ashby, M. Effective properties of the octet-truss lattice material. *Journal of the Mechanics and Physics of Solids* **49**, 1747–1769 (2001).



Algorithms

The algorithms used for automating the matrix analysis are elaborated here. Three algorithms are devised. Two of these, are for analysing unit cells of infinite lattices and the third is for analysing finite lattices. The algorithms slightly differ for infinite and finite lattices. In addition to that, guidelines for designing appropriate unit cells suitable for the devised algorithms are also mentioned. For infinite lattices, unit cells can be designed in two ways: with nodes at the boundary or with elements crossing the boundary. The treatment for both these cases is different. In the former, periodicity is maintained by repeating nodes at the boundary (affects the rows in the equilibrium matrix), and in the latter, periodicity is maintained by repeating members (affects the columns in the equilibrium matrix). Figure A.1a and Figure A.1b represent a suitable unit cell for both cases of a Kagome lattice.

A.1. Repeating members

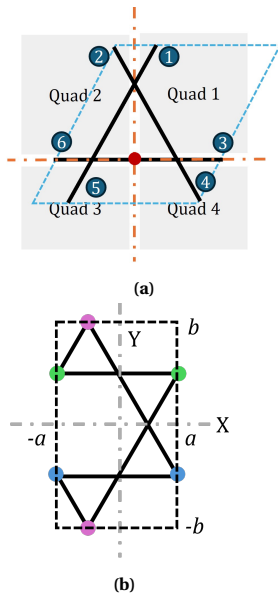
Consider the case of repeating members, or otherwise also referred to as boundary crossing members. It is imperative to choose an appropriate unit cell here. There are pitfalls to not choosing an appropriate unit cell. The set of conditions to be satisfied by the unit cell design for being suitable for the algorithms is termed here as the *criteria-for-design*. The *criteria-for-design* for unit cells with boundary crossing members is as follows,

1. Unit cell should be space/plane filling.
2. Equal number of boundary crossing members in opposing quadrants. The coordinate origin of the unit cell should be adjusted appropriately to ensure this.
3. Boundary crossing members should be of equal lengths - half of an internal member.
4. Boundary crossing members should not be part of two different quadrants. In other words, they should not cross either axis passing through the origin.
5. If a boundary crossing member overlaps with an axis, it is a special member and is counted in the adjacent quadrant in a clockwise sense. This is not physically carried out, rather, is only implemented in the algorithm. However, in these cases, the unit cell origin should be altered *a-priori* such that the adjustment of special members (in the algorithm) does not violate condition 2.

Under these conditions, the algorithm ensures the correct evaluation of the matrices. The heart of these algorithms is identifying the correct pair of repeating elements, which ensures periodicity. For repeating members, this is done based on the slope, quadrants and distance between them. These are called the *criteria-for-analysis*. For example, in Figure A.1a, each member in quadrant 1 has its counterpart in quadrant 3 with the same slope. However, depending on the choice of unit cells, there could be multiple such elements in each quadrant and this creates a problem for pairing. The distance check solves this issue. For an appropriately chosen unit cell, it is a general rule that the correct pairs across all quadrants should have the same absolute distance between them. This fact is used to finalise the correct pairs. For example, assessment of the unit cell in Figure A.1a against the *criteria-for-design* and the *criteria-for-analysis* is elaborated in Figure A.1c. The pseudo-code for evaluating the matrices and nullspace for periodic lattices with boundary crossing members is presented in algorithm 1. The pseudo-code is presented in a block-wise manner (indicated by *procedure* command).

Algorithm 1 Infinite lattice: boundary crossing members

Require: Node set N ▷ Node-set N and their Cartesian coordinates
Require: Member set E (internal) and B (boundary crossing)
Require: Equal number of members ($s_i \in B, i = 1, 2, 3, 4$) in each opposing quadrant
1: **procedure** CONNECTIVITY(N, E, B) for all nodes $n \in N$ ▷ Build connectivity matrix C
2: Build C : matrix with nodes and corresponding connected members from $E \cup B$
3: **end procedure**
4: **procedure** SORTING(C, N, E, B) all members $b \in B$ ▷ Sorting boundary crossing members
5: Build Q : matrix with information regarding members and corresponding quadrants.
6: Build QC : vector indicating total count of members for each quadrant
7: Build S : matrix storing member slope information
8: Build SM : matrix indicating members connected to the same node with same slope
9: Build D : matrix with information regarding distance between members in opposite quadrants.
10: **end procedure**
11: **procedure** PAIRING(C, Q, QC, S, SM, D) ▷ Pairing multiple instances of same members $b \in B$
12: Select members $b \in B$ based on slope, opposing quadrants and distance constraints.
13: Build pairing matrix P with $P[b, 1]$: primary members & $P[b, 2]$: secondary members
14: **end procedure**
15: **procedure** MATRICES(C, N, E, B) ▷ Evaluating A and B matrices
16: Generate A : equilibrium matrix containing all members in $E \cup B$
17: **end procedure**
18: **procedure** REDUNDANCY ELIMINATION(A, B, P) ▷ ':' indicates usage of the all entries of that dimension
19: **for all** $k \in P[:, 1]$ **do**
20: $A \leftarrow A[:, P[k, 1]] + A[:, P[k, 2]]$
21: **end for**
22: Delete $A[:, P[k, 2]]$
23: $B \leftarrow A^T$
24: **end procedure**
25: **procedure** NULLSPACES(A, B) ▷ Calculating linearised modes from dynamical matrices
26: $B' \leftarrow \text{double}(B)$
27: $D \leftarrow B'^T B'$ and $D^h \leftarrow B' B'^T$
28: Solve for smallest eigenvalues using `eigs` MATLAB function
29: **end procedure**

**Table: Criteria-for-design**

Condition	Satisfied (Yes/No)	Remarks
1	Yes	Chosen unit cell is tessellatable in plane
2	Yes	Equal number of boundary crossing elements in opposing quadrants (after application of condition 5)
3	Yes	All external members are halves of internal ones
4	Yes	No members crossing either axes
5	Yes	Member 3 belongs to quad 4 and member 6 belongs to quad 2



All conditions satisfied

Table: Criteria-for-analysis

Condition	Remarks
1: Quadrants	Member 1 is paired with member 5; members 3 and 4 are to be paired with 2 and 6
2: Slope	Indicates the paired member sets are (1,5), (3,6), (2,4)
3: Distance	Since the slopes are unique, this check is not necessary.

Figure A.1: Representation of both *criteria-for-design* and *criteria-for-analysis* on Kagome unit cells: **a.** Kagome unit cell with boundary crossing members suitable for an infinite-model; **b.** Kagome unit cell with periodic nodes suitable for an infinite-model, with set of periodic nodes highlighted by the same colour; **c.** Process flow starts from the selection of appropriate unit cell with boundary crossing members that satisfy *criteria-for-design* to fulfilment of *criteria-for-analysis* which ultimately results in a proper implementation of periodicity in the matrices.

A.2. Repeating nodes

For repeating nodes, the only information available is regarding the quadrants, which on its own is unreliable. Therefore for repeating nodes, the pairing is done manually through GUI-based user input with no *criteria-for-analysis*. The choice of unit cell here is also important, although not as restrictive as in the previous case. The *criteria-for-design* for this case are as follows,

1. Unit cell should be space/plane filling. The choice of the unit cell dictates the directions in which it should repeat in order to model the infinite lattice. For example, the unit cell shown in Figure A.1b, should be repeated along the X and Y directions.
2. Equal number of periodic nodes along each repeating direction on either side of the origin. For example, in Figure A.1b, two sets (green and blue) of periodic nodes along X direction; and one set (pink nodes) along Y direction. It is important to note that for Y direction, the blue and green coloured nodes do not count as they do not participate in periodicity along that repeating direction. Similarly, for X axis, the pink-coloured nodes do not count.

The algorithm for repeating nodes is outlined in algorithm 2.

Algorithm 2 Infinite lattice: repeating nodes

Require: Node set N ▷ Node-set N and their Cartesian coordinates
Require: Member set B
1: **procedure** SORTING(N, B) all members $b \in B$ ▷ Sorting boundary crossing members
2: Build S : matrix storing member slope information
3: **end procedure**
4: **procedure** PAIRING(N) ▷ Pairing multiple instances of same nodes $m \in M \subset N$
5: GUI (user input) based pairing of repeating nodes.
6: Build pairing matrix P with $P[m, 1]$: primary nodes & $P[n, 2]$: secondary members
7: **end procedure**
8: **procedure** MATRICES(S, N, B) ▷ Evaluating A and B matrices
9: Generate A : equilibrium matrix
10: **end procedure**
11: **procedure** REDUNDANCY ELIMINATION(A, B, P) ▷ ':' indicates usage of all entries of that dimension
12: **for all** $k \in P[:, 1]$ **do**
13: $B \leftarrow B[:, P[k, 1]] + B[:, P[k, 2]]$
14: **end for**
15: Delete $B[:, P[k, 2]]$
16: $A \leftarrow B^T$
17: **end procedure**
18: **procedure** NULLSPACES(A, B) ▷ Calculating linearised modes from dynamical matrices
19: $B' \leftarrow \text{double}(B)$
20: $D \leftarrow B'^T B'$ and $D^h \leftarrow B' B'^T$
21: Solve for smallest eigenvalues using `eigs` MATLAB function
22: **end procedure**

A.3. Finite lattices

For finite lattices, the process is relatively straightforward since the aspect of periodicity does not exist. The only challenge here is to incorporate appropriate boundary conditions (if existing). Information regarding boundary conditions is also extracted from the input file generated. Depending on the type of boundary conditions, the rows of the equilibrium matrix (representing nodal information) are modified to incorporate the changes in degrees of freedom. The algorithm for this case is as presented in algorithm 3

Algorithm 3 Finite lattices

Require: Node set N ▷ Node-set N and their Cartesian coordinates
Require: Member set E

- 1: **procedure** CONNECTIVITY(N, E) for all nodes $n \in N$ ▷ Build connectivity matrix C
- 2: Build C : matrix with nodes and corresponding connected members from E
- 3: **end procedure**
- 4: **procedure** MATRICES(C, N, E) ▷ Evaluating A and B matrices
- 5: Generate A : equilibrium matrix
- 6: **end procedure**
- 7: **procedure** BOUNDARY CONDITION APPLICATION(A, B, N, E)
- 8: $P \subset N \quad \forall n \in N$ with $(u_x^n, u_y^n) = (0, 0)$
- 9: $Q \subset N \quad \forall n \in N$ with $u_x^n = 0$
- 10: $R \subset N \quad \forall n \in N$ with $u_y^n = 0$
- 11: **if** $P \cup Q \cup R = \phi$ **then**
- 12: Break out of procedure
- 13: **end if**
- 14: **if** $i \in P$ **then**
- 15: $A[2i - 1, :] = 0$ ▷ Eliminating x degree of freedom
- 16: $A[2i, :] = 0$ ▷ Eliminating y degree of freedom
- 17: **else if** $i \in Q$ **then**
- 18: $A[2i - 1, :] = 0$ ▷ Only eliminating x degree of freedom
- 19: **else if** $i \in R$ **then**
- 20: $A[2i, :] = 0$ ▷ Only eliminating y degree of freedom
- 21: **end if**
- 22: Delete all zero rows
- 23: $B = A^T \leftarrow$ compatibility matrix
- 24: **end procedure**
- 25: **procedure** NULLSPACES(A, B) ▷ Calculating linearised modes from dynamical matrices
- 26: $B' \leftarrow$ double(B)
- 27: $D = B'^T B'$ and $D^h = B' B'^T$
- 28: Solve for smallest eigenvalues using `eigs` MATLAB function
- 29: **end procedure**

The implementation of all these algorithms can be found in repository.

B

Mechanisms

Contents of this appendix supplement the benchmark tests presented in Chapter 2 that verify the proposed dynamical matrix method against traditional matrix method. Metrics like the computation time and the number mechanisms (m) and states of self-stress (s) obtained using both methods are already discussed. To complete the picture, the ensuing mechanisms are also examined. In fact, states of self-stress can also be evaluated following the same procedure. However, comparative results for states of self-stress are assumed to follow the trend in comparative results of mechanisms. Therefore, only mechanisms are studied here. Since the traditional matrix method without augmenting only discovers non strain-producing mechanisms, the comparative study is limited to non strain-producing mechanisms only. For the dynamical matrix case, this indicates the eigenvectors corresponding to eigenvalues of the order of $\approx 10^{-16}$. Furthermore, the obtained mechanisms illustrated in this section are also compared with the corresponding results from literature [20], [31], [40].

Table B.1 illustrates the mechanisms obtained for 3 infinite lattice architectures- the Kagome, KT and Hexagonal Cupola. Since the nullspace vectors can be arbitrarily scaled, a visual disparity could be observed, upon scrutiny, between the mechanisms shown for both methods. However, this is a mere artefact of vector scaling and does not challenge the validity of the results. Moreover, all mechanisms represented here are infinitesimal mechanisms. Therefore they are heavily exaggerated for illustration purposes only. Excellent agreement can be seen between the results obtained using both methods.

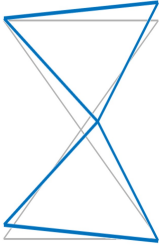




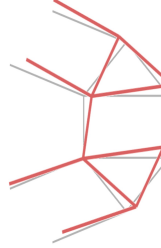
	Kagome	KT	Hexagonal Cupola
Traditional matrix method			
Dynamical matrix method			

Table B.1: Visual comparison of non strain-producing mechanisms of infinite lattices obtained using the traditional matrix method (using symbolic matrices) against the dynamical matrix method. Original unit cells are shown in grey, with mechanisms overlaid.

Mechanisms of finite lattices are also studied. Superhexagon architectures as shown in Figure 2.6f are chosen for this purpose. Superhexagons with an inner loop count of 8 members and 12 members are selected. The mechanisms obtained using both methods are presented in Table B.2. Although the mechanisms shown here seem exaggerated, they correspond to lattice architectures with finite mechanisms and are therefore can be considered as accurate representations.





	Inner loop: 8	Inner loop: 12
Traditional matrix method		
Dynamical matrix method		

Table B.2: Visual comparison of mechanisms of network lattices obtained using the traditional matrix method (using symbolic matrices) against the dynamical matrix method.

Lastly, localised modes observed in polarised lattices are also studied. Mechanisms of the lattice model are shown in Figure 2.7a. Recall that these are in fact unit cells of an infinite lattice.

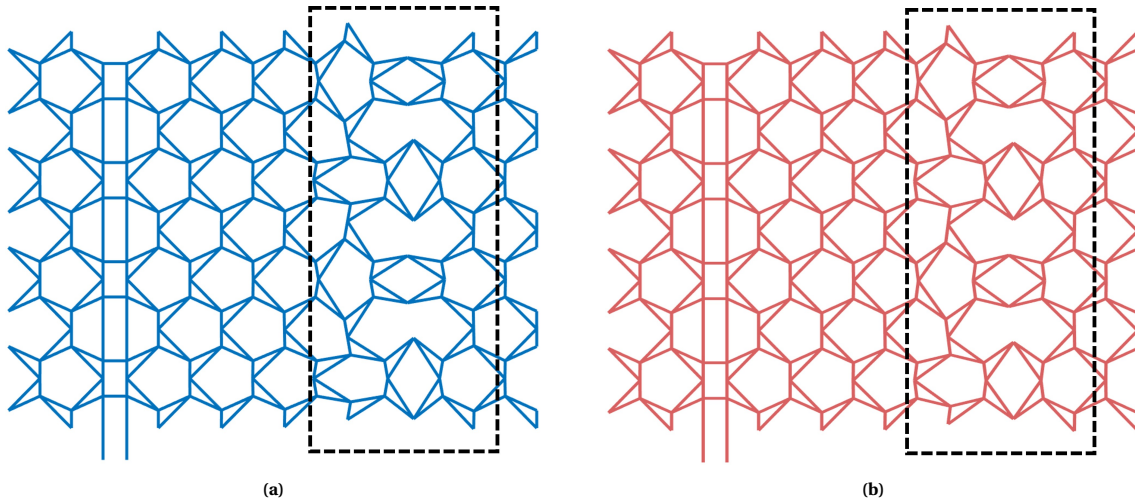


Figure B.1: Visual comparison of the non strain-producing mechanism obtained for the lattice shown in Figure 2.7a. Notice the accumulation of mechanisms near the domain wall (region indicated by the dashed box). Mechanism obtained using: **a.** Traditional matrix method; **b.** Dynamical matrix method.

C

CL designs

C.1. Polarising the Kagome

Polarisation in Kagome is generated by distorting the unit cell such that it causes a gap in the phonon spectrum of the Kagome. This gap is characterised by a winding number that is a system invariant. The winding number (n) when collected with lattice base vectors \mathbf{a} in as in Equation C.1 gives the direction of polarisation. It was noted by Sun *et al.* [34] that the Kagome mechanism (which preserves the shape of triangles in the unit cell) also generates a gap in the phonon spectrum (as discussed in Section 2.1.2). However, the combination of winding numbers and lattice vectors yields a zero polarisation even with a non-zero winding number. Therefore it is important to note that a mere gap in the phonon spectrum does not ensure topological polarisation.

$$\mathbf{P}_T = \sum_i n_i \mathbf{a}_i \quad (\text{C.1})$$

Kane & Lubensky [33] identify 4 independent parameters that govern the distortion of Kagome for polarising it. They are (x_1, x_2, x_3, z) , where x_1, x_2, x_3 indicates the amount of disruption in straight lines (through nodal displacements) along base vectors $\mathbf{a}_1, \mathbf{a}_2$ and \mathbf{a}_3 , and z indicates the asymmetry in sizes of two triangles. Although only two independent base vectors are needed for a complete in-plane representation, a third (dependent) one is considered to make the process simpler. Here, asymmetry in triangles is not considered and therefore $z = 0$. Figure C.1 shows an arbitrary distortion of Kagome. Due to this parametrisation, Equation C.1 reduces to

$$\mathbf{P}_T = \frac{1}{2} \sum_{i=1}^3 \mathbf{a}_i \text{sign}(x_i) \quad (\text{C.2})$$

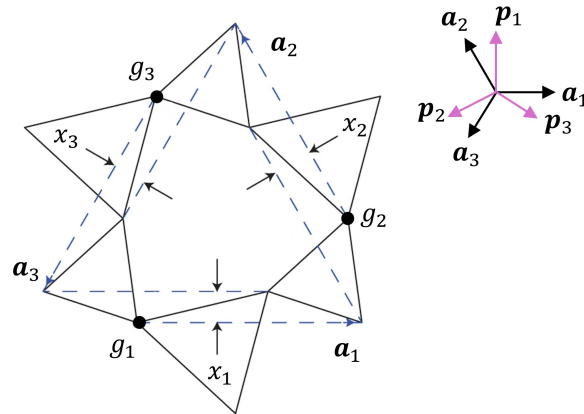


Figure C.1: Convention and associated parameters (x_1, x_2, x_3) for distorting the Kagome to obtain a polarised Kagome. g_i represents nodes of the same triangle but indicated at different sites to aid visualisation of the movement of each of those nodes independently.

Consider the 3 nodes of a single triangle in Kagome. In Figure C.1, these nodes are highlighted at different triangles as g_1 , g_2 and g_3 , which are in essence the same unit. The parametrisation allows freedom to move all 3 nodes independently which results in a distorted Kagome. Distortion of one such triangle can be replicated across symmetry lines to obtain the whole lattice if the asymmetry in two triangles is not allowed. In this example, all nodes are moved outwards from the centroid. This motion is associated with positive x_i . Conversely, if the other 3 nodes are considered ("bigger" triangle nodes), x_i assumes negative values. Both these cases are equivalent in nature. Equation C.2 indicates that eight combinations of x_i are possible with two of them $(+, +, +)$ and $(-, -, -)$ being topologically equivalent to the Kagome lattice in its mechanism state and have no polarisation. The other 6 combinations ensure polarisation. Interestingly, only the sign governs polarisation and not the magnitude of displacement of nodes.

Given an appropriate combination of (x_1, x_2, x_3) , to build the ensuing polarised Kagome out of this, it is useful to first re-make the base vectors that are born out of this distortion. Base vectors of the polarised Kagome is given by,

$$\mathbf{r}_i = \mathbf{r}_i^0 - \sqrt{3}x_i \mathbf{p}_i + x_{i-1} \mathbf{a}_{i+1} \quad (\text{C.3})$$

where, \mathbf{p}_i indicates perpendicular vectors to \mathbf{a}_i , and \mathbf{r}_i^0 stands for the position vectors of nodes i in the original Kagome configuration. Equation C.3 is a slightly modified version adapted from Kane & Lubensky [33]. Consider a triangle of the Kagome as shown in Figure C.2a (in grey). Distortion operations are carried out to this triangle which is then mirrored to obtain the Kagome unit cell since no asymmetry in triangles is considered. The lattice base vectors and their corresponding perpendiculars are given by

$$\begin{aligned} \mathbf{a}_i &= \left[\cos\left(\frac{2(i-1)\pi}{3}\right), \sin\left(\frac{2(i-1)\pi}{3}\right) \right] \\ \mathbf{p}_i &= \left[-\sin\left(\frac{2(i-1)\pi}{3}\right), \cos\left(\frac{2(i-1)\pi}{3}\right) \right] \end{aligned} \quad (\text{C.4})$$

In Figure C.2a, site 3 is assumed to be at the origin and therefore,

$$\mathbf{r}_1^0 = \frac{\mathbf{a}_1}{2}; \quad \mathbf{r}_2^0 = -\frac{\mathbf{a}_3}{2} \quad \text{and} \quad \mathbf{r}_3^0 = \mathbf{0}$$

For the polarised Kagome developed here, (x_1, x_2, x_3) is chosen as $(-0.2, 0.1, 0.03)$. A straightforward substitution of these parameters along with Equation C.4 into Equation C.3 gives the distorted unit cell as shown in Figure C.2a (in black), which when mirrored and repeated forms the polarised lattice as shown in Figure C.2b. The x_i values were chosen so as to facilitate ease of geometrical construction. The polarisation vector of this lattice is determined by Equation C.2, which gives $\mathbf{P}_T = -\mathbf{a}_1$, also indicated in Figure C.2b by the green arrow. Again, three nodes of the same triangle is represented by g'_1 , g'_2 and g'_3 with two of them (g'_2 and g'_3) displaced outwards and one (g'_1) displaced inwards. This is the polarised Kagome lattice used in all CL designs presented in this work.

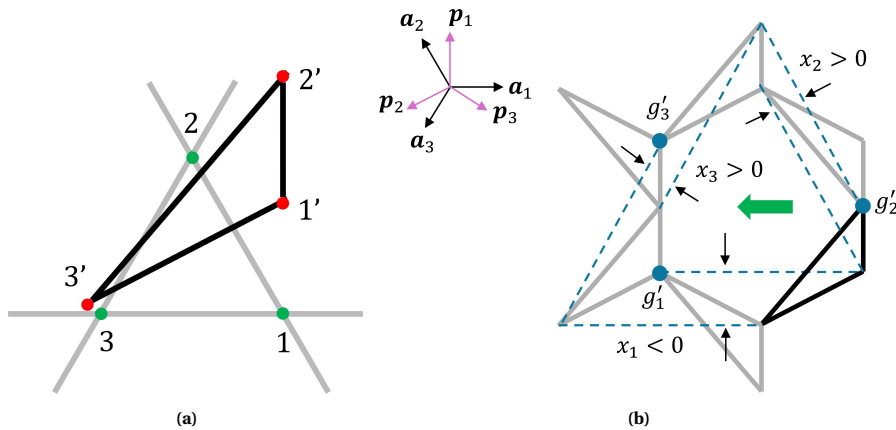


Figure C.2: Polarised Kagome: **a.** Distortion of a single triangle to a polarised one. The original Kagome configuration is illustrated in grey, and the distorted Kagome in black; **b.** Tessellating the obtained triangle to fill the space. Since asymmetry is not allowed, a single triangle (in black) is enough to generate the whole lattice. Blue dots indicate 3 nodes of the same triangle marked by g'_1 , g'_2 and g'_3 . Green arrow indicates the direction of polarisation.

C.2. CL truncation for matrix analysis

The original CL models are considerably large and cause unnecessary computational expense during matrix analysis. The Kagome cores are truncated to reduce this expense yet retain the lattice behaviour. The Kagome core is incrementally reduced till a sudden change is observed in the eigenvalues corresponding to either the Kagome core or outer layer mechanisms. A sudden change indicates a shift in balance between the eigenvalues of the Kagome core and the CL outer layers and hence represents the limiting case. Any truncation beyond this point completely changes the lattice behaviour and would lead to erroneous observations. Three representative cases of the truncation process for the CL2 model are generated, each with a decreasing Kagome core than the previous one. Figure C.3 shows the three cases. A reduction in the Kagome core beyond case 3 is observed to alter the eigenvalues and therefore, the Kagome core size presented in the third case are used as the limit for matrix analysis of CL designs.

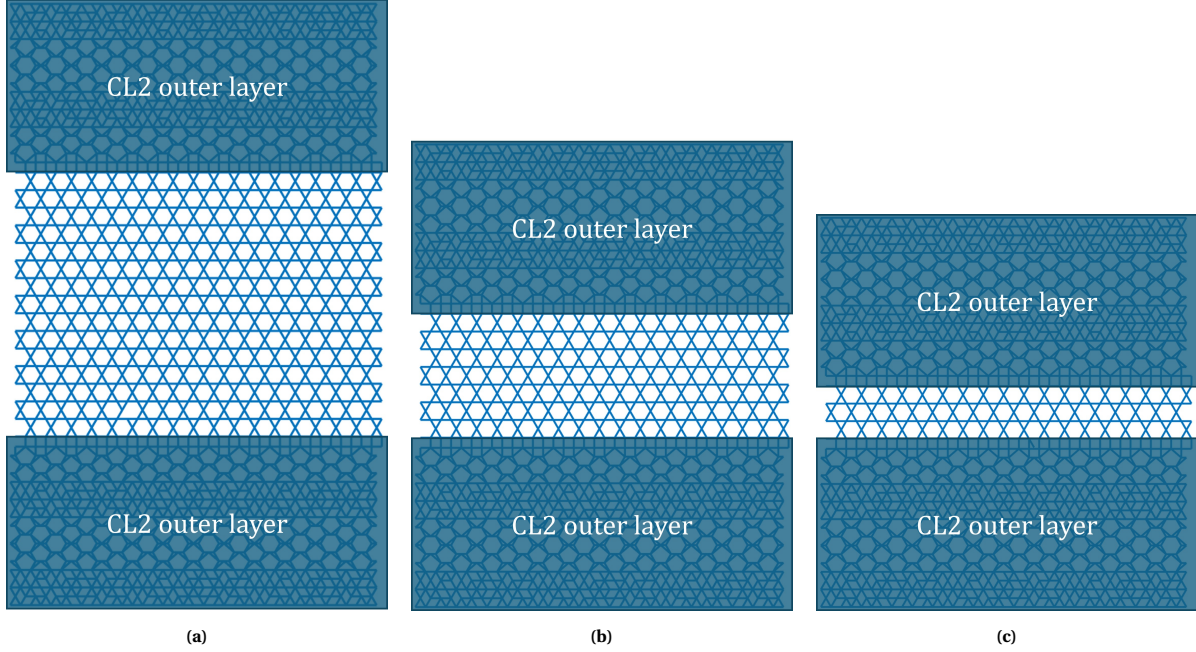


Figure C.3: Incremental truncation of the Kagome core of CL2 model: **a.** Case 1; **b.** Case 2; **c.** Case 3.

For case 1, λ_1 to λ_{18} are observed to be Kagome core mechanisms which are of the order of $\sim 10^{-16}$ and λ_{19} to λ_{22} represent the outer layer mechanisms. λ_{19} and λ_{20} correspond to the mechanisms of the outer-most MT lattice region and associated domain-walls with each having a value of 2.9×10^{-4} . Further, λ_{21} and λ_{22} corresponds to other MT lattice region (closer to the Kagome core) and associated domain walls with each having a value of 2.2×10^{-3} .

For case 2, the number of Kagome mechanisms are reduced, and the outer layer mechanisms have the following eigenvalues. The first two correspond to the outer MT lattice region.

$$\lambda_{11} = 2.9 \times 10^{-4}; \quad \lambda_{12} = 3 \times 10^{-4}; \quad \lambda_{13} = 2.3 \times 10^{-3}; \quad \text{and} \quad \lambda_{14} = 2.4 \times 10^{-3}$$

Along the similar lines, eigenvalues for the outer layer mechanisms of case 3 are,

$$\lambda_8 = 2.9 \times 10^{-4}; \quad \lambda_9 = 3 \times 10^{-4}; \quad \lambda_{10} = 2.1 \times 10^{-3}; \quad \text{and} \quad \lambda_{11} = 2.4 \times 10^{-3}$$

Truncation of the Kagome core beyond this point quantitatively affects the eigenvalues of the lattice and hence core size of case 3 is chosen for all CL matrix analysis. One should be aware that for the imperfect CL models, the amount of nodal defects should also be adjusted to maintain the nodal defect percentage along with this truncation.

C.3. Relative density expressions

Derivation of the expression for relative densities for the MT lattice and polarised regions is elaborated here.

MT lattice

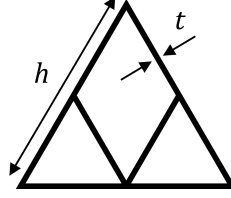


Figure C.4: Schematic of the supertriangle which is the unit cell of the MT lattice.

Consider the supertriangle unit cell as shown in Figure C.4. Total area of the supertriangle is

$$A_{\text{unit}} = \frac{\sqrt{3}h^2}{4}$$

Cumulative area of cell walls,

$$\begin{aligned} A_{\text{walls}} &= 2 \times A_{\text{inner wall}} + \frac{1}{2} (3 \times A_{\text{outer wall}}) \\ &= \frac{5th}{2} \end{aligned}$$

The factor of 0.5 accounts for outer cell walls being shared between two adjacent unit cells. Therefore, the relative density of the MT lattice region is,

$$\begin{aligned} \bar{\rho}_{\text{MT}} &= \frac{A_{\text{walls}}}{A_{\text{unit}}} \\ &= \frac{10t}{\sqrt{3}h} \end{aligned}$$

Polarised Region

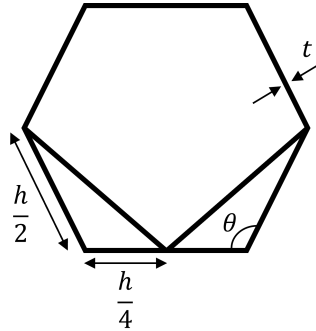


Figure C.5: Unit cell for the polarised Kagome lattice. Distortion of the Kagome is carried out such that the unit cell obtained is a regular hexagon.

Consider the unit cell of the polarised Kagome as shown in Figure C.5. The side lengths of the hexagon shown here are the same as that of the Kagome, which is in fact half the outer wall length of the supertriangle. Therefore, area of the unit cell (regular hexagon) is,

$$A_{\text{unit}} = \frac{3\sqrt{3}h^2}{8}$$

Cumulative area of walls,

$$A_{\text{walls}} = 2 \times A_{\text{inner wall}} + \frac{1}{2} (6 \times A_{\text{outer wall}})$$

where length of inner wall is derived from the rules of cosines as,

$$\begin{aligned} l_{\text{inner wall}} &= \frac{h}{2} \sqrt{\frac{5}{4} - \cos \theta} \\ &= \frac{\sqrt{7}h}{4} \quad \text{as } \theta = \frac{2\pi}{3} \end{aligned}$$

Similar to the previous calculation, the factor of 0.5 accounts for cell walls being shared by adjacent unit cells. Total area of the cell wall then is,

$$A_{\text{walls}} = \frac{\sqrt{7}th}{2} + \frac{3th}{2}$$

Therefore, relative density of the polarised region is,

$$\begin{aligned} \bar{\rho}_{\text{polarised}} &= \frac{A_{\text{walls}}}{A_{\text{unit}}} \\ &= \frac{(4\sqrt{7} + 12)t}{3\sqrt{3}h} \end{aligned}$$